

ISSN 1732-9353 (suspended)
eISSN 2543-7496

Scientific Review

Engineering and Environmental Sciences

Przegląd Naukowy
Inżynieria i Kształtowanie Środowiska

Vol. 32 (4)

2023
Quarterly

Issue 102

SCIENTIFIC REVIEW
ENGINEERING AND ENVIRONMENTAL SCIENCES
Quarterly

EDITORIAL BOARD

Kazimierz Adamowski (University of Ottawa, Canada), **Kazimierz Banasik – Chairman** (Warsaw University of Life Sciences – SGGW, Poland), Andrzej Ciepiewski (Warsaw University of Life Sciences – SGGW, Poland), Tomáš Dostál (Czech Technical University in Prague, Czech Republic), Vidmantas Girklys (Aleksandras Stulginskis University, Kaunas, Lithuania), Małgorzata Gutry-Korycka (University of Warsaw, Poland), Zbigniew Heidrich (Warsaw University of Technology, Poland), Silvia Kohnova (Slovak University of Technology, Bratislava, Slovak Republic), Andrzej J. Kosicki (Maryland State Highway Administration, Baltimore, USA), Hyosang Lee (Chungbuk National University, Korea), Athanasios Loukas (University of Thessaly, Volos, Greece), Jurík Luboš (Slovak Agriculture University, Nitra, Slovak Republic), Viktor Moshynskyi (National University of Water Management and Nature Resources Use, Rivne, Ukraine), Magdalena Daria Vaverková (Mendel University in Brno, Czech Republic)

EDITORIAL OFFICE

Tomasz Gnatowski (Deputy-chairman), Weronika Kowalik, Paweł Marcinkowski (Editorial Assistant Environmental Sciences), Katarzyna Pawluk, **Mieczysław Połoński (Chairman)**, Magdalena Daria Vaverková, Grzegorz Wierzbicki, Grzegorz Wrzesiński (Editorial Assistant Engineering Sciences)

REVIEWERS Vol. 32

Afaq Ahmad, Ahmed Alalikhhan, Muna Al-Rubaye, Najla H. Alshareef, Libor Ansoerge, Vazgen Bagdasaryan, Marek Bajda, Piotr Banaszuk, Isabel Brás, Filip Bujakowski, Armands Celms, Piotr Dąbrowski, Marek Dohojda, Tomasz Dysarz, Sébastien Gadal, Olga Heralová, Maher Murad Jebur, Katarzyna Jeleniewicz, Agnieszka Karczmarczyk, Renata Kędzior, Amina Ahmed Khalil, Gagik Kirakossian, Małgorzata Loga, Mohamed Khatif Tawaf Mohamed Yusof, Erfan Najaf, Paweł Oglęcki, Roberto Pizzolotto, Anna Podlasek, Gabriela Rutkowska, Vasyl Shvabyuk, Zdzisław Skutnik, Urszula Somorowska, Tomasz Stańczyk, Lada Stejskalová, Maciej Szwaśc, Tomasz Szymczak, Roman Trach, Zubeda Ukundimana, Magdalena Vaverková, Eva Vítková, Ivanna Voronkova, Wendelin Wichtmann, Rafał Wyczółkowski, Askar Zhusupbekov, Krzysztof Zima, Kinga Zinowiec-Cieplik

ENGLISH LANGUAGE EDITOR

Ewa Gurdak

EDITORIAL OFFICE ADDRESS

Wydział Budownictwa i Inżynierii Środowiska SGGW, ul. Nowoursynowska 159, 02-776 Warsaw, Poland
tel. (+48 22) 59 35 363, 59 35 210, 59 35 302
e-mail: srees@sggw.edu.pl
<https://srees.sggw.edu.pl>

Electronic version of the Scientific Review Engineering and Environmental Sciences is primary version

All papers are indexed in the data bases as follows: AGRO(Poznań), BazTech, Biblioteka Nauki, **CrossRef**, **DOAJ**, **Google Scholar**, **Index Copernicus**, INFONA, POL-Index, **SCOPUS**, SIGŻ(CBR)

Scientific Review

Engineering and Environmental Sciences

Przegląd Naukowy
Inżynieria i Kształtowanie Środowiska

Vol. 32 (4)

2023

Issue 102

Contents

MEZHOUD S., BADACHE H. Evaluation of physical and mechanical properties of cement-treated base incorporating crushed waste tires	305
JIENMANEECHOTCHAI T., FOYTONG P., KHUNKITTI P., SATA V., CHINDAPRASIRT P. Enhancement of tensile performance of concrete by using synthetic polypropylene fibers	320
MERZA A.N., RAHEEM A.M., NASER I.J., IBRAHIM M.O., OMAR N.Q. Implementing GIS and linear regression models to investigate partial building failures	338
FITRI S.N., SURJANDARI N.S., AS'AD S. A systematic review of clay shale research development for slope construction	357
KOCOURKOVA G., VITKOVA E., PELCAK S. Labor costs in a construction company in the Czech Republic – a case study	376
LAKAWA I., SYAMSUDDIN, HUJIYANTO, ILHAM V.A. Noise mapping due to motor vehicle activities in the by-pass ring road area of the city of Kendari	392

Wydawnictwo SGGW, Warsaw 2023



Wydawnictwo SGGW



wydawnictwosggw

Editorial work – Anna Dołomisiewicz, Tomasz Ruchniewicz

ISSN 1732-9353 (suspended) eISSN 2543-7496

Samy MEZHOUD✉

Hacene BADACHE

University Mentouri of Constantine, Department of Civil Engineering, Laboratoire Matériaux et Durabilité des Constructions, Algérie

Evaluation of physical and mechanical properties of cement-treated base incorporating crushed waste tires

Keywords: crushed waste tires, recycling, cement-treated base, physical evaluation, mechanical performance

Introduction

Pavements are a crucial component of transportation infrastructure, enabling the efficient and safe movement of people and goods (Mezhoud, Clastres, Houari & Belachia, 2018). However, the conventional construction and maintenance of pavements typically require significant amounts of virgin materials, leading to the depletion of natural resources (Li, Xiao, Zhang & Amirkhanian, 2019). In recent years, there has been a growing need to find efficient and sustainable ways to recycle and reuse waste materials in pavement construction to reduce the environmental impact of these activities (Plati, 2019). The incorporation of recycled materials in pavement construction is gaining attention as a potential solution. Such sustainable pavement practices can help promote resource conservation and reduce the carbon footprint of the transportation infrastructure (Correia, Winter & Puppala, 2016). Several recycled materials have been explored for their use in pavement construction, including reclaimed asphalt pavement and recycled concrete aggregate, which have shown promising results in terms of both

mechanical performance and environmental benefits (Siddika et al., 2019). In addition, various other recycled materials such as fly ash, bottom ash, recycled asphalt shingles, lignin, waste plastic, crushed brick, recycled glass, glass powder, glass fibers and crumb rubber have also been examined as replacements for conventional pavement materials (Mezhoud, Houari & Boubaker, 2017; Orouji, Zahrai & Najaf, 2021; Medaoud, Mokrani, Mezhoud & Ziane, 2022; Orouji & Najaf, 2023). While much of the research on recycled materials in pavement construction has focused on asphalt layers, the base and subbase layers have greater potential to incorporate sustainable materials due to their greater thickness (Mohanty, Mohapatra & Nayak, 2022). The use of waste tires in pavement construction has received significant attention in recent years due to its potential to mitigate environmental pollution and promote sustainability. The utilization of waste tires in bituminous layers of pavement has been extensively investigated. Zhang, Li, Ding and Li (2019) studied the use of crumb rubber in asphalt pavements and found that it enhanced the rutting resistance and reduced cracking. Similarly, Lu, Qing, Xin, Alamri and Alharthai (2021) investigated the use of crumb rubber in open-graded friction course (OGFC) pavements and reported improved skid resistance and durability. In addition to bituminous layers, waste tires have also been explored as an additive in base layers. Pham, Zhuge, Turatsinze, Toumi and Siddique (2019) investigated the use of waste tire rubber as an additive in cement-stabilized aggregate and found that it improved the mechanical properties and reduced water absorption. Moreover, studies have shown that using waste tire-derived aggregate in the base layer can reduce the overall cost of pavement construction while improving its durability (Saberian, Perera, Zhou, Roychand & Ren, 2021). Despite the promising results reported in the literature, there are still some challenges and limitations associated with the use of waste tires and plastic in pavement construction. One of the major concerns is the lack of standardization in the manufacturing and characterization of waste tire materials. Another challenge is the limited knowledge of the long-term performance and environmental impact of these materials. Therefore, further research is needed to address these challenges and optimize the use of waste tires and plastic in pavement construction. For this reason, this study aims to investigate the potential of incorporating waste tire aggregates in cement-treated base layers for pavement construction. The purpose is to comprehensively evaluate the physical and mechanical properties of CTB mixtures containing crushed waste tires, with a focus on their deformation capability, compressive strength, tensile strength, modulus of elasticity, and shrinkage behavior. Through this investigation we aim to provide valuable insights into the feasibility and benefits of utilizing waste tire aggregates in cement-treated base layers, thereby supporting the advancement of environmentally conscious and economically viable pavement construction practices.

Methodology

To achieve the objectives, the methodology was structured into the following steps: (1) Material selection and characterization: The initial step involved selecting natural aggregates, including crushed sand and gravel, along with recycled rubber derived from non-reusable tires. Subsequently, a thorough characterization of these materials was conducted to assess their mechanical strength, density, and elasticity, and chemical composition. (2) Mix design and preparation: This phase encompassed the meticulous preparation of cement-treated base (CTB) mixtures under controlled conditions. (3) Compaction and Proctor tests: Proctor compaction tests should be executed; the objective is to ascertain the optimal water content and maximum dry density of the CTB mixtures. (4) Mechanical testing: A series of mechanical tests were conducted to evaluate the performance of the CTB mixtures. Compressive strength tests were performed on cubic specimens ($10 \times 10 \times 10 \text{ cm}^3$) at varying ages (7 and 28 days). Indirect tensile strength tests were carried out on prismatic specimens ($7 \times 7 \times 28 \text{ cm}^3$) at specified time intervals. Furthermore, the modulus of elasticity was evaluated using cylindrical specimens ($10 \times 20 \text{ cm}^3$) after 28 days. (5) Shrinkage analysis: shrinkage behavior was assessed through measurements on prismatic specimens ($7 \times 7 \times 28 \text{ cm}^3$) utilizing a refractometer and digital comparator. Concurrently, the strain was monitored, and correlations were established. (6) Data analysis and interpretation: In the final step, a thorough analysis of test results was undertaken to elucidate the impact of rubber aggregates on mechanical properties and deformations of the CTB mixtures.

Experimental Procedure

Materials

CPJ-CEMII-42.5A cement was used as the binder in the study. This binder is composed of finely ground clinker and additives, with the main addition of pozzolana. The cement has a density of $3,030 \text{ kg}\cdot\text{m}^{-3}$ and an average 28-day compressive strength of 45.1 MPa. Table 1 shows the chemical composition of the cement used.






TABLE 1. Chemical compositions of cement

Chemical compositions [%]		Elements [%]	
C3S	55–65	clinker	≥ 74
C2S	10–25	gypse	4–6
C3A	8–12	calcaire	0
C4AF	9–13	pozzolana	≤ 20

Source: own work.

Two types of aggregates were used in this study: natural aggregates and recycled aggregates. The natural aggregates were sourced from the Mila region in the North of Algeria and consisted of crushed sand (0/3) and crushed gravels (3/8, 8/15, and 15/20 mm) with a measured density of about $2,700 \text{ kg}\cdot\text{m}^{-3}$. The rock is of limestone origin, and the characteristics complies with the normative specifications for use as a road subbase material. In this study, one type of recycled aggregate was used, recycled rubber from non-reusable tires (Table 2), which contained textile fibers. These aggregates come in three forms (0/2 sand, 2/4 gravel, and powder with size less than $500 \mu\text{m}$). The rubber granulates have a density of 1.12. They were used in their raw state and were supplied by local recycling factory.

TABLE 2. Details of granular fractions of natural and recycled aggregates

Type	Origin/Size		
	natural 0/3 sand		natural 3/20 coarse
Natural aggregates			
	powder 0/2 sand		2/4 rubber gravel
Recycled crushed rubber			

Source: own work.

TABLE 3. Physical characteristics of natural aggregates – type according to NF EN 13242+A1 (Association française de Normalization [AFNOR], 2008)

Parameter	Description/Value
Natural aggregates	
Mechanical strength of aggregates	D
Manufacturing characteristics	III
Manufacturing characteristics	B
Angularity of aggregates and sands	$I_c > 30$
Rubber aggregates	
Tensile strength [MPa]	11.8
Breaking strength [$\text{kg}\cdot\text{mm}^{-2}$]	3.1
Elasticity [%]	42
Density [$\text{kg}\cdot\text{dm}^{-3}$]	3 043
UV radiation resistance	excellent
Water permeability	0

Source: own work.

CTB samples and testing procedure

Samples of the cement-treated base (CTB) were studied and formulated according to the NF EN 14227-1 standard (AFNOR, 2005). The grain size of the reconstituted mixture must comply with the specification range. To form the median curve, each fraction must have a well-determined weight. Once the control mixture was reconstituted, a granulometric analysis was carried out to confirm the calculation and then to verify that the curve of the analysis fits into the specification range of the NF EN 13285 standard (AFNOR, 2018; Fig. 1).

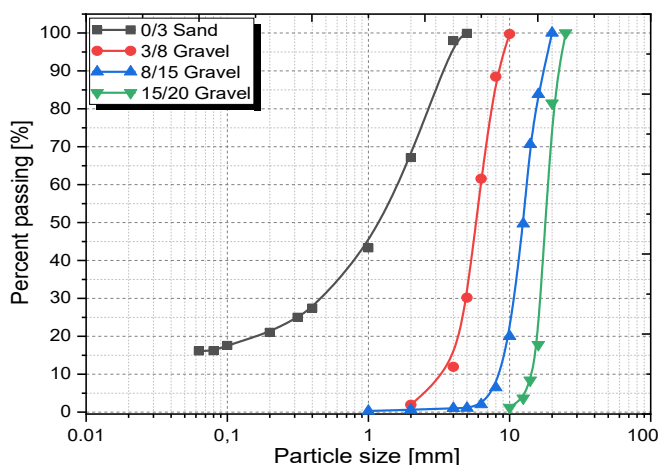


FIGURE 1. Size distribution of natural aggregates according to NF EN 14227 standard (AFNOR, 2005) Source: own work.

For the experimental plan, three gravels were reconstituted from tire waste (Table 4). The first artificial gravel is reconstituted with 100% tire waste, meaning that three artificial fractions (0/2 and 2/4) are introduced into the calculation of the control normative mixture mass. The replacement concerns the 0/2 and 2/4 fractions of natural aggregates, and the other fractions remain unchanged. In the other reconstituted gravels, only the concerned fraction is replaced: 0/2 only and 2/4 only. However, the mass inclusion percentage is 25% and then 50% of the concerned mass. Because suitability tests showed that 100% inclusion gives very low results, the specimens break during demolding.

Furthermore, to valorize the powder of tire waste, other gravels were reconstituted, but this time this artificial ingredient was incorporated as an addition at 10%, 15%, and 20% compared to the dry weight of the normative mixture of Table 4.

TABLE 4. Mixes design

Abbreviation	Natural aggregate content (0/20) [%]				Rubber aggregates content [%]		Rubber powder content [%]
	0/2	2/4	4/15	15/20	0/2	2/4	×
CTB-CTRL	×	×	×	×	×	×	×
CTB-RUS-100	0	×	×	×	100	×	×
CTB-RUS-50	50	×	×	×	50	×	×
CTB-RUS-25	75	×	×	×	25	×	×
CTB-RUG-50	×	50	×	×	×	50	×
CTB-RUG-25	×	75	×	×	×	25	×
CTB-RUP-10	×	×	×	×	×	×	10
CTB-RUP-15	×	×	×	×	×	×	15
CTB-RUP-20	×	×	×	×	×	×	20

Source: own work.

The CTB mixtures were manufactured in a laboratory environment at 20°C and 50% relative humidity using a mixer of 150 l capacity. The mixed materials were placed in molds fixed on the vibrating table, vibrated for 1 min after each layer. After 24 h, the specimens were removed and kept in water at 20°C until the testing age. Tests were performed on the CTB mixes in both fresh and hardened states. Fresh concrete tests included modified Proctor compaction tests. The compaction was carried out with a 4.5 kg hammer dropped from a height of 450 mm into a mold with a diameter of 102 mm and a height of 127 mm. Hardened CTB experiments included compressive strength, tensile strength, and modulus of elasticity. Compressive strength tests were conducted on cubic specimens of 10 × 10 × 10 cm³ at the age of 7 and 28 days according to EN 196-1 standard (European Committee for Standardization [CEN], 2016). Indirect tensile strength tests were performed on cylindrical specimens of 10–20 cm at the age of 7 and 28 days according to EN 196-1 standard. The modulus of elasticity was tested at the age of 28 days.

Results and discussion

Compaction test results

The Proctor compaction test was carried out according to the NF EN 13286-2 standard (AFNOR 2010) to determine the optimal water content and maximum dry density. The results are reported in Figure 2. The Proctor test results show very close

results between mixtures containing rubber and CTB-CTRL. The small observed variability of the maximum dry densities of the different mixtures is directly linked to the percentage of insertion.

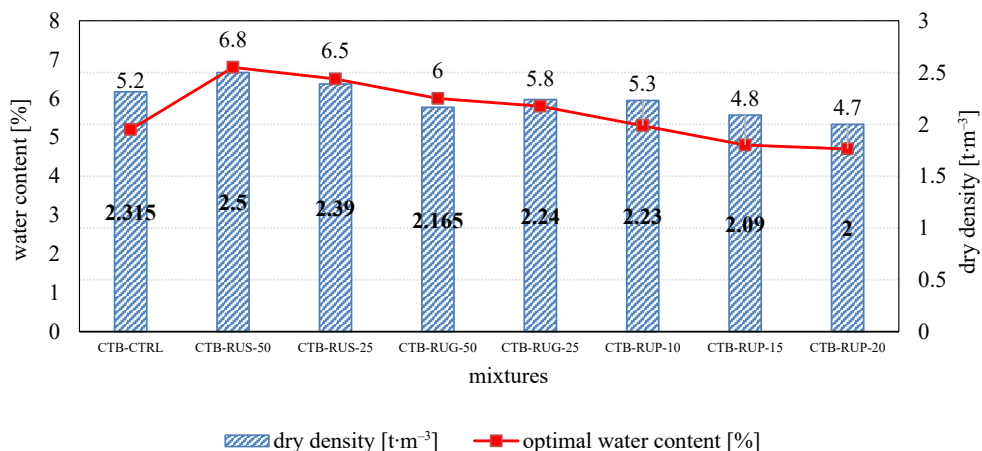


FIGURE 2. Compaction test results

Source: own work.

This observation underscores the inherent advantage of rubber-based aggregates, which have been reported to manifest lower water absorption rates compared to conventional natural aggregates (Prasad, Ravichandran, Annadurai & Rajkumar, 2014).

Compressive test results

Figure 3 shows the variations in compressive strength obtained at 7 and 28 days with respect to the percentage of rubber. For all mixes, they follow the same trend regarding the increase of the percentage of cement. Gradual decrease in compressive strength was noticed as the percentage of rubber increased. The reduction in compressive strength of the mix with 100% of rubber or the case of inclusion of rubber as sand 0/2 were more than the case of inclusion of rubber as gravel 2/4. The results are 50% than the value of the control mix. However, the case of inclusion as gravel or addition of 10% of rubber powder shows appreciable results compared to the control mix. At 7 days, the maximum compressive strength (7 MPa) was obtained for the control mix with 0% rubber and the value 6.18 MPa for the mix with 25% rubber as gravel. Same trend was observed for

the compressive strength at 28 days, a strength above 11 MPa was obtained in the case of mixes containing 25% of rubber and appreciable strength for mixes containing rubber powder at 10%.

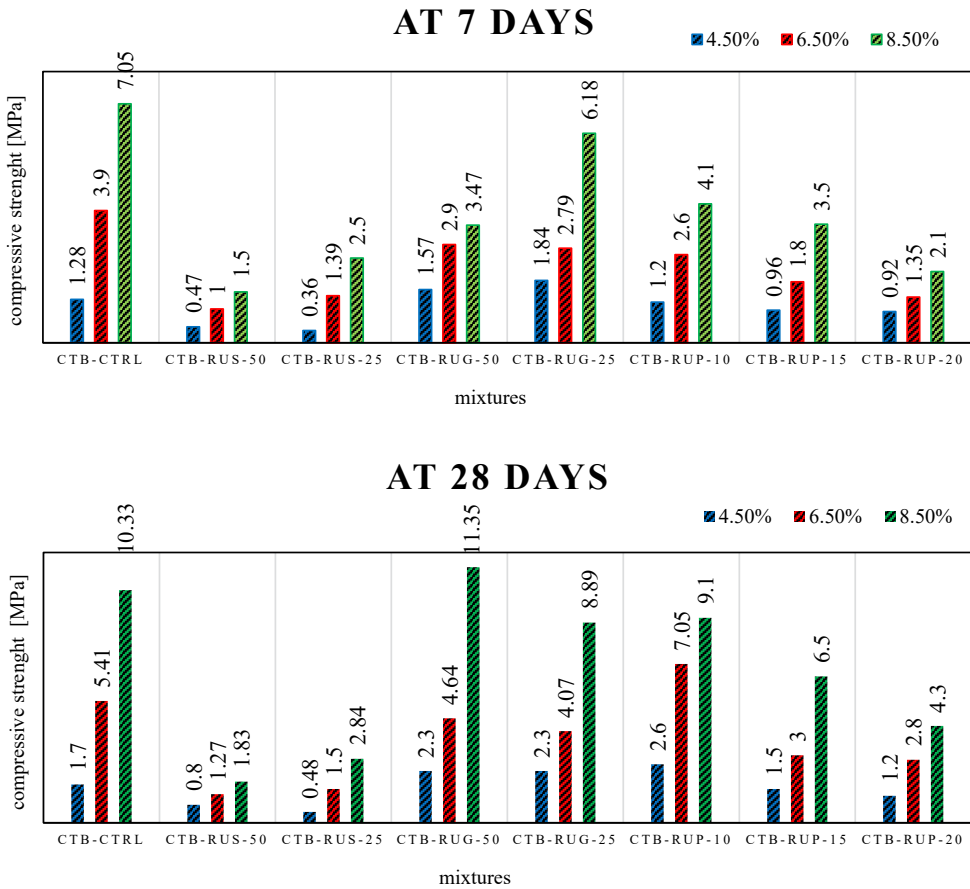


FIGURE 3. Compressive strength at 7 and 28 days for several rate of cement

Source: own work.

The loss in mechanical properties of rubberized concrete was supported by the results obtained by various researchers (Sofi, 2018). The reason for the decrease in compressive and flexural strength of the rubberized concrete is that the aggregate would be surrounded by the cement paste containing rubber particles. This cement paste would be much softer than that without rubber (Ganjan, Khorami & Maghsoudi, 2009).

Indirect tensile test results

Figure 4 presents the test and results of the indirect tensile strength at the laboratory. It can be observed that the mixture including 100% rubber did not yield any results as the specimens break even under minimal stress. The added cement content (8.5%) was unable to achieve the desired bond. It was observed for all mixes that the addition of cement increases the tensile strength. In addition, the results show

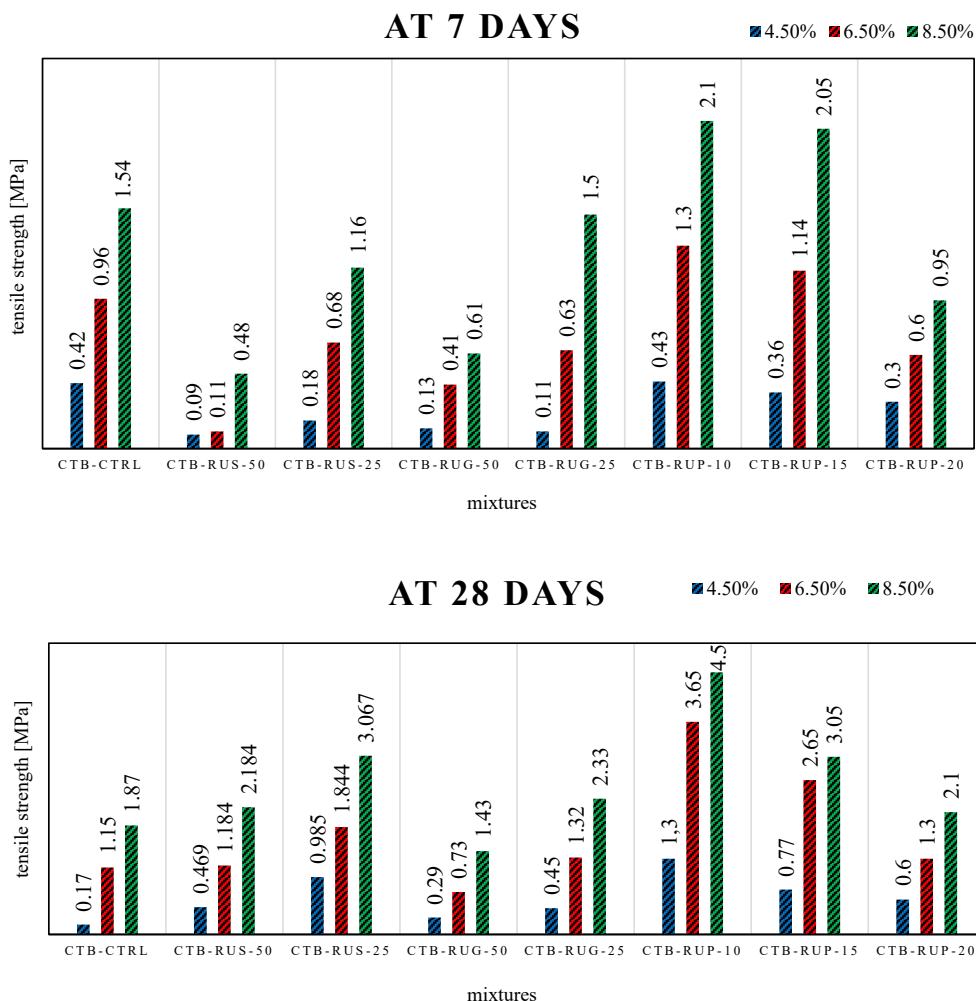


FIGURE 4. Indirect tensile strength at 7 and 28 days for several cement rate

Source: own work.

that the tensile strengths decrease with the increase of the rubber content, however, the results are acceptable compared to those of the control mixture in case of adding the rubber as gravel. The decrease was 18% in case of adding gravel with 25% and cement rate of 8.50%. The results even surpassed the control mix when using rubber powder additions between 10% and 15%. These results are in conformity with Alam, Mahmood and Khattak (2015).

It was initially hypothesized that the presence of tire rubber, acting as a soft material, would enhance the tensile strength of the concrete and serve as a barrier against crack growth. For this reason, these results confirm this hypothesis and demonstrate that the incorporation of artificial aggregates, whether through substitution or addition, improves the tensile strengths. Thus, it provides further support for the use of these materials in road construction. In summary, although the inclusion of rubber in the concrete was expected to enhance tensile strength, the results demonstrated a reduction in tensile strength. This outcome can be attributed to the weak bonding at the interface between rubber and cement, leading to a micro-crack zone and surface segregation between these two materials.

Modulus of elasticity

Figure 5 presents the test and results of elastic modulus at laboratory. The result concerns the mixtures when the binder percentage is 6.5%.

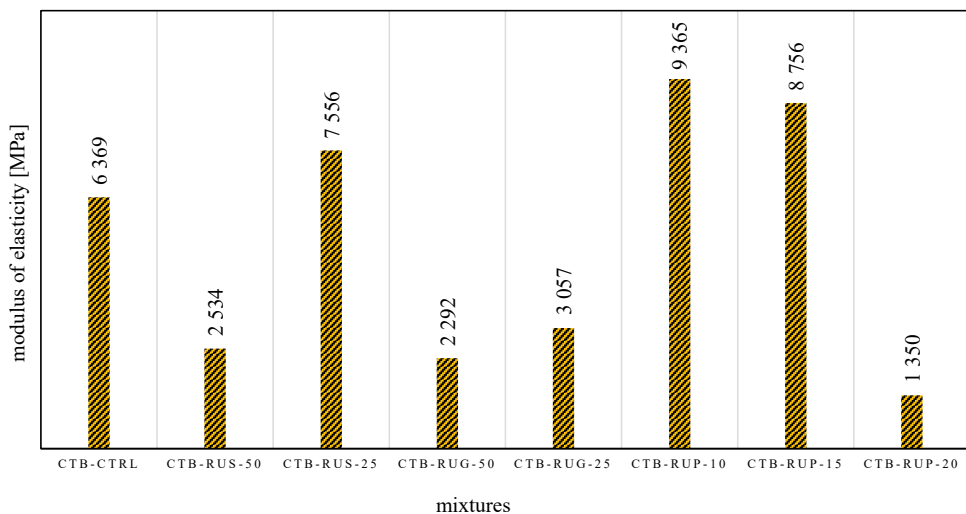


FIGURE 5. Modulus of elasticity at 28 days for cement rate of 6.5%

Source: own work.

It can be observed that increasing the amount of rubber tires in CTB leads to a decrease in the modulus of elasticity. However, in the case of a mixture containing 25% tire rubber sand, a performance superior to that of the control CTB by approximately 20% is exhibited. This observation is evident when tire rubber is added as powder at levels of 10% to 15%, where the results surpass the control CTB by about 47%. This trend is reported by Mohajerani et al. (2020). In addition, when tire rubber is introduced as coarse aggregates, the modulus of elasticity yields lower results. This can be attributed to the fact that the characteristics of coarse aggregates significantly impact the modulus of elasticity. Since concrete can be regarded as a composite material comprising various phases, including coarse or fine aggregates and cement, in which the modulus of elasticity and volumetric ratio in concrete are influenced by the nature of the aggregates. Therefore, if the aggregates have a higher modulus of elasticity than the cement paste, increasing the elastic modulus of aggregates in the concrete mixture will consequently elevate the overall concrete's modulus of elasticity. In simpler terms, the resulting concrete's modulus of elasticity increases when aggregates with higher elastic moduli are employed, particularly when the aggregate volume in the mixture is augmented.

Shrinkage measurement

Shrinkage property, one of durability parameters of CTB, significantly affects their application, especially in mass road structure construction. So far, plenty of investigations have been conducted particularly on the free shrinkage properties of CTB, as a key indicator of the shrinkage phenomena. The results are depicted in Figure 6. The outcomes indicated that the CTB mixtures underwent notable volume fluctuations during the curing of the binder due to water evaporation from capillaries and pores. Across all specimens, the following observations were noted: shrinkage remained below 2%; the control mixture exhibited minimal shrinkage, while mixtures incorporating rubber waste displayed higher shrinkage values. This can be attributed to the additional water content required for achieving optimum compaction during the compaction test and the water absorption capacity of rubber aggregates when compared to natural ones.

However, mixtures incorporating rubber as powder with the percentage of 10% or as sand demonstrated acceptable shrinkage in comparison to the control mixtures. CTB containing rubber gravel exhibit a shrinkage higher about 100% than mixtures containing rubber sand. This observation can be explained by the presence of fine rubber particles in the rubberized concrete, which helped

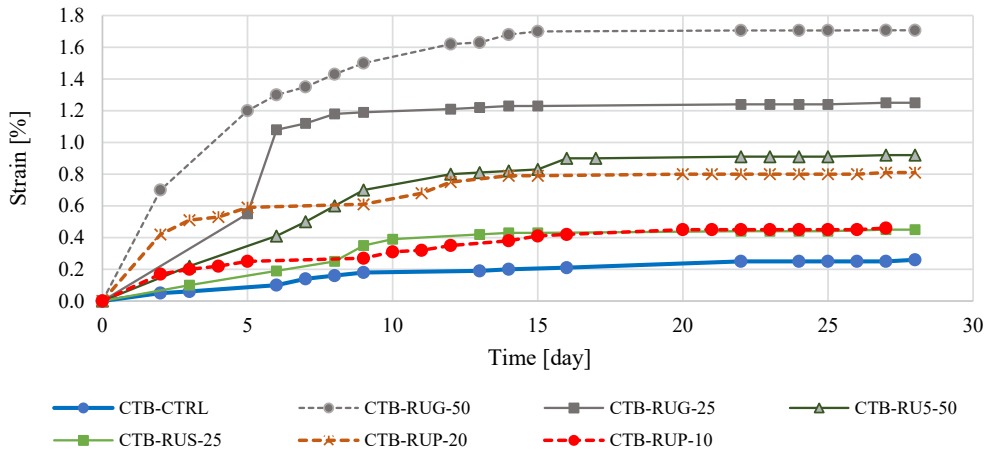


FIGURE 6. Shrinkage measurement results

Source: own work.

maintain the cohesion of constituent particles, preventing crack formation and material separation. Globally, for all specimens, starting from the 15th day onwards, shrinkage became stable.

Conclusions

The following conclusions from this experiment:

1. The compaction test results showed that the mixtures made from waste tires had similar dry densities and water contents to those of the control aggregates, supporting their use in road construction.
2. The compressive strength decreased gradually as the percentage of rubber increased. The substitution of 25% of rubber gravel or the addition of 10% of rubber powder gives acceptable compressive strength. In the tensile strength test, the mixture with 100% rubber did not yield any results, while significant improvement was observed in the tensile strengths of mixtures containing rubber, surpassing even those of the control mixture, especially the case of addition of 10% rubber powder. The addition of cement further increased the tensile strength of all mixtures. The modulus of elasticity decreased when rubber particles were used as replacements for aggregates in hydraulic binder-treated mixtures, while it surpassed the control mix in the case of the addition of 10% to 15% of rubber powder.

3. Shrinkage measurements indicated that the mixtures incorporating rubber waste exhibited higher shrinkage values compared to the control mixture. Incorporating rubber as 10% addition of rubber powder exhibits acceptable shrinkage compared to natural aggregates.

Overall, the results indicate that the addition of 10% of rubber powder exhibits the best performance compared to the natural aggregates.

References

- Association française de Normalisation [AFNOR] (2005). *Mélanges traités aux liants hydrauliques. Partie 1: Mélanges granulaires traités au ciment [Hydraulically bound mixtures – Specifications. Part 1: cement bound granular mixtures]* (EN 14227-1).
- Association française de Normalisation [AFNOR] (2008). *Aggregates for unbound and hydraulically bound materials for use in civil engineering work and road construction* (NF EN 13242+A1).
- Association française de Normalisation [AFNOR] (2018). *Unbound mixtures – specifications* (NF EN 13285).
- Alam, I., Mahmood, U. A. & Khattak, N. (2015). Use of rubber as aggregate in concrete: a review. *International Journal of Advanced Structures and Geotechnical Engineering*, 4 (2), 92–96.
- Correia, A. G., Winter, M. G. & Puppala, A. J. (2016). A review of sustainable approaches in transport infrastructure geotechnics. *Transportation Geotechnics*, 7, 21–28.
- European Committee for Standardization [CEN] (2010). *Unbound and hydraulically bound mixtures. Part 2: Test methods for laboratory reference density and water content – Proctor compaction* (EN-B-13286-2).
- European Committee for Standardization [CEN] (2016). *Methods of testing cement. Part 1: Determination of strength* (EN-T-196-1).
- Ganjian, E., Khorami, M. & Maghsoudi, A. A. (2009). Scrap-tyre-rubber replacement for aggregate and filler in concrete. *Construction and Building Materials*, 23 (5), 1828–1836.
- Li, J., Xiao, F., Zhang, L. & Amirkhanian, S. N. (2019). Life cycle assessment and life cycle cost analysis of recycled solid waste materials in highway pavement: a review. *Journal of Cleaner Production*, 233, 1182–1206.
- Lu, Q., Xin, C., Alamri, M. & Alharthai, M. (2021). Development of porous asphalt mixture with bio-based epoxy asphalt. *Journal of Cleaner Production*, 317, 128404.
- Medaoud, S., Mokrani, L., Mezhoud, S. & Ziane, S. (2022). Characterization of stabilised sewage sludge for reuse in road pavement. *Civil and Environmental Engineering Reports*, 32 (1), 201–217.
- Mezhoud, S., Clastres, P., Houari, H. & Belachia, M. (2018). Field investigations on injection method for sealing longitudinal reflective cracks. *Journal of Performance of Constructed Facilities*, 32 (4), 04018041.

- Mezhoud, S., Houari, H. & Boubaker, F. (2017). Valorisation des fraisât routiers et produits de démolition pour la fabrication de mélanges granulaires traités aux liants hydrauliques [Valorisation of road millings and demolition products for the manufacture of granular mixtures treated with hydraulic binders]. *Algerian Journal of Environmental Science and Technology*, 3 (3), 539–543.
- Mohajerani, A., Burnett, L., Smith, J. V., Markovski, S., Rodwell, G., Rahman, M. T., Kurmus, H., Mirzababaei, M., Arulrajah, A., Horpibulsuk, S. & Maghool, F. (2020). Recycling waste rubber tyres in construction materials and associated environmental considerations: a review. *Resources, Conservation and Recycling*, 155, 104679.
- Mohanty, M., Mohapatra, S. S. & Nayak, S. (2022). Efficacy of C&D waste in base/subbase layers of pavement – current trends and future perspectives: a systematic review. *Construction and Building Materials*, 340, 127726.
- Orouji, M. & Najaf, E. (2023). Effect of GFRP rebars and polypropylene fibers on flexural strength in high-performance concrete beams with glass powder and microsilica. *Case Studies in Construction Materials*, 18, e01769.
- Orouji, M., Zahrai, S. M. & Najaf, E. (2021). Effect of glass powder & polypropylene fibers on compressive and flexural strengths, toughness and ductility of concrete: an environmental approach. *Structures*, 33, 100546.
- Pham, P. N., Zhuge, Y., Turatsinze, A., Toumi, A. & Siddique, R. (2019). Application of rubberized cement-based composites in pavements: suitability and considerations. *Construction and Building Materials*, 223, 1182–1195.
- Plati, C. (2019). Sustainability factors in pavement materials, design, and preservation strategies: a literature review. *Construction and Building Materials*, 211, 539–555.
- Prasad, A. S., Ravichandran, P., Annadurai, R. & Rajkumar, P. (2014). Study on effect of crumb rubber on behavior of soil. *International Journal of Geomatics and Geosciences*, 4, 579–584.
- Saberian, M., Li, J., Perera, S. T. A. M., Zhou, A., Roychand, R. & Ren, G. (2021). Large-scale direct shear testing of waste crushed rock reinforced with waste rubber as pavement base/subbase materials. *Transportation Geotechnics*, 28, 100546.
- Siddika, A., Mamun, M. A. A., Alyousef, R., Amran, Y. H. M., Aslani, F. & Alabduljabbar, H. (2019). Properties and utilizations of waste tire rubber in concrete: a review. *Construction and Building Materials*, 224, 711–731.
- Sofi, A. (2018). Effect of waste tyre rubber on mechanical and durability properties of concrete – a review. *Ain Shams Engineering Journal*, 9 (4), 2691–2700.
- Zhang, J., Li, C., Ding, L. & Li, J. (2021). Performance evaluation of cement stabilized recycled mixture with recycled concrete aggregate and crushed brick. *Construction and Building Materials*, 296, 123596.

Summary

Evaluation of physical and mechanical properties of cement-treated base incorporating crushed waste tires. Pavements play a pivotal role in facilitating safe and efficient transportation. However, conventional pavement construction consumes substantial virgin resources, necessitating a shift towards sustainable alternatives. This study explores the integration of crushed waste tires as partial replacements for sand and gravel in cement-treated base (CTB) layers, aiming to enhance pavement sustainability. The CTB mixtures were meticulously formulated and tested for their physical and mechanical properties. Results revealed that while the presence of waste tire aggregates affected the fresh-state rheology, the cured-state performance remained satisfactory, often exceeding normative requirements. Notably, the addition of 10% rubber powder enhanced the mechanical performance of the CTB mixtures and overall exhibited acceptable shrinkage values. The findings offer insights into designing resilient and sustainable pavement systems by using crushed waste tires, aligning with modern infrastructure demands.

Thunyawee JIENMANEECHOTCHAI¹

Piyawat FOYTONG¹✉

Pirat KHUNKITTI²

Vanchai SATA¹

Prinya CHINDAPRASIRT¹

¹Khon Kaen University, Faculty of Engineering, Department of Civil Engineering, Sustainable Infrastructure Research and Development Center, Thailand

²Khon Kaen University, Faculty of Engineering, Department of Electrical Engineering, Thailand

Enhancement of tensile performance of concrete by using synthetic polypropylene fibers

Keywords: polypropylene fiber, modulus of rupture, toughness

Introduction

Concrete is a material commonly used for construction, consisting of a mixture of aggregates, water, and cement. This material exhibits suitability for a wide range of structural applications, including but not limited to buildings, bridges, roads, and dams. The utilization of concrete in construction is highly preferred due to its remarkable compressive strength and durability. Concrete exhibits a very low tensile strength, which is a fundamental behavior that makes it vulnerable to cracking when subjected to tensile stresses. This limitation often necessitates using reinforcements to improve the tensile performance of concrete structures and maintain their structural integrity under service loads. Improving the tensile strength of the concrete matrix can effectively mitigate the probability of struc-

tural elements developing cracks. The concept prevents corrosion by insulating reinforcement steel from moisture and the atmosphere. Several techniques have been investigated to improve the tensile strength of concrete. According to the established design standards such as Eurocode 2 (European Union [EU], 2004) and ACI 318-14 (American Concrete Institute [ACI], 2014), the tensile strength of concrete depends on a variety of factors, including the concrete grade, curing conditions, age of concrete, and structural member dimensions. The utilization of fiber reinforcements is an interesting approach for its capability to improve the tensile strength of concrete and enhance its overall toughness and durability (Banthia & Sappakittipakorn, 2007).

The utilization of fiber reinforcements in concrete requires a careful selection of the fiber type, which includes steel, glass, polypropylene, or natural, each offering particular characteristics and limitations, which the specific demands of the concrete framework should guide (Bentur & Mindess, 2007). Incorporating steel fibers into concrete has increased its tensile strength and toughness substantially. However, it should be noted that steel fibers are susceptible to corrosion when exposed to harsh environmental conditions (ACI, 2002b; Nanni, 2003). Glass fibers, on the other hand, improve tensile and flexural strength but require alkali-resistant treatments to stop degradation in the high pH environment of concrete (Lau & Anson, 2006; Provis, Palomo & Shi, 2015). Polypropylene (PP) fibers, although having a lower tensile strength than steel or glass, provide outstanding impact resistance and shrinkage control and show impressive resistance to corrosion and chemical stability (ACI, 2002b; Banthia & Sappakittipakorn, 2007; Bentur & Mindess, 2007). Natural fibers, such as sisal, jute, and coir, contribute a certain degree of tensile strength enhancement and crack resistance to a material. However, they require particular treatments to improve their durability in wet environments (Sudin & Swamy, 2006).

Research investigations examining the influence of fiber content on the characteristics of concrete have produced a range of interesting findings throughout the years. In a study by Choi and Yuan (2005), the researchers investigated the effects of incorporating glass and PP fibers into concrete. Their findings contradicted the anticipated relationship between fiber content and strength, suggesting that an increase in strength corresponds to a higher fiber volume of less than 1% (Choi & Yuan, 2005). Similarly, Hasan, Afroz and Mahmud (2011) conducted an experiment investigating various volume ratios of PP fibers. They observed that the compressive strength of concrete reached its maximum value at a 0.51% volume ratio. Varghese and Fathima (2014) investigated the incorporation of crimped steel fibers, hooked-end steel fibers, and PP fibers into their concrete compositions. A PP fiber volume

ratio of 0.5% was determined to yield the highest levels of compressive and flexural strength. Li, Niu, Wan, Liu and Jin (2017) conducted a subsequent study to examine a broader range of volume ratios between glass and PP fibers. The researchers determined that a 0.9% volume ratio marked the critical point at which both compressive and flexural strength started to decline. Similarly, the study by Lee, Cho, Choi and Kim (2016) revealed a reduction in flexural strength as the volume of fibers surpassed 0.5%. In agreement with prior research, the recent study conducted by Al Enezi, Al-Arbeed, Alzuwayed, Al-Zufairi and Awad (2023) confirmed that a 0.65% fiber volume ratio is associated with the highest compressive strength.

This research focuses on the enhancement of the tensile performance of concrete by incorporating synthetic PP fibers at proportions of 0.5% and 1.0% by volume, compared to conventional non-fiber reinforced concrete. The concrete mix is specified to have a compressive strength of 40 MPa, and Type 3 portland cement – famous for its early strength qualities – is chosen as the composition's binder. The research follows the ASTM C39/C39M standard (American Society for Testing and Materials [ASTM], 2003b) for evaluating the produced concrete compressive strength to guarantee consistency and reliability. The performance of the PP fiber-reinforced concrete is evaluated using standardized testing procedures according to the ASTM C1609C/1609M (ASTM, 2019). This test provides a comprehensive examination of the flexural behavior of PP fiber-reinforced concrete (PPFRC). Key performance indicators, such as the modulus of rupture, residual strengths, and toughness indices, are evaluated in detail. Following a thorough analysis of the impact of fiber content on essential performance parameters, it becomes evident that PP fiber reinforcement enhances the tensile strength and overall performance of the concrete.

Materials and concrete mixed design

The present investigation involved formulating a concrete mixture to attain a compressive strength of 40 MPa. According to the ACI 211.1-91 standard (ACI, 2002), the proportion of superplasticizers was appropriately modified to achieve a slump value greater than 10 cm, thereby ensuring uniformity in the amounts of cement, gravel, and sand. The mix proportions for each variation of fiber content utilized in this study are presented in Table 1, providing a comprehensive overview. This research utilized a PP fiber with a remarkable tensile strength of 550 MPa. The fiber's physical characteristics consisted of a diameter measuring 0.71 mm and a length of 48 mm. Table 2 provides an extensive description of the geometry and material properties of the PP fiber.

TABLE 1. Mix proportion of concrete

Synthetic macrofiber [kg·m ⁻³]	Fiber volume fraction [%]	Cement [kg·m ⁻³]	Coarse aggregate [kg·m ⁻³]	Fine aggregate [kg·m ⁻³]	Water [kg·m ⁻³]	Superplasticizer [l·m ⁻³]
0.0	0.0	415	1029	810	114	4.15
4.5	0.5	415	1029	810	114	4.25
9.0	1.0	415	1029	810	114	4.50

Source: own work.

TABLE 2. Geometric and material properties of polypropylene fiber

Type	Specific gravity [-]	Equivalent diameter [mm]	Length [mm]	Tensile strength [MPa]	Modulus of elasticity [GPa]	Melting point [°C]
Macrofiber	0.92	0.71	48	550	6.9	170

Source: own work.

Furthermore, Figure 1 provides a visual representation of the fiber, enabling a better understanding of its physical appearance.

Type 3 portland cement, also known as rapid hardening portland cement, was used for the experiment. This type of cement is characterized by a significant amount of C₃S, which results in a significant exothermic reaction during the hydration process. It also exhibits a higher degree of fineness than Type 1 portland cement. Consequently, this cement type has gained widespread recognition for its exceptional early strength characteristics.

The process of choosing fine and coarse aggregates was conducted with careful attention to adherence to the ASTM C 33 standard (ASTM, 2003a). The specifications mentioned above were carefully selected to uphold experimental consistency and precision. The natural fineness modulus of the fine aggregate was 2.60, and its specific gravity was 2.65. The coarse aggregate, having a maximum particle size of 20 mm, demonstrated a fineness modulus of 3.4 and a specific gravity of 2.7.

The concrete mixture was improved by utilizing Type F superplasticizer,



FIGURE 1. Configuration of the polypropylene fiber
Source: own work.

which is recognized as a high-range admixture that reduces water and increases slump. The superplasticizer was compatible with the standards outlined in ASTM C494/C494M standard (ASTM, 2013). Incorporating the substance resulted in significant improvements in the concrete mixture slump, while the water and cement proportions remained constant. This led to improved workability and compatibility of the various components of the mixture.

To ensure uniform distribution, the mixing process started with dry sand, gravel, cement, and PP fiber mix. After that, water infused with the superplasticizer was added, and the mixing process was sustained until the targeted slump value was achieved. The ultimate concrete mixture was carefully deposited into steel molds with measurements of $150 \times 150 \times 150$ mm for the compression examination and $150 \times 150 \times 500$ mm for the flexural examination.

Test methods and performance parameters

This research aims to investigate the influence of different fiber content (0.0%, 0.5% and 1.0% by volume) on the compressive and flexural strengths of concrete. The experiments involved the results of compressive strength assessments on $15 \times 15 \times 15$ cm³ cubic specimens, and a comparative analysis was carried out between the effects of fiber inclusion and ordinary concrete at the age of 1 day, 7 days, and 28 days, according to the ASTM C39/C39M standard. Beam specimens with the dimensions of $15 \times 15 \times 50$ cm³ were subjected to flexural strength tests at 28 days following the ASTM C 1609/C1609M standard (ASTM, 2019).

The compression test employed cube-shaped concrete specimens with the dimensions of $15 \times 15 \times 15$ cm³. Using a universal testing machine, the loading rate was controlled with $0.15 \text{ MPa} \cdot \text{s}^{-1}$, according to the guidelines specified in ASTM C39/C39M standard (ASTM, 2003b). This experimental study involved the collection of three distinct sets of specimens. The first group comprised conventional concrete specimens, which functioned as the benchmark for comparative analysis. The other two groups consisted of corresponding concrete specimens containing 0.5% and 1.0% fiber content per unit volume. Each group consisted of three specimens. The concrete specimens were tested at different ages, specifically 1 day, 7 days, and 28 days. Following the achievement of the tests, the highest amount of force applied during the compression process was recorded and subsequently used to calculate the compressive strength via the application of Equation 1.

$$f = \frac{P}{A}, \quad (1)$$

where: f – compressive strength [MPa], P – load [N], A – area [mm²].

The flexural strength of concrete was investigated by conducting tests on specimens with the dimensions of 15 × 15 × 50 cm when a concrete age of 28 days. The specimens were placed on a simple support, with the upper surface of the concrete facing sideways during the testing process, according to its position at the casting specimens. The support points were spaced at a distance of 45 cm from each other. The experiment was conducted following the ASTM C 1609C/1609M standard, utilizing a four-point loading method. The load was applied at a distance of one-third of the beam length from both ends, specifically at a point 15 cm away from the end. This generated a pure bending moment at the center region of the beam. The load application rate was controlled at 0.1 mm·min⁻¹ and experienced until the specimen underwent deformation to a magnitude of 3 mm or L/150. The test specimens' displacement was measured using two linear variable differential transducers (LVDTs) located at the applied force point on both sides of the beam, as depicted in Figure 2.

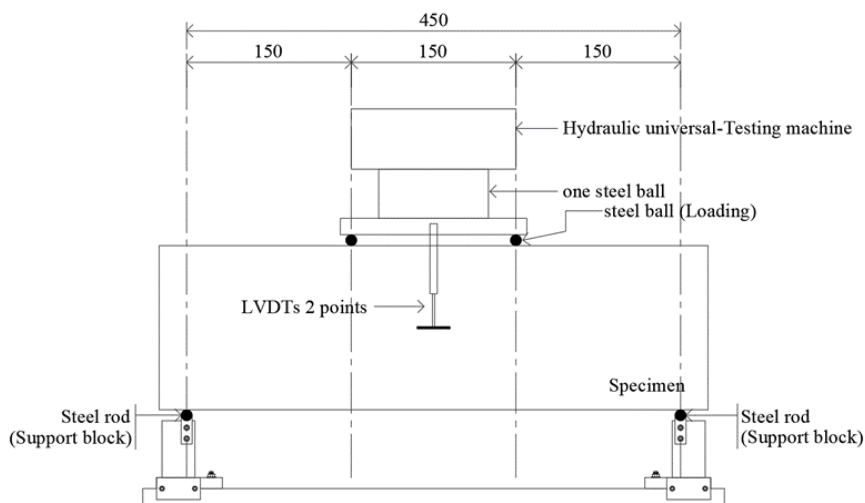


FIGURE 2. Specimen test setup for the flexural test according to ASTM C 1609/1609M standard
Source: own work.

The maximum resistance can be used to determine the initial peak strength or the modulus of rupture using Equation 2.

$$f = \frac{PL}{bd^2}, \quad (2)$$

where: f – strength [MPa], P – load [N], L – span length of beam [mm], b – width of beam [mm], d – depth of beam [mm].

The residual strength at the deformation of L/600 and L/150 also employed Equation 2. The toughness value can also be determined by calculating the area under of load-deformation curve from the starting point to the deformation point equivalent to L/150.

Results and discussion

Compressive strength test

The compressive strength tests carried out according to the ASTM C39/C39M standard provided insights into the strength variations between plain concrete and PPFRC at distinct ages of 1 day, 7 days, and 28 days. The average compressive strength values for each of these concrete mixes are illustrated in Table 3 for a more straightforward comparison. The test results indicate a general trend of increasing compressive strength over the curing period for all mixes. The concrete with PP fiber 0.5% by volume consistently demonstrated the highest average compressive strength at all testing times, reaching 31.07 MPa, 41.51 MPa, and 46.68 MPa at 1 day, 7 days, and 28 days, respectively. This performance indicated an optimal fiber volume of 0.5% for maximizing compressive strength. Even though the concrete mixed with a higher fiber volume of 1.0% consistently exhibited lower average compressive strengths, these values became within the same range as those of plain concrete, demonstrating the fibers' impact on the mix's strength properties. The compressive strengths of concrete with PP fiber 1.0% by volume were reported to be 28.48 MPa, 37.13 MPa, and 42.96 MPa at 1 day, 7 days, and 28 days, respectively. These values were similar to the compressive strengths of plain concrete, which were recorded as 29.05 MPa, 37.50 MPa, and 42.25 MPa at their respective time periods. Therefore, the optimal proportion of PP fiber for achieving maximum compressive strength in the concrete mixture is 0.5% by volume.

The relationship between different volume ratios of compressive strength in fiber-reinforced concrete and non-fiber-reinforced concrete with the various proportions of PP fiber is depicted in Figure 3. This information was derived from previous studies (Choi & Yuan, 2005; Hasan et al., 2011; Varghese & Fathima, 2014; Li et al., 2017; Al Enezi et al., 2023) that utilized type PP macrofibers, which was consistent with the approach employed in this current study. The incorporation of fibers in concrete at volume percentages ranging from 0.3–0.8% increased its compressive strength.

TABLE 3. Compressive strength test result

Fiber volume fractions [%]	Compression strength [MPa]								
	one-day old sample			seven-day old sample			28-day old sample		
0.0	29.36	avg	29.05	36.44	avg	37.50	40.54	avg	42.25
	27.48			37.30			42.67		
	30.30			38.75			43.53		
0.5	31.92	avg	31.07	41.91	avg	41.51	46.43	avg	46.68
	30.13			41.48			45.66		
	31.15			41.14			47.97		
1.0	28.08	avg	28.48	37.13	avg	37.13	42.67	avg	42.96
	28.59			36.70			43.10		
	28.76			37.55			43.10		

Source: own work.

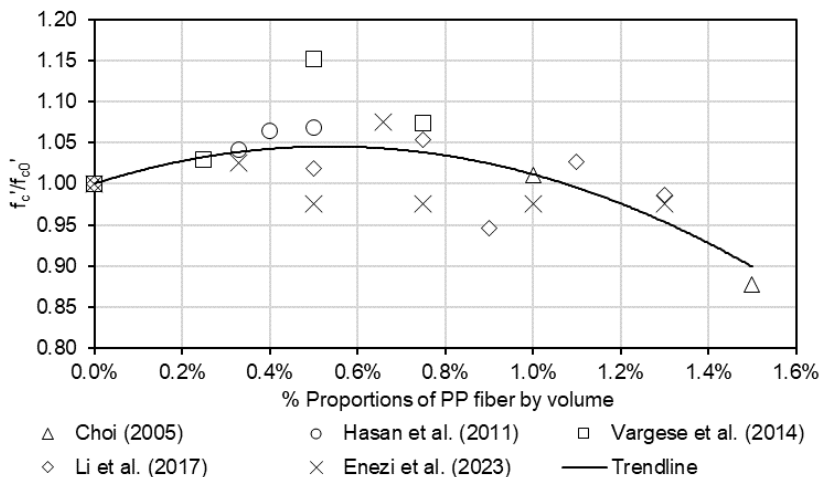


FIGURE 3. The relationship of the ratios of compressive strength in fiber-reinforced concrete and non-fiber-reinforced concrete with the proportion of polypropylene fiber from previous studies

Source: own work based on Choi and Yuan (2005), Hasan et al. (2011), Varghese and Fathima (2014), Li et al. (2017), Al Enezi et al. (2023).

Nevertheless, it can be observed that the compressive strength declines as the fiber-mix ratio increases, which agrees with the results obtained in the present investigation. Based on the observed pattern in the correlation between various volume ratios of compressive strength in fiber-reinforced concrete and non-fiber-reinforced

concrete, a mathematical expression in the form of a second-order polynomial equation, shown as Equation 3, was derived.

$$\frac{f'_c}{f'_{c0}} = -1,577.712x^2 + 16.929x + 1.000. \quad (3)$$

In this experiment, when incorporating fiber mix volume percentages of 0.5% and 1.0% into the equation, the resulting compressive strengths were measured to be 44.16 MPa and 42.74 MPa, respectively. In comparison to the empirical findings, it was observed that the mean compressive strength measurements for concrete specimens incorporating fiber volumes of 0.5% and 1.0% are 46.68 MPa and 42.96 MPa, correspondingly, with the differing percentages of 5.71% and 0.52%, respectively.

Flexural strength test

Concrete beam specimens were tested following the ASTM C 1609C/1609M standard to determine the flexural strength of concrete. Figure 4 illustrates the relationship of force and deformation for plain concrete and concrete with PP fiber 0.5% and 1.0% by volume. The maximum flexural strength of the three different test components had been determined from the force-deformation relationship as similar. The concrete with PP fiber 0.5% by volume has the maximum flexural strength, followed by the concrete with PP fiber 1.0% by volume and the plain concrete sample with the lowest flexural strength. The resulting pattern corresponds to the values of the compressive strength. The modulus of rupture or flexural strength can be determined using the formula for bending stress occurring at the bottom surface of the test specimen cross section at the middle of the beam, as shown in Equation 2. Table 4 presents the calculated flexural strengths of each test specimen. Fiber-reinforced concrete specimens had first peak strengths greater than plain concrete specimens. The concrete with PP fiber 0.5% by volume has the highest value, with an average modulus of rupture of 4.40 MPa. The concrete mixed with PP fiber 1.0% by volume shows a lower modulus of rupture than PP fiber content 0.5% by volume, with an average of 4.27 MPa. The modulus of rupture of plain concrete is the lowest, averaging 3.98 MPa. Notably, the fiber volume in the concrete mix had no immediate effect on the modulus of rupture (Patel, Desai & Desai, 2012; Dopko, Najimi, Shafei & Wang, 2018). According to ACI 318M-11 standard (ACI, 2011), the relationship between the beam samples' compressive strength and bending strength may be used to compute the modulus of rupture of concrete, as shown in Equation 4. The calculated modulus of rupture for plain concrete with a design compressive strength of 40 MPa is 3.92 MPa. Con-

versely, it was found that the experimental findings were 3.98 MPa, demonstrating a strong correlation between the two values.

$$f_r = 0.62\sqrt{f'_c}. \quad (4)$$

Regarding the behavior expressed after reaching the peak flexural strength, it can be observed that the plain concrete's resistance experiences a rapid decline, ultimately resulting in negligible residual strength, as depicted in Figure 4a. The concrete with PP fiber 0.5% by volume exhibits a residual strength of approximately 7,500 N, as shown in Figure 4b, despite experiencing a rapid decline. Moreover, the specimen composed of concrete with PP fiber 1.0% by volume displays the greatest residual strength, approximately 10,000 N, as illustrated in Figure 4c. The strength reduction following the cracks' development depends on the volume of fibers present, whereby a greater fiber volume corresponds to a lower decrease in residual strength. As the deformation state increases, cracks expand while the resistance force remains relatively constant. The softening behavior of strength is observed in PPFRC after the development of cracks. The post-crack behavior of the test samples shows to be independent of the compressive strength.

According to the ASTM C 1609C/1609M standard, the residual strength of concrete, which is calculated after cracking, refers to the material's capacity to endure stress and maintain its structural integrity after damage. The indicators above were compared to the first peak. Two critical values considered were f^D_{600} , which signifies the remaining strength after a deformation of L/600, and f^D_{150} , which represents the strength after a deformation of L/150. The data presented in Table 4 shows that the f^D_{600} values for plain concrete and concrete with PP fiber 0.5% and 1.0% by volume are 0.36 MPa, 1.04 MPa, and 1.61 MPa, respectively. When compared to the first peak strength of each type of concrete, these values represent 9.04%, 23.70%, and 37.73%, respectively. The results indicate an interesting improvement in residual strength with PP fiber, as evidenced by the f^D_{600} values of concrete with PP fiber 0.5% and 1.0% by volume, which are 2.9 and 4.5 times higher than those of plain concrete. The plain concrete exhibited a negligible f^D_{150} value, demonstrating that it cannot sustain residual strength following substantial deformation. In contrast, it had been observed that concrete with PP fiber 0.5% and 1.0% by volume demonstrates f^D_{150} values of 0.74 MPa and 1.16 MPa, respectively. Compared to the first peak strength, these performances accounted for 16.74% and 27.23%, respectively. Therefore, it can be inferred that an increase in the amount of fiber results in a proportional improvement of the residual strength of the concrete. This enhancement in strength is attributed to

the fibers, which bridge the cracks in the concrete, resulting in improved tensile strength and resistance to crack propagation due to the widespread distribution of fibers throughout the cross-section of the concrete.

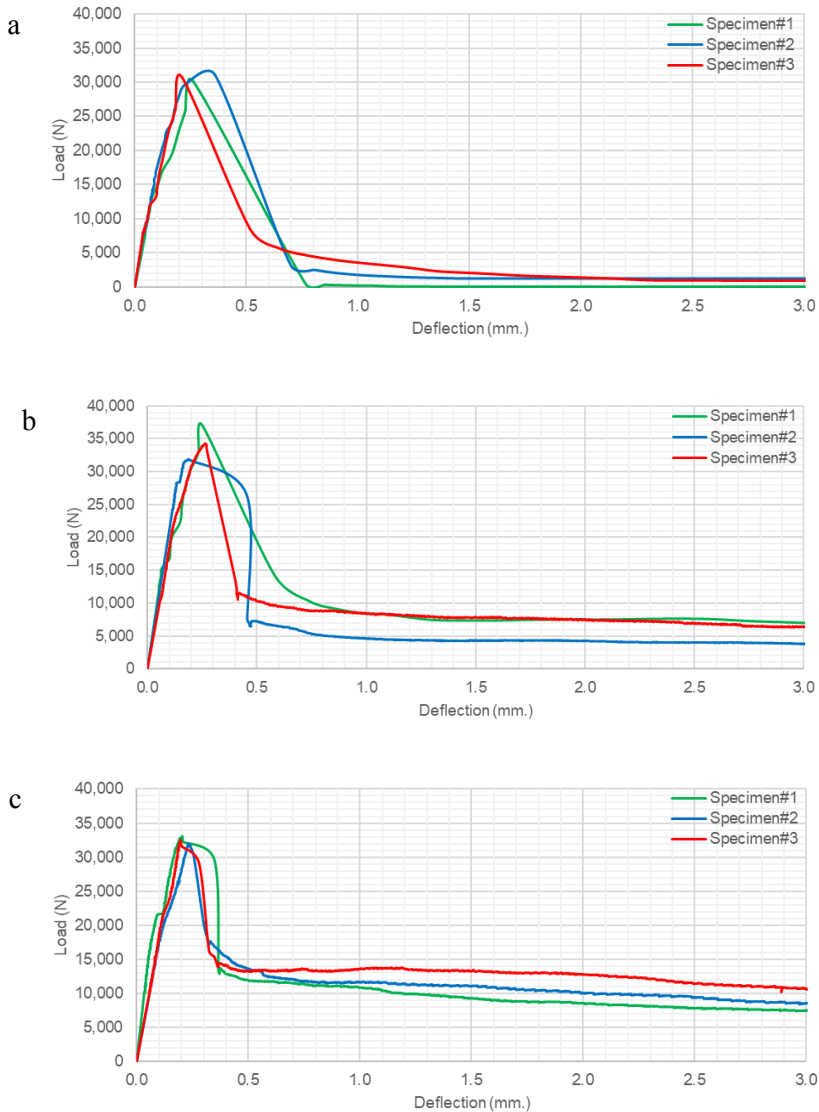


FIGURE 4. The load-deflection curves obtained from the flexural tests conducted on the specimens exhibit variations in fiber content: a – 0.0% by volume; b – 0.5% by volume; c – 1.0% by volume

Source: own work.

Toughness is noteworthy when analyzing the test results according to the ASTM C 1609C/1609M standard. It serves as an essential measure of performance for fiber post-cracking. The toughness principle relates to a material’s capacity to withstand crack propagation or absorb energy when subjected to flexural load. Consistent with the hypothesis proposed in this research, the addition of fibers into concrete has the potential to improve its tensile strength, which leads to a more ductile behavior in the structures. The determination of toughness can be achieved by calculating the integral of the force-deformation curve from the initial point up to the point where the deflection reaches $L/150$. The experimental results indicated that the toughness measurements of plain concrete and concrete with PP fiber, 0.5% and 1.0% by volume, were 13.98 J, 28.19 J, and 36.63 J, respectively. The findings suggest that adding PP fiber in concrete at volume proportions of 0.5% and 1.0% results in a significantly improved toughness, with values approximately twice and 2.6 times higher than those observed in plain concrete. Therefore, it can be inferred that an increase in fiber content leads to an increase in toughness, contributing to a more ductile structure. Consequently, this enhancement allows the concrete to withstand greater tensile forces, underscoring the value of fiber reinforcement in concrete mixtures.

TABLE 4. Flexural strength test results

Fiber volume fraction [%]	Modulus of rupture [MPa]			f_{600}^D [MPa]			f_{150}^D [MPa]			Toughness [J]		
0.0	3.82	avg	3.98	0.05	avg	0.36	0.00	avg	0.00	12.10	avg	13.98
	4.08			0.42			0.00			15.35		
	4.04			0.61			0.00			14.49		
0.5	4.59	avg	4.40	1.28	avg	1.04	0.88	avg	0.74	32.55	avg	28.19
	4.18			0.70			0.50			22.82		
	4.43			1.14			0.83			29.20		
1.0	4.32	avg	4.27	1.49	avg	1.61	0.98	avg	1.16	33.68	avg	36.63
	4.27			1.58			1.14			35.36		
	4.22			1.76			1.37			40.86		

Source: own work.

Figure 5 illustrates the correlation between various volume ratios of the modulus of rupture of fiber-reinforced concrete and the modulus of rupture of non-fiber-reinforced concrete, as evidenced by previous studies (Varghese & Fathima, 2014; Li et al., 2017; Al Enezi et al., 2023). The addition of fibers to concrete in volume percentages ranging from 0.1–0.8% had been found to increase the modulus of rupture value, which agreed well with the obtained results.

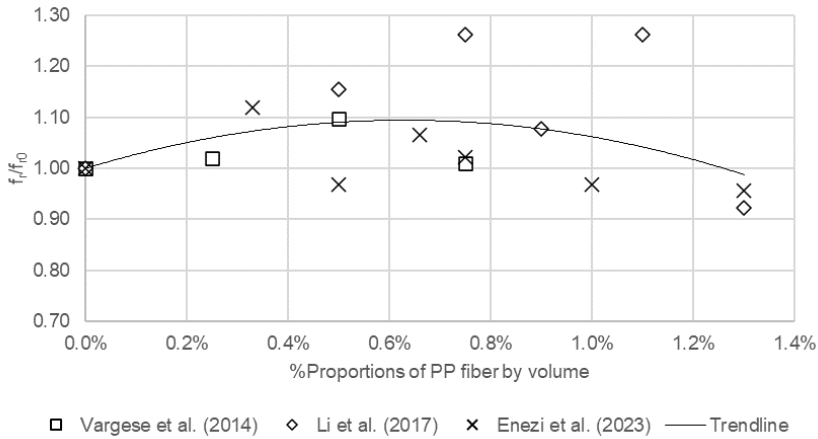


FIGURE 5. The relationship of the ratios of modulus of rupture in fiber-reinforced concrete and non-fiber-reinforced concrete with the proportion of polypropylene fiber from previous studies
Source: own work based on Varghese and Fathima (2014), Li et al. (2017), Al Enezi et al. (2023).

As depicted in Equation 5, the second-order polynomial relationship was derived from the trendline representing the correlation between various volume ratios of modulus of rupture in fiber-reinforced concrete and non-fiber-reinforced concrete.

$$\frac{f_r}{f_{r0}} = -2,372.848x^2 + 29.892x + 1.000. \quad (5)$$

When applying the fiber mix volume percentages of 0.5% and 1.0% obtained from this study to Equation 5, the modulus of rupture was determined to be 4.34 MPa and 4.23 MPa, respectively. The results were consistent with the modulus of rupture values derived from the experimental data. The average MOR of concrete mixed with fiber volumes of 0.5% and 1.0% are 4.40 MPa and 4.27 MPa, respectively. The deviation values for these measurements are 1.41% and 1.06%, respectively.

Distribution of polypropylene fibers

The uniform dispersion of fibers can be observed on the fractured surface of the specimens, as depicted in Figure 6, following their failure. This particular result can be explained by meticulous preparation during the mixing process of the concrete components, in which the fibers were distributed uniformly before adding water. The concrete mixture effectiveness was enhanced by adding superplasticizers, which facilitated suitable workability and effective casting. Examining the fiber distribution at the fracture surface indicates that most fibers remained undamaged, while

only a minor fraction experienced rupture. The primary failure mechanism exhibited by the fibers was ‘pull-out’, which is explained by insufficient bonding between the concrete and fibers.

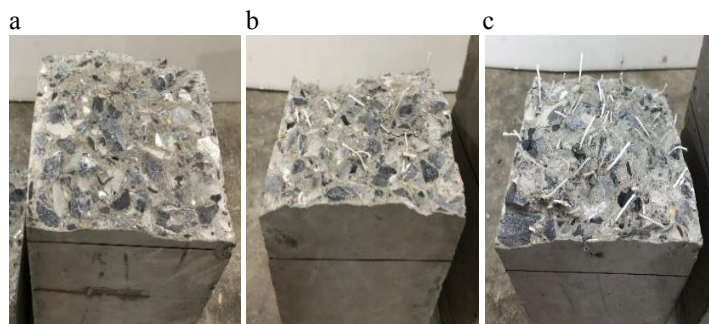


FIGURE 6. Fracture faces of the polypropylene fiber-reinforced concrete beam: a – plain concrete, b – polypropylene fiber 0.5% by volume; c – polypropylene fiber 1.0% by volume

Source: own work.

Consequently, using fibers with a rough texture or increasing the fiber length could improve the interfacial adhesion potency between the fiber and the concrete matrix, thereby eliminating the probability of the pull-out collapse. The utilization of crimped-shaped fibers (Oh, Kim & Choi, 2007) and longer fibers (Singh, Shukla & Brown, 2004) presents the possibility of improving the mechanical properties and durability of fiber-reinforced concrete. The present study highlights the significant influence of fiber dispersion and bond strength on the improvement of post-cracking behavior and overall performance of fiber-reinforced concrete.

Conclusions

The present investigation systematically evaluated the mechanical characteristics of plain concrete and PPFRC. The study included experimental testing utilizing ASTM C39/C39M to evaluate compressive strength and ASTM C 1609C/1609M for assessing flexural performance. The findings of the research can be summarized as follows:

- The concrete with PP fiber 0.5% by volume exhibited consistently high performance, as demonstrated by compressive strength tests conducted following ASTM C39/C39M standard. The mixture based on investigation showed the greatest mean compressive strength across all testing ages, with values of 31.07 MPa, 41.51 MPa, and 46.68 MPa recorded at 1 day, 7 days, and 28 days, respectively.

The mechanical properties indicated by the above values exhibited superior performance compared to plain concrete and concrete with PP fiber 1.0% by volume. Thus, it had been identified that a fiber volume portion of 0.5% represents the most advantageous amount for enhancing the compressive strength of concrete.

- The analysis of the behavior of concrete after cracking demonstrated essential improvements in residual strength and toughness with the addition of PP fibers. The concrete with PP fiber 0.5% and 1.0% by volume resulted in significant enhancements in the f_{600}^D values, which indicate the residual strength of the material after the deformation of L/600. The concrete with PP fiber 0.5% and 1.0% by volume exhibited a f_{600}^D value of 1.04 MPa and 1.61 MPa, respectively. These values represented significant improvements over the 0.36 MPa f_{600}^D value observed in the plain concrete. Furthermore, the addition of PP fiber into concrete at volumes of 0.5% and 1.0% yielded toughness measurements that were 2.0 (28.19 J) and 2.6 times (36.63 J) greater than the value of 13.98 J for plain concrete. The observation above emphasized the critical advantage of adding fiber reinforcement in enhancing the ability of concrete to withstand crack propagation and absorb energy when subjected to flexural load.
- The evaluation of the fractured surfaces of the specimens demonstrated that the realization of these performance improvements depended on the uniform distribution of fibers and the development of adequate bonding with the concrete. The addition of fibers in the concrete matrix resulted in an essential improvement in its overall performance. The predominant failure mode was ‘pull-out’ indicating inadequate bonding between the concrete and fibers. This illustrates the potential of enhancing the mechanical properties of fiber-reinforced concrete by improving the bonding between the fiber and concrete matrix. The approach above could involve the utilization of longer or rough fibers, which denotes a suitable option for future research.

Acknowledgements

The authors gratefully acknowledge the funding supported by Research and Graduate Studies Sustainable Infrastructure Research and Development Center, Department of Civil Engineering, Faculty of Engineering, Khon Kaen University, Khon Kaen 40002, Thailand and the Provincial Electricity Authority (PEA).

References

- Al Enezi, S., Al-Arbeed, A., Alzuwayed, S., Al-Zufairi, R. & Awad, A. (2023). Production, characterization, and application of a polypropylene macrosynthetic fiber for the development of fiber-reinforced concrete. *Available at SSRN 4370921*. <https://dx.doi.org/10.2139/ssrn.4370921>
- American Concrete Institute [ACI] (2002a). *Standard practice for selecting proportions for normal, heavyweight, and mass concrete* (ACI 211.1-91). Farmington Hills: American Concrete Institute.
- American Concrete Institute [ACI] (2002b). *State-of-the-art report on fiber reinforced concrete*. Farmington Hills: American Concrete Institute.
- American Concrete Institute [ACI] (2011). *Building code requirements for structural concrete and commentary* (ACI 318M-11). Farmington Hills: American Concrete Institute.
- American Concrete Institute [ACI] (2014). *Building code requirements for structural concrete* (ACI 318-14). Farmington Hills: American Concrete Institute.
- American Society for Testing and Materials [ASTM] (2003a). *Standard specification for concrete aggregates* (ASTM C33). West Conshohocken: ASTM International.
- American Society for Testing and Materials [ASTM] (2003b). *Standard test method for compressive strength of cylindrical concrete specimens* (ASTM C39/C39M). West Conshohocken: ASTM International.
- American Society for Testing and Materials [ASTM] (2013). *Standard specification for chemical admixtures for concrete* (ASTM C494/C 494M). West Conshohocken: ASTM International.
- American Society for Testing and Materials [ASTM] (2019). *Standard test method for flexural performance of fiber-reinforced concrete (using beam with third-point loading)* (ASTM C 1609/C1609M). West Conshohocken: ASTM International.
- Banthia, N. & Sappakittipakorn, M. (2007). Toughness enhancement in steel fiber reinforced concrete through fiber hybridization. *Cement and Concrete Research*, 37 (9), 1366–1372. <https://doi.org/10.1016/j.cemconres.2007.05.005>
- Bentur, A. & Mindess, S. (2007). *Fibre reinforced cementitious composites*. Boca Racon: CRC Press. <https://doi.org/10.1201/9781482267747-8>
- Choi, Y. & Yuan, R. L. (2005). Experimental relationship between splitting tensile strength and compressive strength of GFRC and PFRC. *Cement and Concrete Research*, 359 (8), 1587–1591. <https://doi.org/10.1016/j.cemconres.2004.09.010>
- Dopko, M., Najimi, M., Shafei, B. & Wang, X. (2018). Flexural performance evaluation of fiber-reinforced concrete incorporating multiple macro-synthetic fibers. *Transportation Research Record*, 2672 (27), 1–12. <https://doi.org/10.1177/0361198118798986>
- European Union [EU] (2004). *Eurocode 2. Design of concrete structures. Part 1-1: General rules and rules for buildings* (EN 1992-1-1). Brussels: The European Union.
- Hasan, M. J., Afroz, M. & Mahmud, H. I. (2011). An experimental investigation on mechanical behavior of macro synthetic fiber reinforced concrete. *International Journal of Civil & Environmental Engineering*, 11 (3), 18–23.

- Lau, A. & Anson, M. (2006). Effect of high temperatures on high performance steel fibre reinforced concrete. *Cement and Concrete Research*, 36 (9), 1698–1707. <https://doi.org/10.1016/j.cemconres.2006.03.024>
- Lee, J., Cho, B., Choi, E. & Kim, Y. (2016). Experimental study of the reinforcement effect of macro-type high strength polypropylene on the flexural capacity of concrete. *Construction and Building Materials*, 126, 967–975. <https://doi.org/10.1016/j.conbuildmat.2016.09.017>
- Li, J., Niu, J., Wan, C., Liu, X. & Jin, Z. (2017). Comparison of flexural property between high performance polypropylene fiber reinforced lightweight aggregate concrete and steel fiber reinforced lightweight aggregate concrete. *Construction and Building Materials*, 157, 729–736. <https://doi.org/10.1016/j.conbuildmat.2017.09.149>
- Nanni, A. (2003). North American design guidelines for concrete reinforcement and strengthening using FRP: Principles, applications and unresolved issues. *Construction and Building Materials*, 17 (6–7), 439–446. [https://doi.org/10.1016/S0950-0618\(03\)00042-4](https://doi.org/10.1016/S0950-0618(03)00042-4)
- Oh, B. H., Kim, J. C. & Choi, Y. C. (2007). Fracture behavior of concrete members reinforced with structural synthetic fibers. *Engineering Fracture Mechanics*, 74 (1–2), 243–257. <https://doi.org/10.1016/j.engfracmech.2006.01.032>
- Patel, P. A., Desai, A. K. & Desai, J. A. (2012). Evaluation of engineering properties for polypropylene fibre reinforced concrete. *International Journal of Advanced Engineering Technology*, 3 (1), 42–45.
- Provis, J. L., Palomo, A. & Shi, C. (2015). Advances in understanding alkali-activated materials. *Cement and Concrete Research*, 78, 110–125. <https://doi.org/10.1016/j.cemconres.2015.04.013>
- Singh, S., Shukla, A. & Brown, R. (2004). Pullout behavior of polypropylene fibers from cementitious matrix. *Cement and Concrete Research*, 34 (10), 1919–1925. <https://doi.org/10.1016/j.cemconres.2004.02.014>
- Sudin, R. & Swamy, N. (2006). Bamboo and wood fibre cement composites for sustainable infrastructure regeneration. *Journal of Materials Science*, 41 (21), 6917–6924. <https://doi.org/10.1007/s10853-006-0224-3>
- Varghese, S., & Fathima, A. (2014). Behavioural study of steel fiber and polypropylene fiber. *International Journal of Research in Engineering & Technology*, 2 (10), 17–24.

Summary

Enhancement of tensile performance of concrete by using synthetic polypropylene fibers. The research attempted to investigate the effect of polypropylene fibers (PP fibers) on the mechanical characteristics of concrete. According to ASTM C39/C39M and ASTM C 1609/C1609M, standard testing methods were used to examine the concrete compressive and flexural strength, post-cracking behavior, and toughness. The mechanical properties were evaluated at different ages of concrete curing, namely 1 day, 7 days, and 28 days, and for different quantities of fiber volume portions, specifically 0.0%, 0.5%, and 1.0%. The results demonstrate that a fiber volume of 0.5% is the most effective in obtaining the highest compressive strength. The recorded values at the related testing ages

were 31.07 MPa, 41.51 MPa, and 46.68 MPa. Additionally, the utilization of 0.5% and 1.0% volume of PP fiber in concrete resulted in improved flexural strength and post-cracking performance. The toughness values for these mixes were 2.0 and 2.6 times higher than those for the plain concrete. Upon analyzing the fracture surface, there was a homogeneous distribution of fibers, which played a significant role in enhancing the overall functionality of the concrete. The research validated that the inclusion of polypropylene fibers substantially enhanced the mechanical characteristics of concrete, emphasizing the potential of fiber reinforcement in concrete-based implementations.

Alaa Nuri MERZA

Aram Mohammed RAHEEM   <https://orcid.org/0000-0002-6889-3939>

Ibrahim Jalal NASER  <https://orcid.org/0000-0001-8986-9711>

Mohammed Omar IBRAHIM

Najat Qader OMAR  <https://orcid.org/0000-0003-2665-7978>

University of Kirkuk, Civil Engineering Department, Kirkuk, Iraq

Implementing GIS and linear regression models to investigate partial building failures

Keywords: GIS, IDW technique, crack identification, linear single, multi-regression models

Introduction

The influence of soil on urban ecology is both direct and indirect (Ouabo, Sangodoyin & Ogundiran, 2020), and creating a digital soil map also has a significant impact on research in terms of time and preventing soil problems, consequently, there is a growing need for information about soil (Zijl, 2019). The data for 56 different soil samples collected from various depths in the city of Kirkuk were combined utilizing the inverse distance weighted (IDW) spatial analysis technique (Raheem & Omar, 2021). Soil behavior and the possible impact of soil issues on structures may be predicted using mathematical models and computer simulations (Addiscott, 1993). Based on prior project observations and data, empirical correlations may be applied to predict soil behavior. These correlations can be used to estimate the soil's

swelling potential and the probable impact on structures (Cantillo, Market & Bird, 2017). Creating models and simulations of how soil would counter or predict some soil characteristics in a particular location requires the use of a geographic information system (GIS) by storing information and data, such as Atterberg limits (liquid limit – *LL*, plasticity index – *PI*), and various soil characteristics denoted by gravel content, sand content, silt content, clay content, gypsum content (*GYP*), total suspended solids (*TSS*), potential of hydrogen (pH), and organic content (*ORG*) components (Raheem, Omar, Naser & Ibrahim, 2022; Raheem, Naser, Ibrahim & Omar, 2023; Salahalden, Shareef & Al Nuaimy, 2023). This information may be utilized to develop predictions regarding soil stability, soil volume change, and other soil qualities. The approach typically involves data collection and mapping, the development of a mathematical model to define soil behavior, and simulation testing to validate the models and provide predictions concerning soil behavior in specific regions (Omer et al., 2018). The accuracy of the findings is determined by the dependability of the models used and the quality of the data used. Machine learning was used to predict continuous dependent soil characteristics from an assortment of independent factors using both single and multi-linear regression models (Matarira, Mutanga & Dube, 2021; Mohsin & Lone, 2021; Pentos, Mbah, Pieczarka, Niedbała & Wojciechowski, 2022).

This study stands out because it employs the IDW method to produce digital maps for several significant soil attributes in a Kirkuk City residential complex. More importantly, no digital maps for apartment buildings in the city of Kirkuk have ever been examined. Planners in Kirkuk, Iraq, will be able to more precisely classify the area's diverse soil sections with the use of these computerized topsoil maps. This will make it possible to put into practice various risk-reduction strategies for structural engineering and make better decisions regarding the potential cracking areas.

The main goal of this study is to utilize a spatial statistical approach determined by the inverse distance weighted (*IDW*) technique to incorporate all available information on the soils of the investigated residential complex in the city of Kirkuk, Iraq. The particular objectives can be represented as geographical data combining the proportions of *LL*, gravel, sand, silt, *GYP*, *TSS*, pH, and *ORG* for the current investigation residential complex in Kirkuk, Iraq. The aim was to investigate the relationship between *PI* and physical soil parameters using a linear single regression model with discrete correlations. The specific correlations between *PI* and the physical, chemical, and compounded physical and chemical soil properties were further examined using linear multi-regression models. The digital maps created using prediction models may be used to visualize the possibility of soil swelling and decrease the anticipated risks for future civil engineering projects.

The study area and problem identification

The site is in the city of Kirkuk, around 750 m from the Kasa Su River and 600 m from the Kirkuk ring motorway. Several apartment buildings are located near the site. The building is about 30,000 m² in size. The project entails the development of one and two-story residential apartments. Figure 1 illustrates the city of Kirkuk, including all governmental buildings, as well as the current investigated study area (Omar & Raheem, 2016). In many buildings in the inspected residential complex, numerous cracks of varied sizes and places have been noticed. Figure 2 illustrates various cracks in size and position for the investigated residential complex.

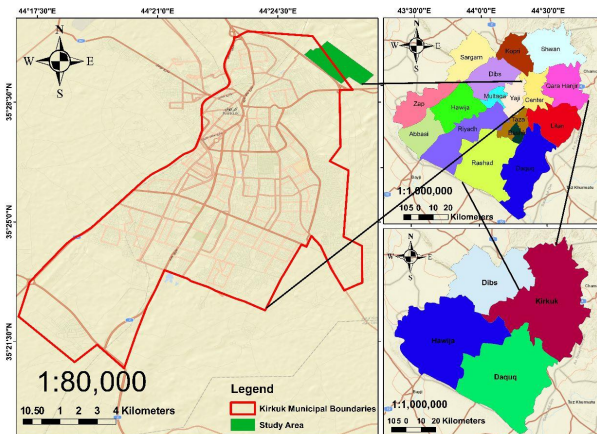


FIGURE 1. Detailed map of Kirkuk City

Source: own work.



FIGURE 2. Various cracks in shape and position in the studied residential complex in Kirkuk City/Iraq

Source: own work.

Methodology

Geographic information system and data collection

Geographic information system applications are used to compile geographic information into databases to save time and money. The data-gathering procedure involves inputting updated data into the GIS application; however, data integration includes adjusting and protecting data integrity. For data acquired arbitrarily, the GIS application enables the evaluation of global auto-correlation (Olmo, Guervos & Rocha, 2019). Seven boreholes in the analyzed area provided a variety of soil data, which is adequate for such an explored area. Physical and chemical soil characteristics such as *PI*, *LL*, gravel, sand, silt, clay, *GYP*, *TSS*, pH, and *ORG* content were obtained. Table 1 provides illustrations of geographical, physical, and chemical soil characteristics for the residential complex in Kirkuk City.

TABLE 1. Geographical and physical soil characteristics of sample examples of the studied residential complex in Kirkuk City/Iraq

FID	BH	North	East	Depth [m]	Gravel content [%]	Sand content [%]	Silt content [%]	Clay content [%]	<i>LL</i>	<i>PI</i>	<i>GYP</i> [%]	<i>TSS</i> [%]	pH	<i>ORG</i> [%]
0	1	3928584.755	448672.088	1.0	10	26	38	26	52	26	1.02	2.81	7.98	0.31
1	2	3928578.675	448641.835	1.0	6	48	24	22	17	2.67	1.95	2.64	7.94	1.42
2	3	3928638.499	448575.699	1.0	54	24	14	8	35	14	3.23	3.53	7.91	2.1
3	4	3928545.745	448585.963	1.0	4	8	49	39	48	26	2.3	2.12	7.92	1.77
4	5	3928580.663	448548.569	1.0	19	25	36	20	41	18	3.02	3.57	7.88	1.05
5	6	3928728.284	448476.17	1.0	40	15	27	18	38	14	2.89	3.9	7.95	1.76
6	7	3928742.614	448462.409	1.0	38	26	17	19	39	15	2.34	4.02	7.88	1.67

BH – borehole, *LL* – liquid limit, *PI* – plasticity index, *GYP* – gypsum content, *TSS* – total suspended solids, pH – potential of hydrogen, *ORG* – organic content.

Source: own work.

Individual data acquired for a specific soil is altered from an Excel file with latitude and longitude to a themed map utilizing Arc Map capabilities. Using the specified coordinates as a starting point, resampling maps were produced using the inverse distance weighted (IDW) interpolation technique. On the studied maps, each borehole position is represented by a small blue point.

Inverse distance weighted (IDW) technique

The IDW technique is simple, comprehensive, and one of the most important approaches to interpolation. A linear sequence of surrounding points is used, which is normalized by an inverse connection of distance between the examined and tested locations (Billah, 2018). Eq. (1) demonstrates how to recognize the IDW approach:

$$Y_o = \sum_{i=1}^N \frac{y_i d_1^{-n}}{d_1^{-n}}, \quad (1)$$

where Y_o is the required quantity of the z factor at the I point; y_i is the known quantity in the I point, d_1 is the Euclidian range between the desired and provided values; N is the weighting factor based on distance; n is the degree of inverse distance weighting.

The retrieved digital maps were utilized to define a surface that is a function of a specified attribute and neighborhood approach. It should be emphasized that the IDW approach conveniently interprets maximum and minimum field values.

Linear single regression model

A linear single regression model was used to estimate the soil PI attribute using field information on the physical and chemical properties of the soil. In Eq. (2), the represented PI soil properties in the linear single regression model are as follows:

$$PI [\%] = L \cdot \text{physical or chemical soil property} [\%] + M, \quad (2)$$

where L and M are model parameters.

Parameters such as LL , gravel content, sand content, silt content, clay content, gypsum content, TSS , pH, and organic content percentages are physical and chemical model factors that may be directly associated with PI content. However, PI requires a rigorous laboratory analysis and may be the primary cause of soil swelling. As a result, the suggested linear single regression model can estimate PI using physical and chemical soil parameters.

Linear multi-regression model

A linear multi-regression model was used to calculate the PI soil attribute using field measurements for physical and chemical soil factors. The linear multi-regression model represents the following soil characteristics: LL , gravel, sand, silt, clay, gypsum, TSS , pH, and organic percentages. Three distinct linear multi-regression models were employed. Equations (3), (4), and (5) reveal the model forms as follows:

$$PI [\%] = A \cdot LL + B \cdot \text{gravel} [\%] + C \cdot \text{sand} [\%] + D \cdot \text{silt} [\%] + E \cdot \text{clay} [\%] + F, \quad (3)$$

$$PI [\%] = G \cdot GYP [\%] + H \cdot TSS [\%] + I \cdot \text{pH} [\%] + J \cdot ORG [\%] + K, \quad (4)$$

$$PI [\%] = N \cdot LL + O \cdot \text{gravel} [\%] + P \cdot \text{sand} [\%] + Q \cdot \text{silt} [\%] + R \cdot \text{clay} [\%] + S \cdot GYP [\%] + T \cdot TSS [\%] + U \cdot \text{pH} [\%] + V \cdot ORG [\%] + W, \quad (5)$$

where the model parameters are $A, B, C, D, E, F, G, H, I, J, K, N, O, P, Q, R, S, T, U, V,$ and W .

The PI component can be predicted using varying percentages of physical and chemical soil variables based on the specified multi-regression model characteristics.

Results

Physical soil distribution

The IDW method was used to estimate the gravel distribution for the examined residential complex in the city of Kirkuk, as shown in Figure 3a. The percentage of gravel is accurately divided into five regions: very low, low, medium, high, and very high. The maximum and minimum gravel concentrations obtained by the IDW interpolation approach were used to characterize these zones. The ranges were as follows: from 4.016 to 13.997, 13.998 to 23.979, 23.980 to 33.961, 33.962 to 43.943, and 43.944 to 53.925. The first region has a maroon color and appears as a single spot near one of the field boreholes. The second zone is identified by its red color and may be found in the analyzed residential complex's northern and western zones. The third region is designated by the pink color and situated in the center of the investigated residential complex. The fourth region is designated by a light pink color and located in the south-eastern zone of the investigated residential complex. The fifth zone is designated by a white color and divided into tiny areas around two of the boreholes.

Figure 3b illustrates the findings of an IDW technique study utilizing a GIS to evaluate the distribution of sand in a residential complex in the city of Kirkuk. The distribution of sand follows the same five zones as the distribution of gravel. The interpolation by IDW method was used to calculate the maximum and minimum sand contents for each zone. The very low, low, medium, high and very high regions started from 12.005 to 17.202, 17.203 to 22.400, 22.401 to 27.598, 27.599 to 32.795, and 32.796 to 37.993, respectively. The first zone is maroon in color and dispersed as a spot near one of the

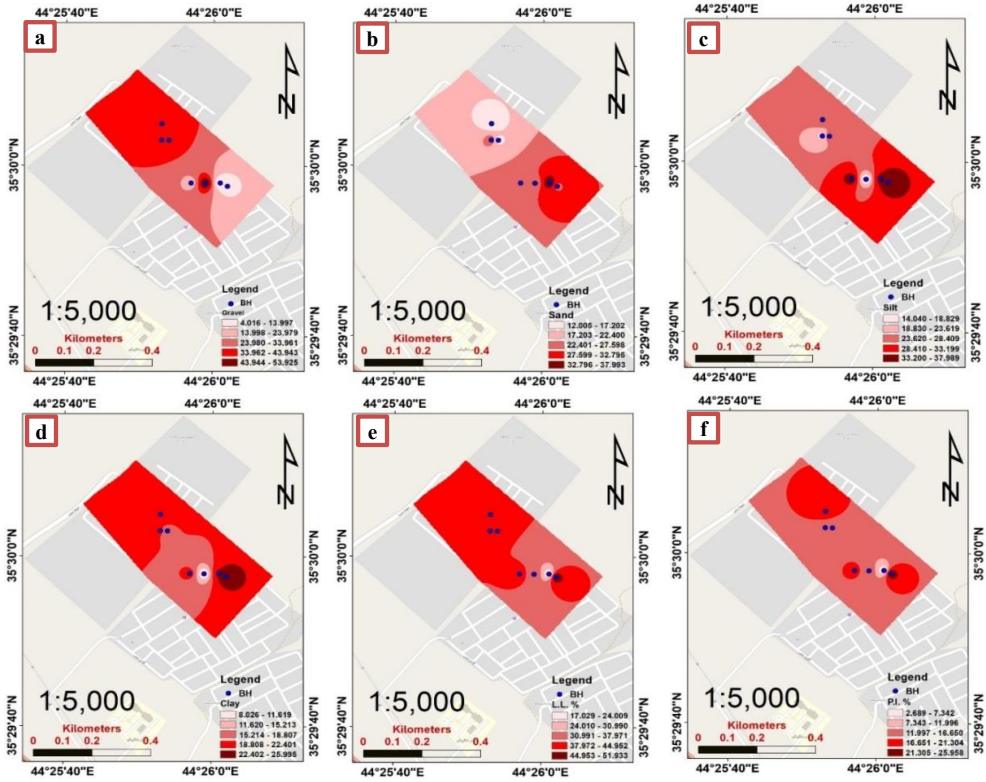


FIGURE 3. Inverse distance weighted technique for physical soil distributions in the studied residential complex in Kirkuk City/Iraq: a – gravel, b – sand, c – silt, d – clay, e – liquid limit (*LL*), f – plasticity index (*PI*)

Source: own work.

boreholes. The second zone is located in the complex’s southeast corner. The third region extends from the complex’s geographic center to the south. The fourth region is located in the examined residential complex’s center to the northern zone. The fifth zone is separated into little portions in the complex’s central northern zone.

As demonstrated in Figure 3c, the silt distribution has been consistently evaluated using the IDW approach combined with the GIS technology for the residential complex in the city of Kirkuk. The silt has been divided into five zones, ranging from extremely low to very high. The IDW interpolation method was used to compute the highest and lowest silt contents in each zone. The first zone is maroon in color and scattered throughout the complex’s south and east zones. The second zone is positioned in the complex’s center, to the south. The third section stretches from the complex’s geographic center to the north. The fourth area is represented by locations

in the complex's center and north. The fifth zone is divided into discrete locations across the complex.

Using IDW with the GIS technique, we mapped out the residential complex of Kirkuk clay distribution as identified in Figure 3d. The clay has been divided into five zones ranging from extremely low to very high. To calculate the maximum and minimum clay concentrations for each zone, the IDW interpolation method was utilized. Starting from 8.026 to 11.619, 11.620 to 15.213, 15.214 to 18.807, 18.808 to 22.401, and 22.402 to 25.995, consecutively, the extremely low, low, medium, high, and very high regions were constructed. The first zone is maroon in color and appears as a spot in the complex's southern zone. The second zone covers up the majority of the complex's space. The third segment extends westward from the complex's geographic center. A site close to one of the boreholes in the examined complex represents the fourth area. The fifth zone is represented by a little piece in the complex's southern zone.

We mapped out the residential complex of Kirkuk *LL* distribution using IDW and the GIS approach, as shown in Figure 3e. The *LL* is separated into five zones ranging from extremely low to extremely high. The IDW interpolation method was used to compute the maximum and minimum *LL* concentrations for each zone. From 17.029 to 20.009, 24.010 to 30.990, 30.991 to 37.971, 37.972 to 44.952, and 44.953 to 51.933, the extremely low, low, medium, high, and very high zones were built in sequence. The first zone is a maroon-colored region in the complex's southern zone. The second zone covers much of the complex's north space. The third segment encompasses the complex's southern portion. The fourth area is located near one of the boreholes in the investigated complex. A little section in the complex's southern zone represents the fifth zone.

The residential complex of Kirkuk *PI* distribution was mapped out using IDW and the GIS technique, as illustrated in Figure 3f. The *PI* is divided into five zones, which range from extremely low to very high. The highest and lowest *PI* concentrations for each zone were calculated using the IDW interpolation method. Extremely low, low, medium, high, and very high zones were developed in order from 2.689 to 7.342, 7.343 to 11.996, 11.997 to 16.650, 16.651 to 21.304, and 21.305 to 25.958. The first zone is a maroon patch in the complex's southern zone. The second zone is represented by three circular shapes in red that are scattered over the study area. The third portion covers the majority of the site. The fourth region is near one of the studied complex's boreholes. The fifth zone is represented by a small part of the complex's southern zone.

It should be noted that the analyzed maps have shown that the maximum values for both silt and clay concentrations are higher than the corresponding values for

both gravel and sand values. Thus, attributed geotechnical complications such as soil swelling is expected that may lead to partial building cracks in the absence of required appropriate engineering protections.

Chemical soil distribution

As shown in Figure 4a, the IDW approach was utilized to estimate the *GYP* distribution for the investigated residential complex in the city of Kirkuk. The proportion of *GYP* is classified into five categories: very low, low, medium, high, and very high. These zones were defined using the maximum and minimum *GYP* concentrations determined using the IDW interpolation method. The ranges were as follows: from 1.023 to 1.464, 1.465 to 1.906, 1.907 to 2.348, 2.349 to 2.790, and 2.791 to 3.232. The first section is maroon in color and appears as a single circular pattern in the complex's southern zone. The second zone is distinguished by its red color and placed in the complex's center. The pink color represents the third region, which is located in the northern and southern parts of the examined residential complex. The fourth region is represented by little spots in the northern and southern zones of the analyzed residential complex and marked by a light pink color. The fifth zone is identifiable as a little spot in the complex's southern zone with a white color.

As shown in Figure 4b, we used IDW and the GIS technique to map out the Kirkuk TSS distribution residential complex. The TSS is divided into five zones ranging from extremely low to extraordinarily high. The greatest and lowest TSS concentrations for each zone were calculated using the IDW interpolation method. Starting from 2.670 to 2.940, 2.941 to 3.211, 3.212 to 3.482, 3.483 to 3.753, and 3.754 to 4.024, consecutively, the extremely low, low, medium, high, and very high regions were constructed. The first zone, which is maroon in color, may be observed in the complex's central zone. The second zone encompasses the majority of the center zone. The third portion extends from the complex's northern zone to its southern region. The fourth location in the investigated complex is towards the complex's southern corner. The fifth zone is represented by white spots in the complex's northern and southern regions.

We mapped out the Kirkuk pH distribution residential complex using IDW and the GIS approach, as shown in Figure 4c. The pH is composed of five zones, from very low to very high. The highest and lowest pH concentrations for each zone were calculated using the IDW interpolation technique. The extremely low, low, medium, high, and very high zones were developed systematically from 7.850 to 7.875, 7.876 to 7.901, 7.902 to 7.927, 7.928 to 7.953, and 7.954 to 7.979. A spot in the complex's southern zone is designated as the first zone, which is symbolized by the maroon color. The complex's southern zone includes one circular shape that

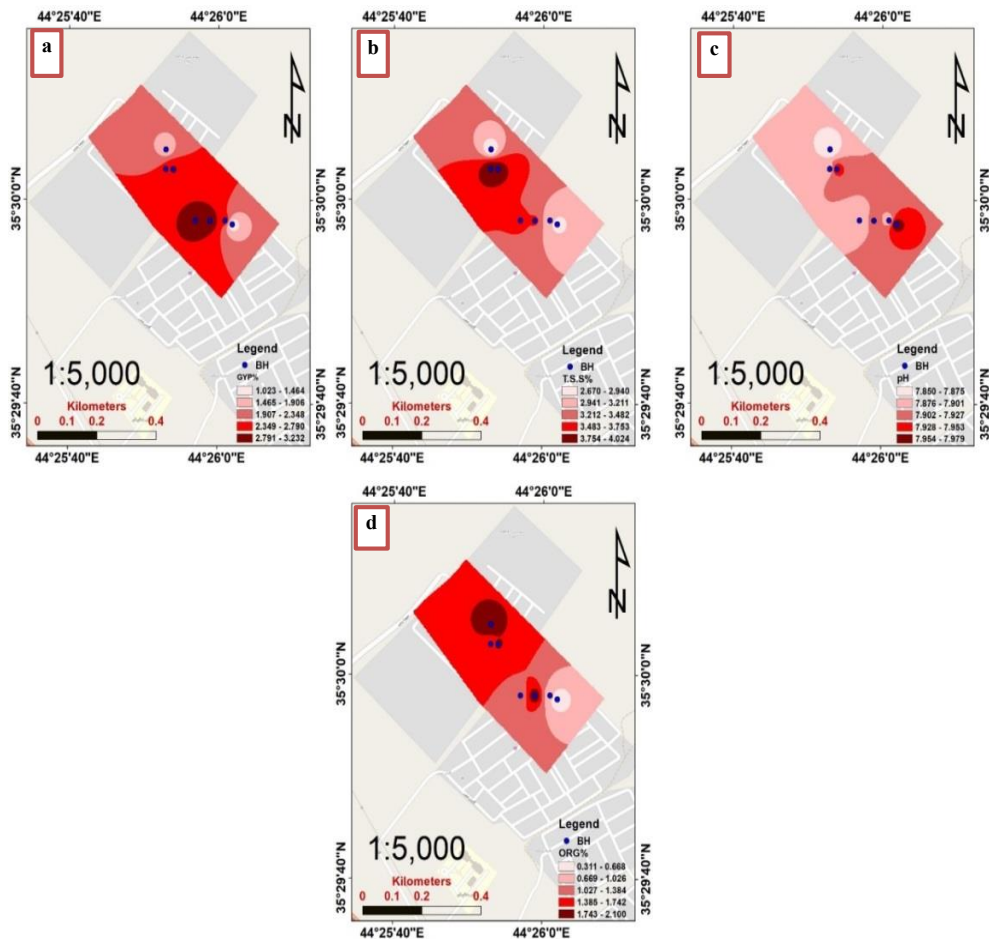


FIGURE 4. IDW technique for chemical soil distributions in the studied residential complex in Kirkuk City/Iraq: a – gypsum content, b – total suspended solids, c – pH, d – organic content
Source: own work.

represents the second zone, which is designated by a red color. The third and fourth zones cover the majority of the southern and northern zones of the study area respectively. The fifth zone is represented by two spots in the complex’s northern and southern zones.

As illustrated in Figure 4d, we mapped the Kirkuk *ORG* distribution residential complex using IDW with the GIS method. Five zones, ranging from incredibly low to very high, constitute the *ORG*. Using the IDW interpolation technique, the highest and lowest *ORG* concentrations for each zone were determined. The extremely low, low, medium, high, and very high regions were built sequentially starting

from 0.311 to 0.668, 0.669 to 1.026, 1.027 to 1.384, 1.385 to 1.742, and 1.743 to 2.100. The first zone, which is maroon in color, may be observed in the complex's north-central zone. The second zone encompasses the majority of the northern zone. The third portion occupies the southern zone of the complex. The fourth location in the investigated complex is located towards the complex's southeastern corner. The fifth zone is represented by a white spot in the complex's southern region.

It should be observed that the highest values for both gypsum and organic concentrations are greater than the equivalent values for pH and TSS values, according to the evaluated maps. Hence, zones with high gypsum and organic contents are more susceptible to geotechnical difficulties such as voids development due to gypsum melting and excessive settlement because of weak soil with high organic content. Consequently, partial building cracks can be caused due to the presence of such problematic soils.

Correlation between plasticity index and soil characteristics

The relationships between *PI* and soil characteristics such as *LL*, gravel, sand, silt, clay, gypsum, *TSS*, pH, and organic components and *PI* are summarized in Table 2.

TABLE 2. Correlations between plasticity index and soil characteristics for studied residential complex in Kirkuk City/Iraq

×	<i>PI</i> [%]	<i>LL</i> [%]	Gravel [%]	Sand [%]	Silt [%]	Clay [%]	<i>GYP</i> [%]	<i>TSS</i> [%]	pH	<i>ORG</i> [%]
<i>PI</i> [%]	1.000	–	–	–	–	–	–	–	–	–
<i>LL</i> [%]	0.345	1.00	–	–	–	–	–	–	–	–
Gravel [%]	–0.298	0.063	1.00	–	–	–	–	–	–	–
Sand [%]	–0.427	–0.369	0.159	1.00	–	–	–	–	–	–
Silt [%]	0.323	0.316	–0.750	–0.611	1.00	–	–	–	–	–
Clay [%]	0.431	0.116	–0.716	–0.700	0.692	1.00	–	–	–	–
<i>GYP</i> [%]	–0.379	–0.026	0.451	–0.021	–0.180	–0.337	1.00	–	–	–
<i>TSS</i> [%]	–0.234	0.125	0.299	–0.231	0.011	–0.086	0.577	1.00	–	–
pH	0.022	0.084	0.091	0.145	–0.147	–0.137	0.106	0.037	1.00	–
<i>ORG</i> [%]	–0.410	–0.138	0.612	–0.061	–0.415	–0.281	0.412	0.304	0.211	1.00

PI – plasticity index, *LL* – liquid limit, *GYP* – gypsum content, *TSS* – total suspended solids, pH – potential of hydrogen, *ORG* – organic content.

Source: own work.

Positive and negative correlations have been identified between the *PI* characteristic and various soil parameters, with degrees of correlation ranging from -0.427 to 0.431 . Furthermore, correlations between the *LL* and gravel, sand, silt, clay, *GYP*, *TSS*, pH, and *ORG* varied from -0.369 to 0.316 . Moreover, satisfactory relationships between gravel content and the amounts of sand, silt, clay, *GYP*, *TSS*, pH, and *ORG* substances are observed, with degrees of correlation ranging from -0.750 to 0.612 . Positive and negative relationships between sand content and proportions of silt, clay, *GYP*, *TSS*, pH, and *ORG* substances have also been identified, with degrees of correlation ranging from -0.700 to 0.145 . Likewise, relationships between silt content and clay, *GYP*, *TSS*, pH, and *ORG* material percentages have been established, with degrees of correlation ranging from -0.415 to 0.692 . Clay content has been found to have negative associations with chemical soil percentages, with degrees of association ranging from -0.337 to -0.086 . Positive relationships exist between soil chemical concentrations, with degrees of correlation ranging from 0.037 to 0.577 . It is essential to establish accurate correlations between *PI* and physical and chemical soil contents that may be utilized to determine the critical swelling feature indirectly with no cost or effort.

Linear single regression model

Table 3 summarizes the properties of the proposed linear single regression model [Eq. (2)]. The least squares approach was used to solve the proposed linear single regression model. Table 3 shows the model parameters (*L* and *M*) as well as R^2 values for the suggested model for all of the analysed situations. The model's coefficients *L* and *M* have comparable ranges from -4.851 to 3.587 and -8.650 to 28.573 . Furthermore, the R^2 ranges from 0.001 to 0.186 .

The variation of *PI* with the physical soil properties has been illustrated in Figure 5a–e. Different negative and positive associations have been observed between *PI* and physical soil contents. The *PI* has demonstrated positive correlations with *LL*, silt content, and clay content, whereas the *PI* has revealed negative associations with both gravel and sand contents. It is obviously indicated that the *PI* has positive associations with fine particle contents and negative associations with coarse particle substances. A decent relationship between *PI* and *LL* is observed for *LL* values higher than 30, with slight changes in gravel concentration over 10%. In addition, reasonable correlations between *PI* with sand, silt and clay contents have been observed except for sand and silt values in the range of 20–30% and for clay content in the range of 30–40%.

TABLE 3. Linear regression model analysis for swelling soil characteristics of studied residential complex in Kirkuk City/Iraq

Swelling property [%]	Physical and chemical properties [%]	<i>L</i>	<i>M</i>	Equation	<i>R</i> ²
<i>PI</i>	<i>LL</i>	0.277	8.255	$PI = 0.277 \cdot LL + 8.255$	0.120
<i>PI</i>	gravel	-0.136	22.679	$PI = -0.136 \cdot \text{gravel} + 22.679$	0.089
<i>PI</i>	sand	-0.236	25.486	$PI = -0.236 \cdot \text{sand} + 25.486$	0.182
<i>PI</i>	silt	0.197	13.879	$PI = 0.197 \cdot \text{silt} + 13.879$	0.104
<i>PI</i>	clay	0.263	13.550	$PI = 0.263 \cdot \text{clay} + 13.550$	0.186
<i>PI</i>	<i>GYP</i>	-4.851	28.573	$PI = -4.851 \cdot GYP + 28.573$	0.144
<i>PI</i>	<i>TSS</i>	-2.415	26.635	$PI = -2.415 \cdot TSS + 26.635$	0.055
<i>PI</i>	pH	3.587	-8.650	$PI = 3.587 \cdot \text{pH} - 8.650$	0.001
<i>PI</i>	<i>ORG</i>	-4.003	23.888	$PI = -4.003 \cdot ORG + 23.888$	0.169

Source: own work.

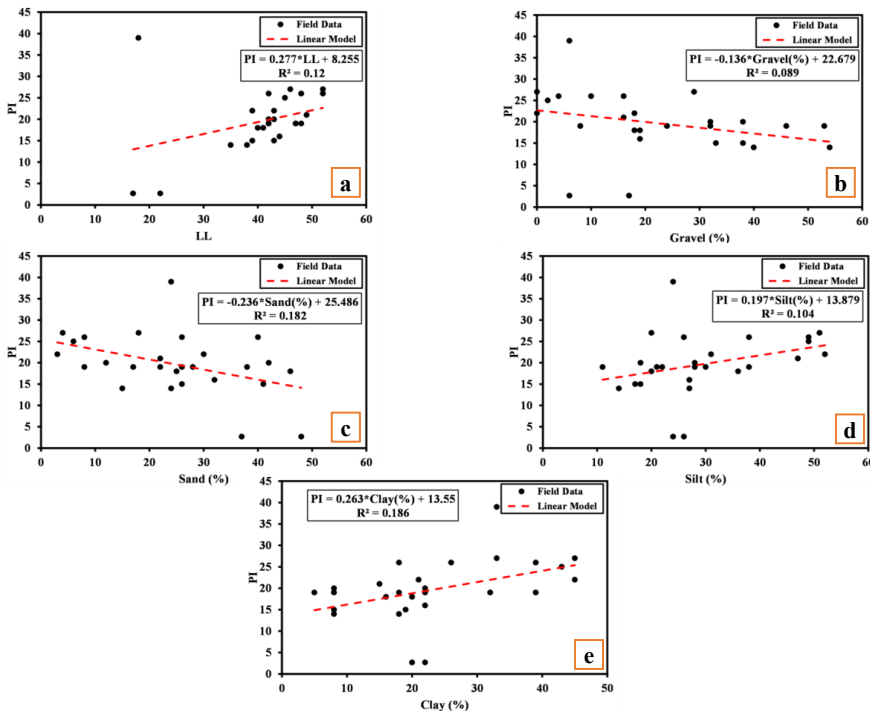


FIGURE 5. The variation of plasticity index content with the physical soil contents of studied residential complex in Kirkuk City using linear single regression model: a – correlation between plasticity index (*PI*) and liquid limit (*LL*), b – correlation between plasticity index (*PI*) and gravel content [%], c – correlation between plasticity index (*PI*) and sand content [%], d – correlation between plasticity index (*PI*) and silt content [%], e – correlation between plasticity index (*PI*) and clay content [%]

Source: own work.

The variation of *PI* with chemical soil properties has been demonstrated in Figure 6a–d. The *PI* has revealed negative correlations with *GYP* [%], *TSS* [%], and *ORG* [%] contents while a positive correlation between *PI* and pH has been noticed. The *PI* values have shown good correlations with both *GYP* [%] and *TSS* [%] for most values greater than 1% and 2% respectively. A reasonable variation between *PI* and pH values has been noticed except for a pH value close to 7.9, whereas *PI* and *ORG* values were correlated rationally for *ORG* values greater than 0.5.

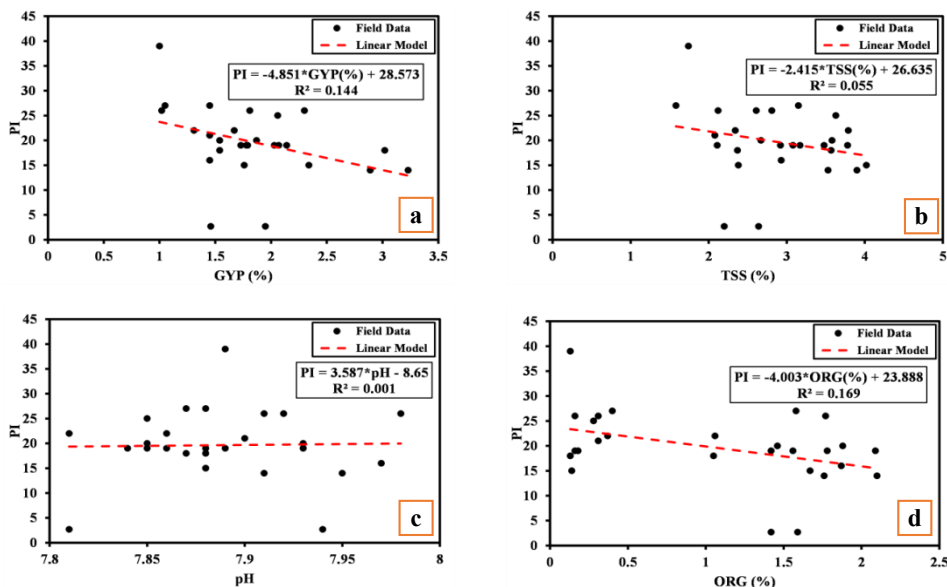


FIGURE 6. The variation of plasticity index content with the chemical soil contents of studied residential complex in Kirkuk City/Iraq using linear single regression model: a – correlation between plasticity index (*PI*) and gypsum content (*GYP*) [%], b – correlation between plasticity index (*PI*) and total suspended solids (*TSS*) [%], c – correlation between plasticity index (*PI*) and pH, d – correlation between plasticity index (*PI*) and organic content (*ORG*) [%]

Source: own work.

Linear multi-regression model

Information about the linear multi-regression framework [Eqs (3), (4) and (5)] is provided in Table 4. The least squares approach was used to solve the linear multi-regression equations. Table 4 shows the proposed model parameters (*A–W*) as well as the predicted values of the multiple *R* model. The multiple *R* value ranges from 0.485 to 0.921.

TABLE 4. Linear multi-regression model analysis for swelling soil characteristics of studied residential complex in Kirkuk City/Iraq

Swelling property [%]	Equation number	Linear multi-regression coefficients						Multiple R
		A	B	C	D	E	F	
PI	3	0.637	-2.661	-2.645	-2.625	-2.560	254.478	0.921
		G	H	I	J	K		
PI	4	-3.369	0.141	19.801	-3.232	-127.336		0.485
		N	O	P	Q	R		
PI	5	0.647	-2.688	-2.665	-2.645	-2.590		
		S	T	U	V	W		
		-0.261	0.010	-4.952	0.259	295.696		0.921

Source: own work.

The variations in the expected and actual soil PI characteristics using the multi-linear regression model [Eqs (3)–(5)] are displayed in Figure 7a–c. The proposed linear multi-regression analysis of Eqs (3) and (5) estimate PI values successfully in Figures 7a and 7c, with multiple R values of 0.921.

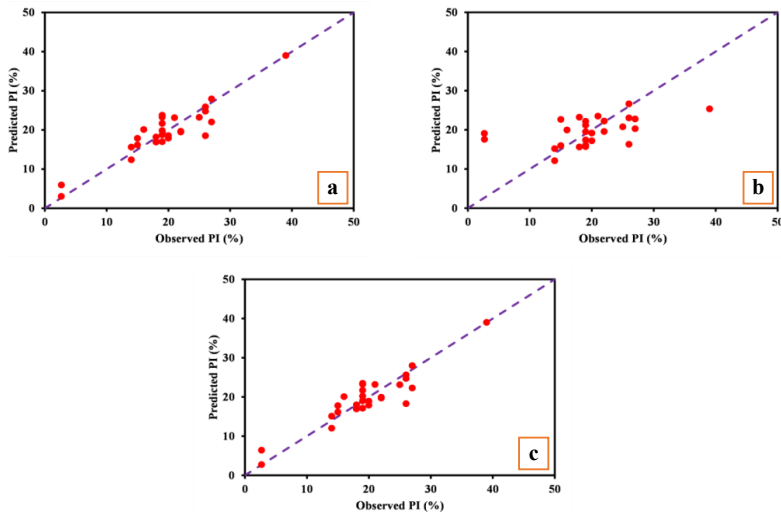


FIGURE 7. The variation of PI content with the chemical soil contents of studied residential complex in Kirkuk City/Iraq using linear single regression model: a – correlation between plasticity index (PI) and gypsum content (GYP) [%], b – correlation between plasticity index (PI) and total suspended solids (TSS) [%], c – correlation between plasticity index (PI) and pH, d – correlation between plasticity index (PI) and organic content (ORG) [%]

Source: own work.

However, a lower multiple R value of 0.485 has been noticed for the predicted PI values of Eq. (4) as presented in Figure 7b. It is evident that PI values can be approximated more conveniently based on physical or integrated physical and chemical soil features rather than chemical attributes alone. Moreover, it has been demonstrated that PI values, which are the primary cause of cracks, may be predicted more accurately using multi-regression models than single-regression models.

Discussion

The arrangement of soil granules is a key factor in assessing the possibility of soil swelling. When contrasted to soil with a more consistent particle size distribution, known as poorly graded soil, soil with a broader range of sizes has greater drainage and a slighter propensity for swelling. It's due to the fact that properly graded soil facilitates the ability for water to drain, which lowers the risk of soil swelling carried on by excessive water absorption. Poorly graded soil, on the contrary, has a larger water-holding capacity and may not drain as efficiently, which might increase the probability of swelling. The particulate distribution might provide useful data for analyzing the possibility of soil swelling and contributing to the design of suitable foundation alternatives. Soils with a substantial clay concentration have a significant possibility for swelling compared to soils with low clay content. Although clay particles are tiny and have a high surface area to volume ratio, they may absorb and retain a lot of water. Since water is absorbed by the soil, the clay particles acquire additional water and expand in volume, leading the soil to swell. The swelling would be determined by the type of clay content, the proportion of clay in the soil, and the amount of water absorbed. As a result, while assessing the possibility of soil swelling, the clay concentration of the soil is an important component to be evaluated. The soil type content in neighboring locations where samples are collected can be predicted using the GIS procedure and IDW approach. It is clear that the TSS , GYP , and ORG concentrations are insufficient to be active throughout the entire examined region. The LL and PI can be utilized to predict the possibility of soil swelling. These two factors provide useful information regarding soil behavior when subjected to moisture fluctuations. Swelling is more likely in soils with high LL and PI levels. This is due to the fact that soils with high LL and PI may hold more water and have a greater tendency to alter volume concerning moisture variations. Such soils can swell as they retain moisture, causing volume changes and possible collapse. According to LL and PI , most regions have swell potentials ranging from moderate to high.

Conclusions

The geographical analysis in this work was carried out using the distance weighted (IDW) approach, based on information received from seven field boreholes obtained from a residential complex in the city of Kirkuk. The physical and chemical properties of field soil samples were used to perform investigations on the existing cracks in the structures of the examined complex. In particular, the plasticity index and soil characteristics relationships, as well as linear single and linear multi-regression models were used in statistical analysis. Based on the available data and findings of this investigation, the following research conclusions have been proposed:

1. Gravel soil is mostly spread in three zones across the examined residential complex, according to the IDW approach combined with the GIS technique.
2. Using the GIS and IDW analysis, the examined residential complex has the greatest sand and silt percentages in the northern part.
3. According to the IDW approach combined with the GIS procedure, clay soil covers the majority of the analyzed residential complex.
4. The investigated residential complex has the highest gypsum concentration in the central part, according to GIS and IDW examinations.
5. The majority of the soil in the examined residential complex area has liquid limit and plasticity index values between 37.972 and 44.952 and 11.997 and 16.650, respectively, according to the GIS and IDW analyses.
6. The analyzed residential complex has the highest total suspended solids in the central and western regions, according to GIS and IDW assessment.
7. All of the soil in the investigated residential complex is alkaline, with small variations in pH values between 7.850 and 7.979, according to the GIS approach and IDW technique.
8. Most of the soil between the north and center of the analyzed residential complex has organic content values between 1.385% and 1.742%, according to the GIS methodology and IDW approach.
9. Significant positive and negative associations between the physical and chemical parameters of the soil and the plasticity index as a swelling indicator have been observed.
10. The presented linear multi-regression models of the physical and integrated physical and chemical soil properties successfully predicted the plasticity index values, with multiple R values of 0.92 for both models.
11. The proposed statistical models can thus offer comprehensive geographic and mechanical interpretations for the crack origins in the analyzed residential complex.

References

- Addiscott, T. M. (1993). Simulation modelling and soil behaviour. *Geoderma*, 60 (1–4), 15–40. [https://doi.org/10.1016/0016-7061\(93\)90016-E](https://doi.org/10.1016/0016-7061(93)90016-E)
- Billah, M. M. (2018). Mapping and monitoring erosion-accretion in an alluvial river using satellite imagery – the river bank changes of the Padma river in Bangladesh. *Quaestiones Geographicae*, 37 (3), 87–95. <https://doi.org/10.2478/quageo-2018-0027>
- Cantillo, V., Market, V. & Bird, C. (2017). Empirical correlations for the swelling pressure of expansive clays in the city of Barranquilla, Colombia. *Earth Sciences Research Journal*, 21 (1), 45–49. <https://doi.org/10.15446/estj.v21n1.60226>
- Matarira, D., Mutanga, O. & Dube, T. (2021). Landscape scale land degradation mapping in the semi-arid areas of the Save catchment, Zimbabwe. *South African Geographical Journal*, 103 (2), 183–203. <https://doi.org/10.1080/03736245.2020.1717588>
- Mohsin, S. & Lone, M. A. (2021). Modeling of reference evapotranspiration for temperate Kashmir Valley using linear regression. *Modeling Earth Systems and Environment*, 7, 495–502. <https://doi.org/10.1007/s40808-020-00921-8>
- Olmo, J. C., Guervos, R. C. & Rocha, I. M. (2019). The spatial effects of violent political events on mortality in countries of Africa. *South African Geographical Journal*, 101 (3), 285–306. <https://doi.org/10.1080/03736245.2019.1612770>
- Omar, N. Q. & Raheem, A. M. (2016). Determining the suitability trends for settlement based on multi criteria in Kirkuk, Iraq. *Open Geospatial Data, Software and Standards*, 1 (10), 1–9. <https://doi.org/10.1186/s40965-016-0011-2>
- Omer, M., Shanableh, A., Mughieda, O., Arab, M., Zeiada, W. & Al-Ruzouq, R. (2018). Advanced mathematical models and their comparison to predict compaction properties of fine-grained soils from various physical properties. *Soils and Foundations*, 58 (6), 1383–1399. <https://doi.org/10.1016/j.sandf.2018.08.004>
- Ouabo, R. E., Sangodoyin, A. Y. & Ogundiran, M. B. (2020). Assessment of ordinary Kriging and Inverse Distance Weighting methods for modeling Chromium and Cadmium soil pollution in E-Waste sites in Douala, Cameroon. *Journal of Health and Pollution*, 10 (26), 1–20. <https://doi.org/10.5696/2156-9614-10.26.200605>
- Pentos, K., Mbah, J. T., Pieczarka, K., Niedbała, G. & Wojciechowski, T. (2022). Evaluation of multiple linear regression and machine learning approaches to predict soil compaction and shear stress based on electrical parameters. *Applied Sciences*, 12 (17), 8791. <https://doi.org/10.3390/app12178791>
- Raheem, A. M. & Omar, N. Q. (2021). Investigation of distinctive physico-chemical soil correlations for Kirkuk city using spatial analysis technique incorporated with statistical modeling. *International Journal of Geo-Engineering*, 12 (18), 1–21. <https://doi.org/10.1186/s40703-021-00147-2>
- Raheem, A. M., Naser, I. J., Ibrahim, M. O. & Omar, N. Q. (2023). Inverse distance weighted (IDW) and kriging approaches integrated with linear single and multi-regression models to assess particular physico-consolidation soil properties for Kirkuk city. *Modeling Earth Systems and Environment*, 2023, 1–23. <https://doi.org/10.1007/s40808-023-01730-5>

- Raheem, A. M., Omar, N. Q., Naser, I. J. & Ibrahim, M. O. (2022). GIS implementation and statistical analysis for significant characteristics of Kirkuk soil. *Journal of the Mechanical Behavior of Materials*, 31 (1), 691–700. <https://doi.org/10.1515/jmbm-2022-0073>
- Salahalden, V. F., Shareef, M. A. & Al Nuaimy, Q. A. M. (2023). Characterization of the Chemical Properties of Deposited Red Clay Soil Using GIS Based Inverse Distance Weighted Method in Kirkuk City, Iraq. *Ecological Engineering & Environmental Technology*, 24 (7), 46–60. <https://doi.org/10.12912/27197050/169571>
- Zijl, G. (2019). Digital soil mapping approaches to address real world problems in southern Africa. *Geoderma*, 337 (1), 1301–1308. <https://doi.org/10.1016/j.geoderma.2018.07.052>

Summary

Implementing GIS and linear regression models to investigate partial building failures. One of the most dangerous field problems in the civil engineering discipline is the suddenly developed cracks in the building, which could be caused by the swelling of the subsurface soil. Thus, this work has focused on employing a procedure in the geographic information system known as the inverse distance weighted (*IDW*) technique, to analyze the extent of cracks in a residential complex in the city of Kirkuk in Iraq using the physical and chemical soil data for seven boreholes from the field of the study. Physical soil parameters such as liquid limit (*LL*), gravel, sand, silt and clay percentages were characterized first, followed by chemical properties such as gypsum content (*GYP*), total suspended solids (*TSS*), potential of hydrogen (pH), and organic content (*ORG*). Furthermore, statistical studies such as plasticity index (*PI*) and soil characteristics association, linear single, and various linear multi-regression models were used. The data analysis shows that there are significantly positive and negative relationships between *PI* as a swelling indicator and the physical and chemical soil properties, although weak to moderate correlations were observed between *PI* and these variables. The *PI* values were accurately predicted by the proposed linear multi-regression models of the physical and integrated physical and chemical soil characteristics, with multiple *R* values of 0.92 for both models. As a result, the suggested statistical models can provide complete geographic and mechanical explanations for the crack sources in the investigated residential complex.

Siti N. FITRI¹  <https://orcid.org/0009-0007-3127-154X>

Niken S. SURJANDARI²

Solihin AS'AD³

^{1,2}Sebelas Maret University, Faculty of Engineering, UNS Geoscience Research Group, Indonesia

¹Sebelas Maret University, Disaster Research Center, Indonesia

³Sebelas Maret University, Faculty of Engineering, Smartcrete Research Group, Indonesia

A systematic review of clay shale research development for slope construction

Keywords: clay shale, systematic review, VOSviewer, slope, bibliometric

Introduction

Clay shale conditions in certain projects have a huge problem that usually occurs. Most of these issues are due to the clay minerals in shale swelling expanding too much, resulting in subsidence, cracking, and loss of bearing capacity. Due to its characteristics, which store water much better than sandy soil, clayey soil is frequently recognized as troublesome soil. These conditions induce more engineering issues because of the soil creeping. Furthermore, another study claims that because clay shale is a transitional element between soil and rock, it loses durability quickly, leading to issues in the geotechnical industry (Agrawal, Manhas & Sharda, 1993; Sharma, 1995; Sharma, 1996; Powell, Siemens, Take & Remenda, 2013; Pardoyo, Kresno, Fahreza & Maulana, 2020; Khairul & Musta, 2022; Simatupang, Alatas, Redyananda & Purnomo, 2022). Furthermore, according to Zanzinger, Koerner & Gartung (1986), unweather clay shale has a maximum cohesion of 85 kPa and an internal angle of friction of 41°.

However, when the material was exposed to air, its shear strength reduced to zero cohesion and its friction angle was only 9 (Zanzinger et al., 1986).

The characteristic of the clay shale problem was found in several areas in Indonesia. An engineering method exercise for clay shale cutting slope was provided first by Shields in Bukit Asam locations (Shields, 1986). Another research is the water-based application that is both cost-effective and inhibitive offshore in East Kalimantan (Huadi, Aldea, Mackereth & Mukhlis, 2010). In addition, the clay shale slope investigation was also conducted on the Cisomang Bridge on the toll route between Purwakarta and Bandung (Hendry, Somantri, Febriansya & Nurhadi, 2020), as well as clay-shale cutting slope in the Karawang Area (Zhang, Wang, Zhou & Huang, 2022), Cipularang highway (Agung, Pramusadi & Damianto, 2017), Semarang, Central Java (Rahardjo, Halim & Wisanto, 2012), and Tana Toraja airport project (Gouw et al., 2016). The visual characteristic in several cutting clay shale slopes is described in Figure 1, which presents the clay shale slope on certain toll road project in Indonesia. In addition, the picture depicts the disintegration of clay shales after only a few days of exposure to the atmosphere; even if they still resemble rock, they are readily spalled off and disintegrated by applying small forces.



FIGURE 1. Clay shale slope in toll road project in Indonesia

Source: own work.

The action to solve the clay shale problem has been described in a particular area. On a problematic clay shale, a 25–37 m high retaining structure was built to support a Tana Toraja runway (Gouw et al., 2016). In addition, by adding 38 pile foundations into the existing foundation layout, reinforcement has been designed to minimize the movement of the particular pier on the Cisomang Bridge (Hendry et al., 2020). The optimal solution was the hybrid reinforced soil slope (HRSS), a combination of anchored gabion units and geogrids. The anchored gabion units were constructed from hexagonal double twisted wire mesh 8 × 10 Galmac® (Zn-Al 5%) polymer coated steel wire measuring 2.7/3.7 mm in diameter. Geogrids with an initial tensile strength of 300 kN·m⁻¹ were utilized, which comprised of high-tenacity polyester yarn tendons encased in polyethene (Gouw, 2018). However, the information on the further topic related clay shale study has not been presented in clay shale slope stability research.

Several article issues describe the clay shale performance. Table 1 presents published review studies about clay shale. Table 1 divides the categories into five areas: case study, rock mechanics, clay mineralogy, slope stability, and bibliometric analysis. A “YES” means the article examines certain criteria, and “NO” vice versa. The percentile of review articles shows most of these describe rock mechanics in clay shale, which reaches 100%. Moreover, the case study analysis is the second topic

TABLE 1. Summary of review articles and published research on clay shale

Year	Reference	Examined case study	Discussed rock mechanics	Discussed clay mineralogy	Analysis for slope stability	Provided bibliometric review
2000	Einstein, 2000	YES	YES	NO	NO	NO
2003	Picarelli et al., 2003	YES	YES	YES	NO	NO
2003	Nomura, 2003	YES	YES	NO	YES	NO
2004	Mesri & Shahien, 2004	YES	YES	NO	YES	NO
2009	Bonini, Debernardi, Barla & Barla, 2009	YES	YES	YES	NO	NO
2014	Al-Arfaj, Amanullah, Sultan, Hossain & Abdulraheem, 2014	NO	YES	YES	NO	NO
2016	Herbosch, Liégeois & Pin, 2016	YES	YES	YES	NO	NO
2021	Mo et al., 2021	NO	YES	YES	NO	NO
2021	Sharifigaliuk, Mahmood, Rezaee & Saeedi, 2021	YES	YES	NO	NO	NO
2021	Rosly, Mohamad, Bolong & Harith, 2022	YES	YES	NO	YES	NO
2022	An, Zagorščak & Thomas, 2022	NO	YES	YES	NO	NO
2022	Pingquan et al., 2022	NO	YES	YES	NO	NO
2022	Jinhua et al., 2022	YES	YES	NO	NO	YES

Source: own work.

with 76.9%. The clay mineralogy and slope stability are the third and fourth levels, with 53.8% and 23%, respectively. Lastly, the article that utilizes bibliometric analysis is the lowest topic, under one-tenth (7.69%).

This review study summarizes the published research for clay shale beginning in 1980 and presents a bibliometric analysis to identify the published studies based on year and country, and provides various research prospective in particular maps using the VOSviewer program.

Methods

Bibliometric review by sequence

The overview organizes the body of research on clay shale structures into categories and provides reinforcement for clay shale slope design. The best technique for ensuring the best quality of the reference lists is to do a systematic literature evaluation (Snyder, 2019) by performing a bibliometric analysis (Morrisey, 2020; Donthu, Kumar, Mukherjee, Pandey & Lim, 2021). The most recent research findings from publications that have been published and conference proceedings linked to clay shale have been statistically evaluated in a bibliometric assessment. In addition, the VOSviewer software was successfully analysed in the civil engineering study (Yu, Xu & Antuchevičiene, 2019; Wang, Xu, Ge, Zavadskas & Skačkauskas, 2020; Aristizabal, Lara, Payares & Alzate, 2021; Mulyawati & Ramadhan, 2021; Videras Rodríguez, Melgar, Cordero & Márquez, 2021; Shahbazi, Elahi & Khalili, 2022) and other topic research (van Eck & Waltman, 2010; van Eck & Waltman, 2017; Nandiyanto & Al Husaeni, 2021; Ding & Yang, 2022; Kuzior & Sira, 2022; McAlister, Lennertz & Atencio Mojica, 2022; Soegoto, Soegoto, Luckyardi & Rafdhi, 2022; Tamala, Maramag, Simeon & Ignacio, 2022). Figure 2 presents the method of bibliometric analysis.

First step: Entering keywords in two groups. For a list of the groups (see Table 2).

Second step: Collect electronic resources from the Scopus search engines.

Third step: The bibliometric analysis identifies the published research for clay shale by year and nation. Then, use VOSviewer to generate a bibliometric map to show the most recent developments in clay shale research and clay shale reinforcement slope.

Fourth step: Extraction of data from the third step, including the goals of the study, the procedures followed, and any conclusions that could be relevant for further research.

Fifth step: The bibliometric analysis identifies the published papers for the clay shale research by year and nation. Then, to display the most recent trends linked to the issue, generate the bibliometric map using VOSviewer.

Sixth step: Data extraction from the fifth step, which summarizes the objectives of the study.

Seventh step: Generate discussions for bibliometric evaluation.

Eighth step: This study’s concluding statement.

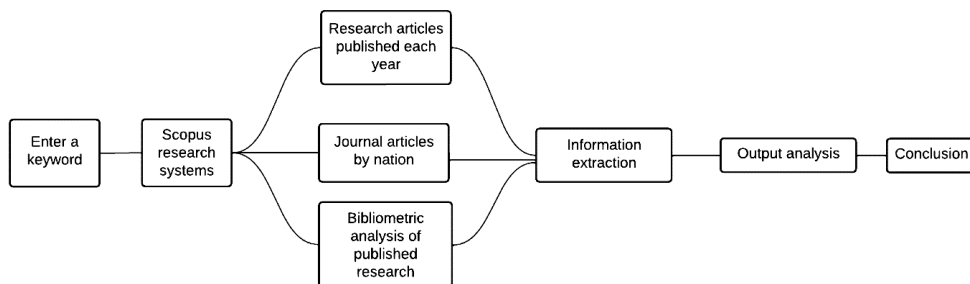


FIGURE 2. The bibliometric review method

Source: own work.

The data was collected in the Scopus website system on 1 May 2023. Table 1 shows the various keyword for this study. The first is “clay shale OR clay-shale”, with the output reaching 597 articles, while another specific keyword, such as “clay-shale, slope”, generates 89 articles, and the last is “clay-shale, landslide”, with 67 items.

TABLE 2. Generated keywords for this review

No	Source	Keyword	Number of articles
1	Scopus	“clay shale OR clay-shale”	597
2	Scopus	“clay-shale, slope”	89
3	Scopus	“clay-shale, landslide”	67

Source: own work.

The Scopus is used as a database version because of the open access factor. Moreover, the Indonesian regulation utilized the Scopus index as the key factor of the institutional performance index. An organization must decide based on institutional needs if it can only afford a systematic review (Burnham, 2006).

The timeline for searching for relevant documents began in 1980 as the published year (Hobson, 1980). The measurement of the published research from 1980

to 2022 was the main goal of the search. The inquiry also included the most recent 5 years of records, from 2018 to 2022. Review articles, research articles, conference proceedings, books, and book chapters that were written and published in English were all included in the search criteria. The file format for these digital resources is Research Information System (RIS), which makes it possible for citation management software to combine data with it.

Clay shale published research by year

The output of annual publication in the keyword “clay shale OR clay-shale” is shown in Figure 3. According to Figure 3, the oldest article was in 1980 and generally increased through the period’s end. Although the fluctuating condition occurs several times, the average use of a trendline as a control that shows the value of the rise is $R^2 = 0.843$.

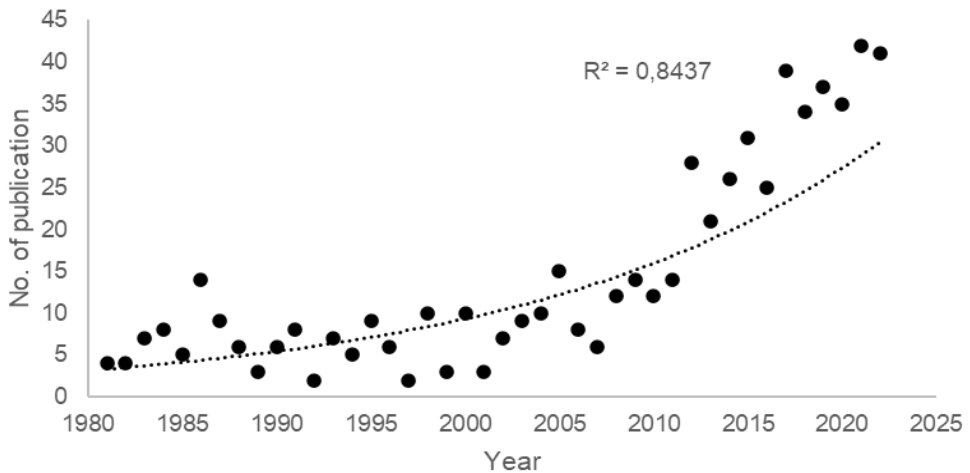


FIGURE 3. Research for clay shale by year of publication

Source: own work.

In terms of other keywords, namely “clay-shale, slope” and “clay-shale, landslide”, they have also been described in Figure 4. The result shows a similar trend to the previous one, the increasing value throughout the year. However, these 2 categories have different specific trendlines, depicted in R^2 0.5275 and 0.3992. The lower R^2 because the total article that smaller than the keyword “clay shale OR clay-shale”.

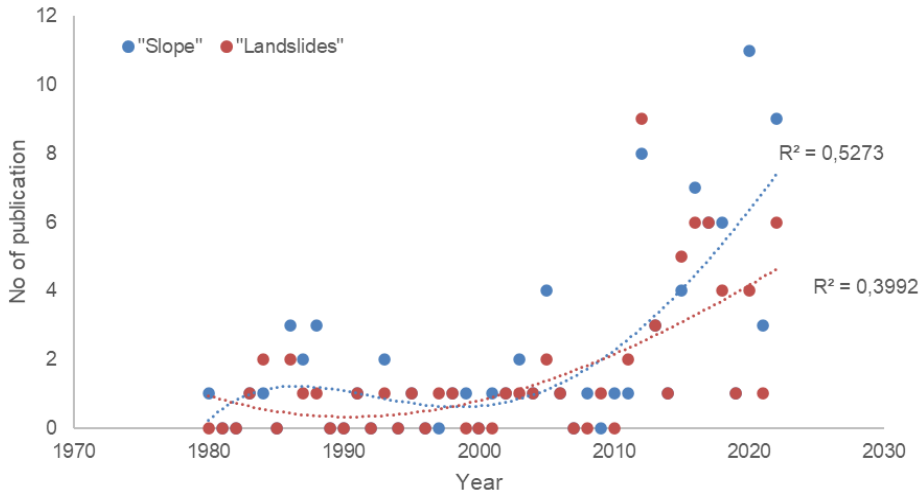


FIGURE 4. Research for clay shale by year of publication with specific keyword
Source: own work.

Clay shale published research by country

Figure 5 shows the bibliometric evaluation in bar chart style and lists the top 14 area of origin for the papers from the 1980–2022 collection that were searched.

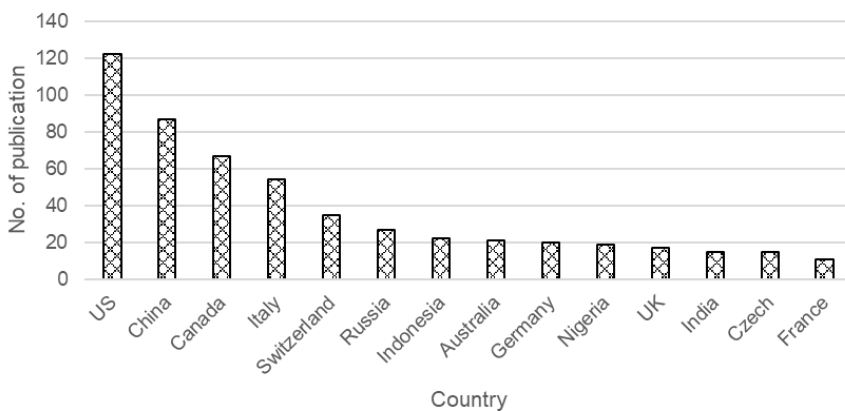


FIGURE 5. Published article based on country with keyword “clay shale”
Source: own work.

In general, the highest publication is from the United States (US) with 122 articles, and France has ranked fourteen with 11 publications. The number 14 is picked because of the big gap between the fifteen 15th range rather than the total number of another level. Another country is China with 87 items, Canada with 67 publications, Italy is 54 items, Switzerland with 35 publications, Russia with 27 numbers, Indonesia is 22 items, Australia is 21 items, Germany with 20 publications, Nigeria is 17 items, the United Kingdom 17 publications, India is 15 items, and Czech with 15 items.

The analysis of another keyword produces different outputs based on the country published. The resulting detail of the keywords “clay-shale, slope” and “clay-shale, landslide” have presented in Figure 6. The highest article was published in Italy and was in a different location from the previous keyword, “clay shale OR clay-shale,” with 26 and 27, respectively. Canada is the second level, with 16 and 8 items, respectively.

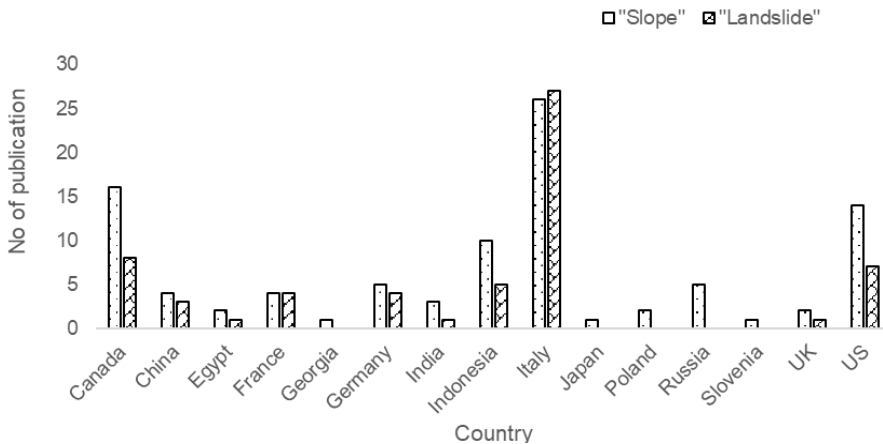


FIGURE 6. Published article based on country with different specific keyword
Source: own work.

Moreover, the United States moved three positions with slope keywords in 14 articles and 7 ones for the landslide category. Indonesia is the next level which describes the large gap among the 5–15 ranks with 10 and 5 publications. In addition, in two different keywords, the process shows the significant output for Georgia, Japan, Poland, Russia, and Slovenia that only have the keyword “clay-shale, slope” in their clay shale publication.

Map of published research for the clay shale research

The bibliometric analysis using VOSviewer, based on the Scopus index from 1980 to 2022, has been described in Figure 7 with 5,432 keywords and 308 meet the threshold. The input keyword is “clay shale OR clay-shale”. There are 5 clusters with different color.

First cluster presents the big keyword “clay shale” with blue color. This topic is linked with soil mechanics, foundations, and rocks. Furthermore, this category is connected with clay minerals, rock mechanics, and landslides.

Second cluster is green in color with the large topic being rock mechanics. This scope interconnects with anisotropy, excavation, and deformation. Moreover, this scope is connected with clay minerals and clay shale.

Third cluster is red in color with the theme of clay minerals which is linked to clay shale and rock mechanics. This section is interconnected with porosity, pore structure, and silica.

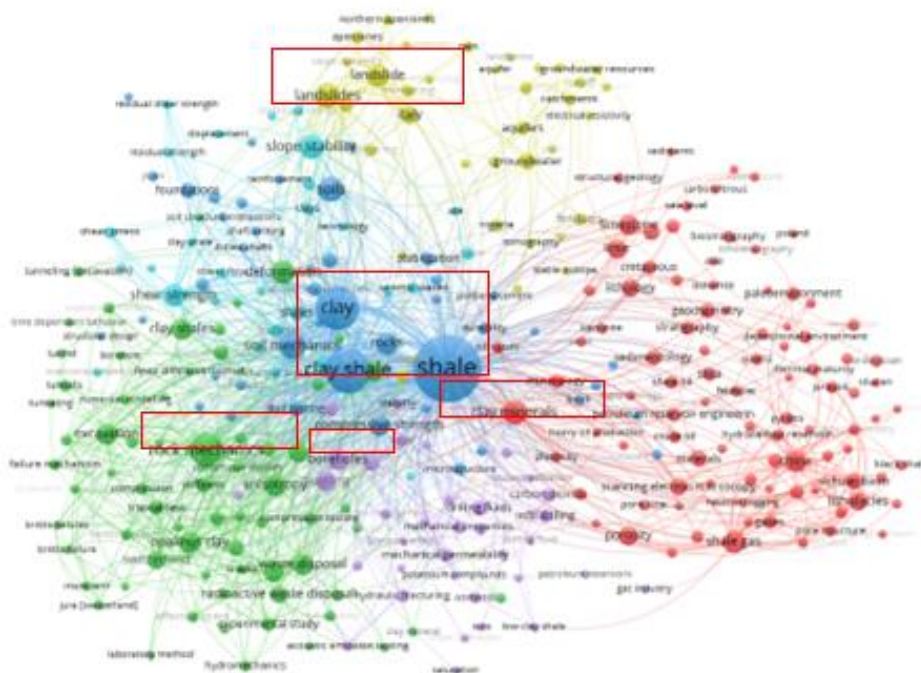


FIGURE 7. VOSviewer's output map of published clay shale research

Source: own work.

Fourth cluster is landslides with a yellow presentation. This topic is interconnected with rain, groundwater, and hydrogeology. In addition, this category is linked with clay shale only. Although it connects with deformation, there is no relationship along clay mineral, swelling and also rock mechanics.

Fifth is purple color with big theme is swelling. It is interconnected with permeability. Furthermore, this part is linked to clay shale and rock mechanics. However, there is no connection with the other section, namely landslides and clay minerals.

Map of published research for the clay shale slope research

The output of VOSviewer investigation with keyword “clay-shale, slope” has been depicted in Figure 8. According to Figure 8, the cluster is divided into 3 criteria.

The first category is green, with clay shale being the main topic. It is interconnected with slope failure, stability analysis, and rock mechanics. Meanwhile, the clay-shale theme is linked to landslide and slope stability. However, the slope

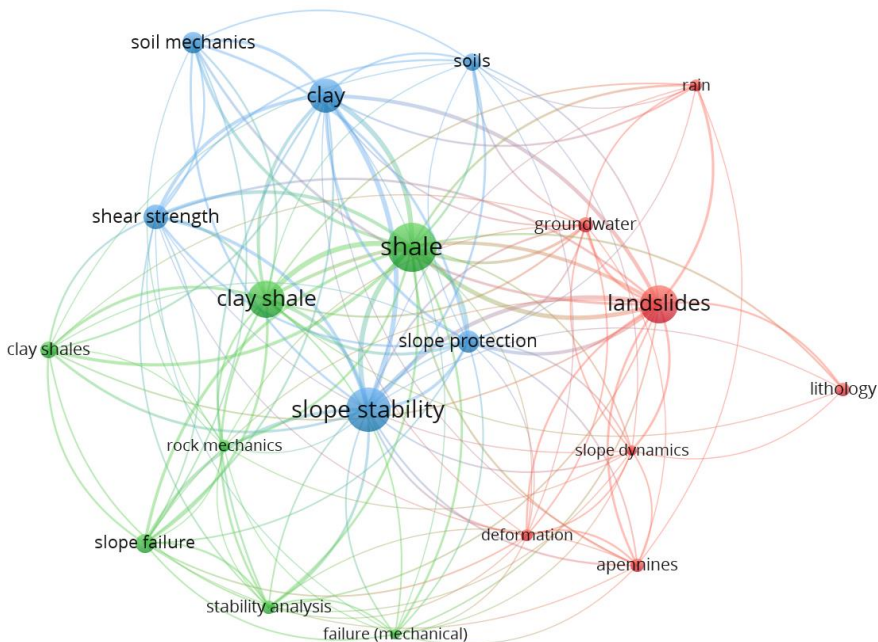


FIGURE 8. VOSviewer's output map of published clay shale slope research

Source: own work.

dynamic and deformation are excluded from this description. The second is a red color, with the big topic being landslides. It includes slope dynamics, deformation, rain, and groundwater. Also, this general topic is connected to clay shale and slope stability. The last color is blue, with the topic being slope stability related to all sub-categories in this map.

Extrapolation of data from published research on clay shale

The collection of information from the most recent studies is accomplished by summarizing the main objectives, useful procedures, and significant findings that may be applicable to future research investigations on clay shale. Table 3 provides a summary of the most recent studies published from 2020 to 2023 that contained the keywords “clay shale” and combined by “landslide” and “slope”.

TABLE 3. Generated keywords for this review

Year	Detailed description of the study	Keyword
2023	This study proposed a methodology and evaluate the outcomes. Within a weathering clay shale and undisturbed clay shale, an interface direct shear test was conducted until its residual state. Using a two-day wetting-drying cycle, the weathering condition of the bottom clay shale is accomplished by soaking and drying the bottom of the sample. Results revealed dispersed values and distinct behavior for wet and dry conditions as weathering days increase. The wet condition increased cohesion, increased the average stress ratio, and decreased the friction angle. The lack of hydration decreased cohesion, increased friction angle, and increased the average stress ratio (Sagitaningrum, Kamaruddin, Nazir, Soepandji & Alatas, 2023).	“clay-shale, slope”
2022	A series of triaxial compression experiments were performed on reconstituted clay shale specimens with normal consolidation. On the basis of laboratory results, an empirical correlation for the secant entirely softened friction angle was derived for clay compositions with a plasticity index between 10 and 250% and an effective normal stress between 10 and 700 kPa. Stability analyses of 63 first-time collapses of slopes in 38 geologic materials were used to investigate the field utilization of a secant totally softened friction angle. There are 45 slope failures with a portion of observed slip surface at residual condition and the back-scarp generating fully softened shear strength, and 18 slope failures with the entire observed slip surface being fully softened (Mesri, Wang & Kane, 2022).	“clay-shale, slope”
2022	In the Apennines, tectonized clay shales are prominent. The poor mechanical properties of these structurally complex materials cause their sloping deposits extremely unstable. In fact, small mountain communities and the infrastructure that services them are constantly at risk of becoming ineffective, requiring high maintenance costs. The analysis of the effects of slope movements on structures and individual artifacts is an especially difficult task that requires specific and targeted approaches. This paper examines the interaction between the unsteady movement of slopes in tectonites clay shales and tunnels in a number of cases (Comegna & Picarelli, 2022).	“clay-shale, landslide”

TABLE 3 (cont.)

2021	Investigations conducted primarily in the United Kingdom and Italy indicate that the accumulation of significantly positive excess pore pressures induced by the processes of undrained loading is the cause of these specific slope movements. In the case of tectonized clay shales, this interpretation warrants further investigation; in fact, given the structure and stress background of such overconsolidated deposits, the rise of high certain excess pore pressures is not an expected consequence of undrained loading. This research attempts to interpret this not-so-minor aspect of the issue by providing experimental data that emphasize the high susceptibility of these soils to dramatic degradation due to chemistry changes in the pore fluid (Picarelli, Di Maio & De Rosa, 2021).	“clay-shale, slope”
2021	This study presents the findings of an extensive examination of the sluggish movements of two underground earthflows in the tectonized clay shales of the southern Apennines. The accumulated movements have caused extensive damage to structures and infrastructure over the years, resulting in significant social and economic costs. Since 2005, depth and superficial displacements, as well as pore water pressures, have been monitored; in some areas of the slope, inclinometers have been used to monitor displacements for roughly three decades. Utilize satellite interferometry to monitor the area. To mitigate this issue, the most granular analysis was performed on satellite data pertaining to regions where displacements and paths are definitely identified through inclinometers and GPS. The data confirmation allowed for the confident application of remote sensing results over a larger region. Consequently, images obtained by the COSMO-SkyMed satellite structure, supplemented by the European remote sensing satellites (ERSs) data sets and Envisat data, enabled an analysis of the kinematic history of the urbanized area, even though inclinometer displacement series were only available for limited periods (Vassallo et al., 2021).	“clay-shale, landslide”

Source: own work.

Discussion

The whole research about clay shale analysis is spread around the world. America, Europe, and Asia are the continents that dominate clay shale research. However, the landslide and slope issues in the clay shale subgrade are presented in different countries. Although the United States does the highest research on clay shale, the study about the slope of clay shale needs to be shown in this area. Italy has the biggest number of publications related to the clay shale slope. This result is suitable because Italy has the Apennines area that has a huge issue with clay shale, which provides research about clay shale slope investigations in the southern and northern Apennines (Dondi, 1999; Veniale, Delgado, Marinomi & Setti, 2002; Di Leo, Dinelli, Mongelli & Schiattarella, 2002; Picarelli, Urciuoli, Mandolini & Ramondini, 2006; Mongelli, Critelli, Dinelli, Paternoster & Perri, 2010; Cavalcante, Belviso, Piccarreta & Fiore, 2014; Bayer, Simoni, Mulas, Corsini & Schmidt, 2018; Costanzo, d’Onofrio & Silvestri, 2019; Smeraglia et al., 2021;

Squarzoni, Bayer, Franceschini & Simoni, 2020; Veniale, Pellegrino, Marinomi & Setti, 2023).

In terms of year of publication, 2 research studies about clay shale and clay shale slope have a similar trend. The number of articles increases slightly in the first year through 2010. In addition, after 2010 until the end of the period, this study goes up rapidly. These conditions happen because of the development of technology and system that support the clay shale research and investigation. Furthermore, the need for an infrastructure construction project leads the engineer to deal with the clay shale issue as a subgrade site.

The output of the VOSviewer analysis has shown 5 clusters with different themes. The topic of the landslide has few links with other clusters, such as clay mineralogy and rock mechanics. Meanwhile, the strong link is only in deformation, slope stability, and clay shale. These circumstances present a gap among these categories and require further study.

Regarding the result of the clay shale slope from VOSviewer, the output shows the domination of links among all clusters. Three clusters have been depicted in this analysis. In addition, the wide gap is described as a link between slope dynamics and other topics. This output means potential research is required to conduct dynamic force issues for clay shale slope study.

Conclusions

the article examines the published research on clay sale and clay shale slope study using bibliometric analysis. All of the results suggest the need for further investigation to fill the knowledge gap regarding clay shale, landslide, and clay mineralogy. Moreover, the clay shale slope has presented the need for further research about dynamic force and its deformation through clay shale slope analysis.

References

- Agrawal, V. K., Manhas, G. S. & Sharda, Y. P. (1993). Problems of an earth dam on weak rocks in Outer Himalayas, Punjab, India. *Engineering Geology Special Publication*, 8, 441–446. [https://doi.org/10.1016/0148-9062\(94\)90801-x](https://doi.org/10.1016/0148-9062(94)90801-x)
- Agung, P., Pramusandi, S. & Damianto, B. (2017). Identification and classification of clayshale characteristic and some considerations for slope stability. *African Journal of Environmental Science and Technology*, 11 (4), 163–197. <https://doi.org/10.5897/ajest2014.1792>
- Al-Arfaj, M. K., Amanullah, M., Sultan, A. S., Hossain, E. & Abdulraheem, A. (2014). Chemical and mechanical aspects of wellbore stability in shale formations: a literature review. *Society*

- of Petroleum Engineers – 30th Abu Dhabi International Petroleum Exhibition and Conference, ADIPEC 2014: Challenges and Opportunities for the Next 30 Years, 1*, 1–11. <https://doi.org/10.2118/171682-ms>
- An, N., Zagorščak, R. & Thomas, H. R. (2022). Adsorption characteristics of rocks and soils, and their potential for mitigating the environmental impact of underground coal gasification technology: a review. *Journal of Environmental Management*, 305, 114390. <https://doi.org/10.1016/j.jenvman.2021.114390>
- Aristizabal, D., Lara, A. J., Payares, V. & Alzate, A. (2021). Bibliometric analysis and research trends of a journal: Magazine of Civil Engineering. *Library Philosophy and Practice*, 5414. Retrieved from: <https://digitalcommons.unl.edu/libphilprac/5414> [accessed: 31.07.2023].
- Bayer, B., Simoni, A., Mulas, M., Corsini, A. & Schmidt, D. (2018). Deformation responses of slow moving landslides to seasonal rainfall in the Northern Apennines, measured by InSAR. *Geomorphology*, 308, 293–306. <https://doi.org/10.1016/j.geomorph.2018.02.020>
- Bonini, M., Debernardi, D., Barla, M. & Barla, G. (2009). The mechanical behaviour of clay shales and implications on the design of tunnels. *Rock Mechanics and Rock Engineering*, 42, 361–388. <https://doi.org/10.1007/s00603-007-0147-6>
- Burnham, J. F. (2006). Scopus database: a review. *Biomedical Digital Libraries*, 3 (1), 1–8. <https://doi.org/10.1186/1742-5581-3-1>
- Cavalcante, F., Belviso, C., Piccarreta, G. & Fiore, S. (2014). Grain-size control on the rare earth elements distribution in the late diagenesis of cretaceous shales from the Southern Apennines (Italy). *Journal of Chemistry*, 2014, 841747. <https://doi.org/10.1155/2014/841747>
- Comegna, L. & Picarelli, L. (2022). Experience about landslide-tunnel interaction in tectonized clay shales [Esperienze sull'interazione franagalleria in argilliti tettonizzate]. *Rivista Italiana Di Geotecnica*, 56 (1), 17–31. <https://doi.org/10.19199/2022.1.0557-1405.017>
- Costanzo, A., d'Onofrio, A. & Silvestri, F. (2019). Seismic response of a geological, historical and architectural site: the Gerace cliff (southern Italy). *Bulletin of Engineering Geology and the Environment*, 78, 5617–5633. <https://doi.org/10.1007/s10064-019-01515-0>
- Di Leo, P., Dinelli, E., Mongelli, G. & Schiattarella, M. (2002). Geology and geochemistry of Jurassic pelagic sediments, Scisti silicei Formation, southern Apennines, Italy. *Sedimentary Geology*, 150 (3–4), 229–246. [https://doi.org/10.1016/S0037-0738\(01\)00181-6](https://doi.org/10.1016/S0037-0738(01)00181-6)
- Ding, X. & Yang, Z. (2022). Knowledge mapping of platform research: a visual analysis using VOSviewer and CiteSpace. *Electronic Commerce Research*, 22 (3), 787–809. <https://doi.org/10.1007/s10660-020-09410-7>
- Dondi, M. (1999). Clay materials for ceramic tiles from the Sassuolo District (northern Apennines, Italy). Geology, composition and technological properties. *Applied Clay Science*, 15 (3–4), 337–366. [https://doi.org/10.1016/S0169-1317\(99\)00027-7](https://doi.org/10.1016/S0169-1317(99)00027-7)
- Donthu, N., Kumar, S., Mukherjee, D., Pandey, N. & Lim, W. M. (2021). How to conduct a bibliometric analysis: an overview and guidelines. *Journal of Business Research*, 133, 285–296. <https://doi.org/10.1016/j.jbusres.2021.04.070>
- Einstein, H. H. (2000). Tunnels in Opalinus Clayshale – a review of case histories and new developments. *Tunnelling and Underground Space Technology*, 15 (1), 13–29. [https://doi.org/10.1016/s0886-7798\(00\)00025-0](https://doi.org/10.1016/s0886-7798(00)00025-0)

- Gouw, T. L. (2018). Geosynthetics application in Indonesia – a case histories. *Geotechnical Engineering Journal of the SEAGS & AGSSEA*, 49 (4), 132–144. Retrieved from: <https://www.scopus.com/inward/record.uri?eid=2-s2.0-85057556087&partnerID=40&md5=-fae89e00e7214f6e7db4af67f592bf0a> [accessed: 31.07.2023].
- Gouw, T. L., Lelli, M., Cerro, M., Meinata, L. E., Laneri, R. & Rimoldi, P. (2016). High hybrid reinforced soil slope as runway support – Tana Toraja airport case study. In *GA 2016 – 6th Asian Regional Conference on Geosynthetics: Geosynthetics for Infrastructure Development, Proceedings, 2016*, 364–374. <https://www.scopus.com/inward/record.uri?eid=2-s2.0-85009080866&partnerID=40&md5=ac6044bb584e6b2f291f7f3175dd070e> [accessed: 31.07.2023].
- Hendry, H., Somantri, A. K., Febriansya, A. & Nurhadi, M. D. (2020). Substructure reinforcement study of Cisomang bridge at Purwakarta-Bandung-Cileunyi toll road, West Java Province, Indonesia. *IOP Conference Series: Materials Science and Engineering*, 732 (1), 012027. <https://doi.org/10.1088/1757-899X/732/1/012027>
- Herbosch, A., Liégeois, J. P. & Pin, C. (2016). Coticules of the Belgian type area (Stavelot-Venn Massif): Limy turbidites within the nascent Rheic oceanic basin. *Earth-Science Reviews*, 159, 186–214. <https://doi.org/10.1016/j.earscirev.2016.05.012>
- Hobson, G. D. (1980). *Developments in Petroleum Geology – 2*. Amsterdam: Elsevier Science.
- Huadi, F., Aldea, C., Mackereth, B. & Mukhlis, T. (2010). Successful KCl-free, highly inhibitive and cost-effective water-based application, offshore East Kalimantan, Indonesia. *Society of Petroleum Engineers – IADC/SPE Asia Pacific Drilling Technology Conference 2010, 2010*, 125–131. Retrieved from: <https://www.scopus.com/inward/record.uri?eid=2-s2.0-79953115141&partnerID=40&md5=700d1d1f80306a5c23762a3d5c6a06a6> [accessed: 31.07.2023].
- Jinhua, F., Shixiang, L., Qiheng, G., Wen, G., Xinping, Z. & Jiangyan, L. (2022). Enrichment conditions and favorable area optimization of continental shale oil in Ordos Basin. *Shiyou Xuebao/Acta Petrolei Sinica*, 43 (12), 1702. <https://doi.org/10.7623/syxb202212003a>
- Khairul, N. A. S. & Musta, B. (2022). Engineering properties and slope inventory of clayey soil from the Trusmi Formation in Bundu Tuhan, Sabah. *IOP Conference Series: Materials Science and Engineering*, 1229 (1), 012010. <https://doi.org/10.1088/1757-899x/1229/1/012010>
- Kuzior, A. & Sira, M. (2022). A bibliometric analysis of blockchain technology research using VOSviewer. *Sustainability*, 14 (13), 8206. <https://doi.org/10.3390/su14138206>
- McAllister, J. T., Lennertz, L. & Atencio Mojica, Z. (2022). Mapping a discipline: a guide to using VOSviewer for bibliometric and visual analysis. *Science & Technology Libraries*, 41 (3), 319–348. <https://doi.org/10.1080/0194262X.2021.1991547>
- Mesri, G. & Shahien, M. (2004). Closure to “Residual Shear Strength Mobilized in First-Time Slope Failures” by G. Mesri and M. Shahien. *Journal of Geotechnical and Geoenvironmental Engineering*, 130 (5), 548–549. [https://doi.org/10.1061/\(asce\)1090-0241\(2004\)130:5\(548\)](https://doi.org/10.1061/(asce)1090-0241(2004)130:5(548))
- Mesri, G., Wang, C. & Kane, T. (2022). Meaning, measurement, and field application of fully softened shear strength of stiff clays and clay shales. *Canadian Geotechnical Journal*, 59 (6), 952–964. <https://doi.org/10.1139/cgj-2020-0663>

- Mo, K. H., Ling, T. C., Tan, T. H., Leong, G. W., Yuen, C. W. & Shah, S. N. (2021). Alkali-silica reactivity of lightweight aggregate: a brief overview. *Construction and Building Materials*, 270, 121444. <https://doi.org/10.1016/j.conbuildmat.2020.121444>
- Mongelli, G., Critelli, S., Dinelli, E., Paternoster, M. & Perri, F. (2010). Mn-and Fe-carbonate rich layers in Meso-Cenozoic shales as proxies of environmental conditions: A case study from the southern Apennine, Italy. *Geochemical Journal*, 44 (3), 211–223. <https://doi.org/10.2343/geochemj.1.0064>
- Morrisey, L. J. (2020). Bibliometric and bibliographic analysis in an era of electronic scholarly communication. In W. Wei (Ed.), *Scholarly Communication in Science and Engineering Research in Higher Education* (p. 12). Abingdon-on-Thames: Routledge.
- Mulyawati, I. B. & Ramadhan, D. F. (2021). Bibliometric and visualized analysis of scientific publications on geotechnics fields. *ASEAN Journal of Science and Engineering Education*, 1 (1), 37–46. <https://doi.org/10.17509/ajsee.v1i1.32405>
- Nandiyanto, A. B. D. & Al Husaeni, D. F. (2021). A bibliometric analysis of materials research in Indonesian journal using VOSviewer. *Journal of Engineering Research (Kuwait)*, 9, 1–16. <https://doi.org/10.36909/jer.ASSEEE.16037>
- Nomura, R. (2003). Assessing the roles of artificial vs. natural impacts on brackish lake environments: foraminiferal evidence from Lake Nakaumi, southwest Japan. *The Journal of the Geological Society of Japan*, 109 (4), 197–214. <https://doi.org/10.5575/geosoc.109.197>
- Pardoyo, B., Kresno, W. S., Fahreza, D. A. & Maulana, T. A. (2020). The effect of clay shale drying on the reduction of compressive strength and durability in bawen sub-district, semarang regency. *Civil Engineering and Architecture*, 8 (6), 1359–1369. <https://doi.org/10.13189/cea.2020.080619>
- Pellegrino, L., Natalicchio, M., Birgel, D., Pastero, L., Carnevale, G., Jordan, R. W., Peckmann, J., Zanellato, N. & Dela Pierre, F. (2023). From biogenic silica and organic matter to authigenic clays and dolomite: insights from Messinian (upper Miocene) sediments of the Northern Mediterranean. *Sedimentology*, 70 (2), 1–33. <https://doi.org/10.1111/sed.13053>
- Picarelli, L., Di Maio, C. & De Rosa, J. (2021). Processes and mechanisms governing the transition of slides in tectonized clays and clay shales into rapid earthflows. *Rivista Italiana Di Geotecnica*, 55 (4), 53–67.
- Picarelli, L., Olivares, L., Di Maio, C., Silvestri, F., Di Nocera, S. & Urciuoli, G. (2003). *Structure properties and mechanical behaviour of the highly plastic intensely fissured Bisaccia clay shale*. Retrieved from: https://www.researchgate.net/profile/Caterina-Di-Maio/publication/284054317_Structure_properties_and_mechanical_behaviour_of_the_highly_plastic_intensely_fissured_Bisaccia_clay_shale/links/57ac770208ae0932c9748245/Structure-properties-and-mechanical-behaviour-of-the-highly-plastic-intensely-fissured-Bisaccia-clay-shale.pdf [accessed: 31.07.2023].
- Picarelli, L., Urciuoli, G., Mandolini, A. & Ramondini, M. (2006). Softening and instability of natural slopes in highly fissured plastic clay shales. *Natural Hazards and Earth System Sciences*, 6 (4), 529–539. <https://doi.org/10.5194/nhess-6-529-2006>
- Pingquan, W., Tao, T., Junlin, S., Qiurun, W., Ping, Y. & Yang, B. (2022). Review of application of molecular simulation in inhibiting surface hydration expansion of clay minerals. *Chemistry and Technology of Fuels and Oils*, 58 (1), 63–76. <https://doi.org/10.1007/s10553-022-01352-0>

- Powell, J. S., Siemens, G. A., Take, W. A. & Remenda, V. H. (2013). Characterizing the swelling potential of Bearpaw clayshale. *Engineering Geology*, 158, 89–97. <https://doi.org/10.1016/j.enggeo.2013.03.006>
- Rahardjo, P. P., Halim, Y. & Wisanto, H. (2012). The use of geotechnical instrumentation and finite element analysis for assessment of bridge foundation stability due to breccia resliding over clayshale. In S. Miura, T. Ishikawa, N. Yoshida, Y. Hisari & N. Abe (Eds), *Advances in Transportation Geotechnics II* (pp. 737–742). CRC Press/Balkema.
- Rosly, M. H., Mohamad, H. M., Bolong, N. & Harith, N. S. H. (2022). An overview: relationship of geological condition and rainfall with landslide events at East Malaysia. *Trends in Sciences*, 19 (8), 3464–3464. <https://doi.org/10.48048/tis.2022.3464>
- Sagitaningrum, F. H., Kamaruddin, S. A., Nazir, R., Soepandji, B. S. & Alatas, I. M. (2023). Lesson learned from weathering clay shale residual interface shear strength testing method. *Proceedings of the 5th International Conference on Rehabilitation and Maintenance in Civil Engineering, 2023*, 523–531. https://www.scopus.com/inward/record.uri?eid=2-s2.0-85137766973&doi=10.1007%2f978-981-16-9348-9_46&partnerID=40&md5=1a1a9d5aa49ba7d3e8ebe345d2fe06dc [accessed: 31.07.2023].
- Shahbazi, R., Elahi, J. & Khalili, L. (2022). Scientific outputs and co-authorship patterns in the fields of electronic, civil and mechanical engineering of Azarbaijan Shahid Madani University (2000–2019): a scientometric analysis. *International Journal of Information Science and Management*, 20 (2), 181–200.
- Sharifigaliuk, H., Mahmood, S. M., Rezaee, R. & Saeedi, A. (2021). Conventional methods for wettability determination of shales: a comprehensive review of challenges, lessons learned, and way forward. *Marine and Petroleum Geology*, 133, 105288. <https://doi.org/10.1016/j.marpetgeo.2021.105288>
- Sharma, V. K. (1995). Probable risk estimation due to reservoir induced seismicity at Jamrani dam Project, Kumaon Himalaya, India. *Bulletin of the International Association of Engineering Geology*, 52 (1), 103–108. <https://doi.org/10.1007/bf02602687>
- Sharma, V. K. (1996). Probable risk estimation due to reservoir induced seismicity at Jamrani dam project, Kumaon Himalaya, India. (1996). *International Journal of Rock Mechanics and Mining Sciences & Geomechanics Abstracts*, 33 (6), 266A. [https://doi.org/10.1016/0148-9062\(96\)81877-8](https://doi.org/10.1016/0148-9062(96)81877-8)
- Shields, D. H. (2022). Preliminary design of a deep open pit mine (Bukit Asam): an exercise in the engineering method. In *Geotechnical Stability in Surface Mining* (pp. 11–22). Boca Raton: CRC Press. <https://www.scopus.com/inward/record.uri?eid=2-s2.0-0022937442&partnerID=40&md5=5dd6f0080d2e8c42065bd6e13d121154> [accessed: 31.07.2023].
- Simatupang, P. T., Alatas, I. M., Redyananda, A. K. & Purnomo, E. A. (2022). Shear strength and durability behaviors of compacted weathered clay shale mixture using portland cement. *Journal of the Civil Engineering Forum*, 8 (2), 169–178. <https://doi.org/10.22146/jcef.3491>
- Smeraglia, L., Giuffrida, A., Grimaldi, S., Pullen, A., La Bruna, V., Billi, A. & Agosta, F. (2021). Fault-controlled upwelling of low-T hydrothermal fluids tracked by travertines in a fold-and-thrust belt, Monte Alpi, Southern Apennines, Italy. *Journal of Structural Geology*, 144, 104276. <https://doi.org/10.1016/j.jsg.2020.104276>

- Snyder, H. (2019). Literature review as a research methodology: an overview and guidelines. *Journal of Business Research*, 104, 333–339. <https://doi.org/10.1016/j.jbusres.2019.07.039>
- Soegoto, H., Soegoto, E. S., Luckyardi, S. & Rafdhi, A. A. (2022). A bibliometric analysis of management bioenergy research using vosviewer application. *Indonesian Journal of Science and Technology*, 7 (1), 89–104. <https://doi.org/10.17509/ijost.v7i1.43328>
- Squarzoni, G., Bayer, B., Franceschini, S. & Simoni, A. (2020). Pre-and post-failure dynamics of landslides in the Northern Apennines revealed by space-borne synthetic aperture radar interferometry (InSAR). *Geomorphology*, 369, 107353. <https://doi.org/10.1016/j.geomorph.2020.107353>
- Tamala, J. K., Maramag, E. I., Simeon, K. A. & Ignacio, J. J. (2022). A bibliometric analysis of sustainable oil and gas production research using VOSviewer. *Cleaner Engineering and Technology*, 7, 100437. <https://doi.org/10.1016/j.clet.2022.100437>
- Wang, X., Xu, Z., Ge, Z., Zavadskas, E. K. & Skačkauskas, P. (2020). An overview of a leader journal in the field of transport: A bibliometric analysis of computer-aided civil and infrastructure engineering from 2000 to 2019. *Transport*, 35 (6), 557–575. <https://doi.org/10.3846/transport.2020.14140>
- Eck, N. J. van & Waltman, L. (2010). Software survey: VOSviewer, a computer program for bibliometric mapping. *Scientometrics*, 84 (2), 523–538. <https://doi.org/10.1007/s11192-009-0146-3>
- Eck, N. J. van & Waltman, L. (2017). Citation-based clustering of publications using CitNetExplorer and VOSviewer. *Scientometrics*, 111, 1053–1070. <https://doi.org/10.1007/s11192-017-2300-7>
- Vassallo, R., De Rosa, J., Di Maio, C., Reale, D., Verde, S. & Fornaro, G. (2021). In situ and satellite long-term monitoring of two earthflows of the Italian southern Apennines and of the structures built on them [Monitoraggio di lungo periodo in situ e satellitare di due colate di terreni argillosi dell'Appennino meridionale e delle strutture su di esse costruite]. *Rivista Italiana Di Geotecnica*, 55 (4), 77–95. <https://doi.org/10.19199/2021.4.0557-1405.077>
- Veniale, F., Delgado, A., Marinoni, L. & Setti, M. (2002). Dickite genesis in the 'varicoloured' clay-shale formation of the Italian Apennines: an isotopic approach. *Clay Minerals*, 37 (2), 255–266. <https://doi.org/10.1180/0009855023720032>
- Videras Rodríguez, M., Melgar, S. G., Cordero, A. S. & Márquez, J. M. A. (2021). A critical review of unmanned aerial vehicles (Uavs) use in architecture and urbanism: scientometric and bibliometric analysis. *Applied Sciences*, 11 (21), 9966. <https://doi.org/10.3390/app11219966>
- Yu, D., Xu, Z. & Antuchevičienė, J. (2019). Bibliometric analysis of the journal of civil engineering and management between 2008 and 2018. *Journal of Civil Engineering and Management*, 25 (5), 402–410. <https://doi.org/10.3846/jcem.2019.9925>
- Zanzinger, H., Koerner R. M. & Gartung, E. (Eds) (1986). *Clay geosynthetic barriers*. London: A.A. Balkema. <https://doi.org/10.1201/9781003078777>
- Zhang, Q., Wang, J., Zhou, B. & Huang, J. (2022). Failure Mode and Countermeasures of Clay-shale Cutting Slope in Karawang Area, Indonesia [印尼Karawang地区泥页岩路堑边坡破坏模式及对策]. *Journal of Railway Engineering Society*, 39 (8), 35–39.

Summary

A systematic review of clay shale research development for slope construction.

The issue of stability controlling cutting slopes is particularly important in clay-shale slopes, a typical expanding sedimentary layer with poor engineering geological conditions and mechanical characteristics. Therefore, research on the causes of failure and remedies for clay-shale cutting slopes is required to serve as an overview for handling and preserving clay-shale slopes in identical conditions. However, the trusted information about the need for further related clay shale research and clay shale in slope stability has yet to be specifically presented. This review study summarizes the published research for clay shale beginning in 1980, presents a bibliometric analysis to examine the published research based on year and country, and provides various study trends in cluster diagram using the VOSviewer program. The analysis also summarized some key goals, effective methodology, and significant findings from the most recent studies to extract information from them that would benefit future research. In conclusion, the results show the need for developing research to fill the knowledge gap regarding clay shale, landslide, and clay mineralogy. In addition, the clay shale slope analysis has revealed the need for additional research into dynamic force and its deformation.

Gabriela KOCOURKOVA¹  <https://orcid.org/0000-0002-7710-767X>

Eva VITKOVA²  <https://orcid.org/0000-0002-2028-953X>

Svatopluk PELCAK³  <https://orcid.org/0000-0002-5812-9865>

Brno University of Technology, Faculty of Civil Engineering, the Czech Republic

Labor costs in a construction company in the Czech Republic – a case study

Keywords: labor costs, construction company, wage costs

Introduction

Nowadays, the inflation rate in the Czech Republic reaches two-figure digits which results in a great pressure on the increase in wages of the employees, both generally and in the construction industry. At the same time, the fact that some professions are highly specialized and there tend to be fewer professional workers in production, forces the construction companies to keep these professions as a part of their workforce. This, however, entails increased costs per such worker and thus increased costs per construction contract. Every company monitors all production costs very carefully; however, it is also necessary to have a detailed overview associated with the labor costs on each construction contract, both the company's own labor costs and the subcontractor's labor costs. If wages or even other costs associated with employees increase, it could have a significant impact on the profitability of the contract.

The aim of the article is to quantify the total labor costs of the company in percent. Moreover, it aims to show the labor costs on a construction contract both from

the terms of the company's labor costs of its own employees and the subcontractors' labor costs.

The construction industry represents one of the pillars of the country's economy. It is a sector that is closely connected to the development of the territory, including environmental impacts. Construction productivity is very important for the growth of the national economy and plays a significant role in the industry by Naoum (2016). It contributes to the development of the territory by expanding infrastructure, creating conditions for the development of the economy and the associated increase in jobs during the construction period in the region together with investment construction by the Stavebnictví České Republiky 2019 (2020).

The construction sector provides employment for a wide range of the population in terms of education, being able to absorb workers with lower or different qualifications. The construction sector employs 8% of the total number of persons employed in the Czech Republic. It provides jobs for foreign minorities, whose employment in the Czech construction sector is currently crucial for the smooth and economical operation of construction companies due to the shortage of domestic workers. This reflects the normal operation of the construction industry in the world by Jang, Kim, Kim and Kim (2011), and Smart Stavebnictví (2012). According to Rabušić (2001), the biggest benefit of such migration is the taxes that immigrants working in the Czech Republic have to pay on their income.

According to Šimková (2016), the importance of migration in the construction sector is that foreign workers are willing to work in worse conditions with lower financial remuneration. Moreover, the construction sector faces the issue of labor productivity as one of the biggest problems. There are several factors related to productivity, one of them being the lack of motivation, where one of the main motivation tools is the financial reward of workers in Hamza, Shahid, Bin Hainin and Nashwan (2022). Although motivation in the form of financial remuneration is directly reflected in an increase in labor costs, its increase is also directly linked to an increase in labor productivity. Thus, it can be stated that the work productivity increases with the increase of the labor costs in Chen, Wu and Van Ark (2009).

Companies are constantly struggling with their labor costs. On the one hand, some companies value their employees more and thus have more benefits to motivate them which is associated with higher costs, and on the other hand, some companies pay only what is required by the state's labor laws. The composition and magnitude of the companies' labor costs of own employees varies from company to company. In the case of contracted outsourced workers, companies have only one total cost to pay the hired person only for the work done.

According to the Czech Ministry of Industry and Trade (MIT CZ, 2023), labor costs in the period under observation 2016–2020 amounted to 13.60% on average in relation concerning the sales revenues for the construction sector (Table 1). Labor costs include the sum of wage costs per employee, compulsory social and health insurance and other costs related to, for example, employer contributions to life insurance or pension schemes.

TABLE 1. Percentage of labor costs to sales revenue from profit and loss statement from 2016 to 2020 period

Specification	2016	2017	2018	2019	2020
Labor costs [%]	13.87	13.96	13.40	13.35	13.46
Wage costs [%]	10.01	10.86	9.51	9.49	9.51
Social and health insurance costs [%]	3.58	3.89	3.63	3.62	3.96
Other costs [%]	0.29	0.32	0.25	0.25	0.16

Source: own work according to MIT CZ (2023).

The above-stated values are taken from construction companies of various sizes operating in the Czech Republic. On average, 32 construction companies entered this analysis for the period 2016–2020. The above-stated costs are classified according to the profit and loss statements, which is determined by Act No. 563/1991 Coll. on accounting. As mentioned earlier, Labor costs form the sum of the following:

- wage costs including wages under an agreement to perform work or under agreements to complete the job,
- social and health insurance costs, which in the Czech Republic amount to 33.8% of gross wages,
- other costs incurred in connection with the payment of life insurance or pension contributions or costs associated with food allowances, etc.

A wage is a reward for work done, i.e., the price of work. Act No. 1/1992 Coll. on wages states that it is a monetary remuneration or remuneration of monetary value provided by an employer to an employee in return for work.

It is provided to the employee according to 3 indicators, namely according to the complexity, responsibility and difficulty of the work (assessment according to the education, knowledge and skills needed to perform the work), according to the difficulty of the working conditions (it means the division of working time, for example, into shifts, or work at night, on holidays, the risk level of the working environment is also taken into account) and according to the work performance and the results achieved (the main point is the quality of the work performed).

The basis of the remuneration system is the wage regulations. They are divided into legal norms at the state level and at the internal company level. The defining legal standard is Act No. 262/2006 Coll. Labor Code. Other important legal standards influence the working environment and remuneration in the Czech Republic. These are mainly government laws and regulations: Act No. 435/2004 Coll. on employment, Act No. 2/1991 Coll. on collective bargaining, Act No. 592/1992 Coll. on general health insurance contributions, Act No. 589/1992 Coll. on social security contributions and contributions to the State Employment Policy, Act No. 586/1992 Coll. on income tax, as amended, Act No. 110/2019 Coll., on the processing of personal data, Government Regulation No. 567/2006 Coll. on the minimum wage and Government Regulation No. 531/2021 Coll. on salary rates in Public Services and Administration. Each company may have its own internal regulations for rewarding and motivating its employees.

The wage costs of a company consist primarily of the sum of the gross wages of all employees plus the social and health insurance paid by the employer on behalf of the employees. The gross wage is calculated by adding the basic wage and the variable wage. Under current legislation, the social insurance paid by the employer on behalf of the employee is 24.8% of the gross wage and the health insurance is 9% of the gross wage according to Act No. 592/1992 Coll. and Act No. 589/1992 Coll.

Although these costs are high, there are other costs associated with the employees; mainly costs related to education and mandatory training of employees, mandatory liability insurance of the company, compensation for sick leave, purchase of protective equipment and equipment for employees, medical allowances, bonus system – e.g. food allowances, contributions to retirement savings, recreational allowances, etc. However, the company does not have all these additional costs if it hires an external company or a tradesman to do the work. There is a constant decision-making process in every company whether it is more economically advantageous to employ a worker or just to use the work of external subcontractors.

Currently, a high inflation rate is one of the parameters affecting wage growth. It is evident, based on the studies carried out, that the rise in prices in the society puts pressure on the increase of wages. This fact is mainly proved by the correlation between the growth of the price level and the level of wages in the economy by Darrat (1994). However, it has to be taken into account that in most cases this is a reaction to the currently rising inflation. Therefore, as inflation rises, wages rise, but the rise in wages is slower and more gradual than the rise in the price level Domash and Summers (2022), and Jordà and Nechio (2023) too. It must also be taken into account that wage increases do not necessarily lead to higher productivity,

but may only keep workers productive at the same level in Cruz (2023). This especially applies if there is an increase in the price level in the economy.

The Czech Statistical Office (CSO) publishes an overview of retrospective data from the field of labor market statistics. The data was obtained from surveys of economic entities or from administrative sources. The survey of economic entities is carried out depending on the number of employees, either by comprehensive or sample surveys. In the case of a sample survey, the transformation to the base set is carried out on all active units included in the CSO register of economic entities. The overview contains the development of the most important indicators in the sectoral and territorial classifications. The sectoral classification is based on the “Classification of Economic Activities CZ-NACE”, valid since 1 January 2008, which fully corresponds to the international classification NACE Rev. 2 at the reported level. The territorial classification is made according to the CZ-NUTS classification, which is in accordance with the Regulation of the European Parliament and the Council of Europe on the establishment of a common classification of territorial units for statistics (NUTS).

Wages rise as the productivity of the economy rises. The evolution of average wages for the whole economy and the construction sector in the Czech Republic from 2005 to 2022 can be seen in Figure 1.

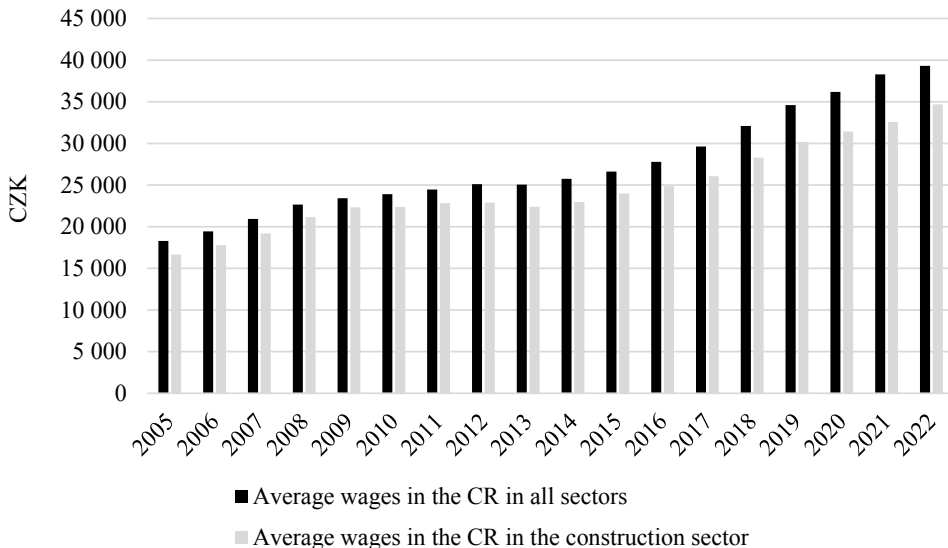


FIGURE 1. Development of average wage in all sectors/construction sector in the Czech Republic (1 EUR = 24.50 CZK)

Source: own work according to CSO (2023).

The development of the average wage in the Czech construction industry has been lower than the average wage in the economy as a whole over the entire period. This difference has been gradually increasing over time. Whereas in 2005 the difference was around 9%, in 2022 it is already almost 12%. This disparity can be explained mainly by the significantly increasing wages in sectors of the economy such as banking, information technology and logistics, where wages are rising faster than in the construction sector.

Looking specifically at the South Moravian Region, where the company used in the case study in this article is located, it can be found that the average wage in its construction sector essentially mirrors the average wage in the construction sector in the whole country. This can be seen in Figure 2.

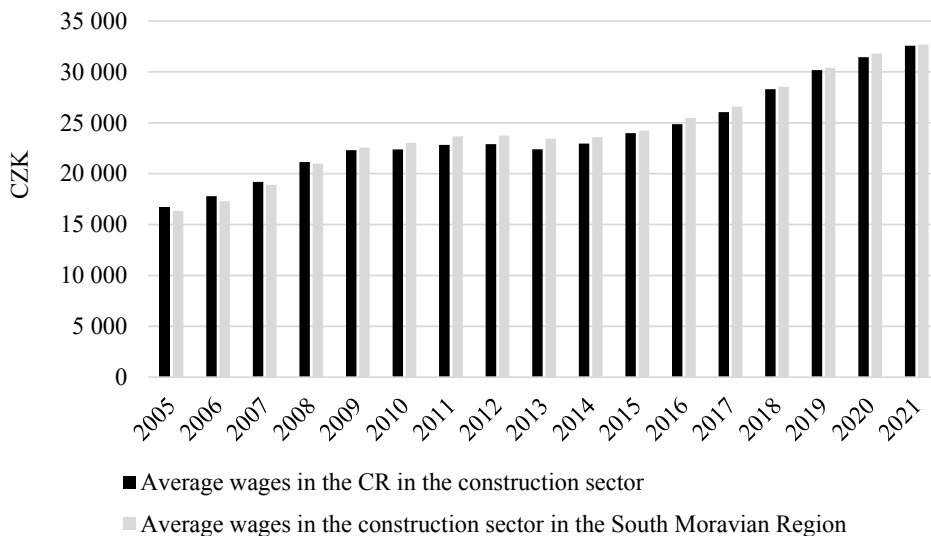


FIGURE 2. Development of average wage in the construction industry in the Czech Republic and the South Moravian Region (1 EUR = 24.50 CZK)

Source: own work according to CSO (2023).

Material and methods

Mainly analytical methods were used in the case study, which deals with the determination of labor costs in a construction company and a construction contract. These analytical methods were applied to the basic financial statements, namely the profit and loss statement. As part of the introduction to the case study, the observed

period was selected, namely the period 2016–2020. For further detailed analysis of labor costs in the company, 2019 was chosen as a sample year, due to the stable reporting of these costs.

The accounting statements like profit and loss statements were used for the case study, this statement can be referred to as income statement. This statement records the income and expenses associated with the operating and financial areas of the entities.

The financial analysis method used in the case study was the vertical method. This method belongs to the elementary methods that are commonly used in the financial management of companies. Vertical analysis is based on the percentage representation of a given item to the total item. The formula of vertical analysis can be expressed as follows:

$$\text{determination of percentage} = \frac{\text{research quantity}}{\text{basic quantity}} 100. \quad (1)$$

An arithmetic average was established to determine the value of the monitored items according to the formula below:

$$\bar{x} = \frac{1}{n}(x_1 + x_1 + \dots + x_n) = \frac{1}{n} \sum_{i=1}^n x_i. \quad (2)$$

The median was determined for the relevance of the outcome of the monitored items as follows:

$$Me(X) = x_{(N+1)/2} \quad (3)$$

In the case study, the methods described above were used in the following steps:

1. Vertical analysis was used in the cost analysis from profit and loss statements for the 2016–2020 period.
2. Individual analysis is used to quantification of all labor costs from the internal company documents for the year 2019.
3. The product of the wage rates and the number of hours worked is used to analysis of labor costs for a specific contract of the given company.
4. Final evaluation of the findings.

Results and discussion

The case study focuses on the analysis of the labor costs in a selected construction company. The period researched from the perspective of the whole company was the 2016–2020 period. The determination of the labor costs directly on the construction

contract was dated to 2019. The determination of the case study directly in the construction company was conditioned by the willingness of the company to cooperate and provide internal company information.

The research into the labor costs of the company was carried out in the following steps:

1. Cost analysis from profit and loss statements for the 2016–2020 period.
2. Quantification of all labor costs from the internal company documents for the year 2019.
3. Analysis of labor costs on a specific contract of a given company.
4. Final evaluation of the findings.

The labor costs are described in the case study using a real medium-sized construction company and its specific real contract. The construction company is based in the South Moravian Region of the Czech Republic (the Czech Republic is divided into 14 regions). The average sale revenues of the selected construction company are about CZK 400 million. The construction company employs about 130 employees. They are divided into production workers and technical and economic employees in the ratio of about 80 production workers and 50 technical and economic employees (percentage ratio is 62 : 38).

Workers are defined as those employees who are directly involved in the production process. Their work is predominantly physical and involves the use of tools. The result of the work of such a worker may be material goods or their repair or maintenance. A worker is for example a welder, a bricklayer, a roofer, etc.

Technical and economic employees are known as administrative staff, most often with a vocational or technical background. They operate mainly in the administration and management departments of a company. A technical and economic employee is for example the director himself, a secretary, an accountant, an economist or a budgeter, etc.

Input values to the analyses come from the financial statements of the accounting units (entities), which contain two basic financial statements, namely the profit and loss statement and the balance sheet, i.e. the balance sheet of assets and sources of coverage of these assets. The specification of these documents is determined by Act No. 563/1991 Coll. on accounting. They are published by the Ministry of Justice on its website.

Firstly, the profit and loss statement from the 2016–2020 period was used to determine data related to the company's sales remuneration and labor costs, which consist of wage costs, social and health insurance paid by the employer on behalf of employees and other personnel costs. This can be seen in Table 2.

TABLE 2. Revenues and personnel costs of the company from 2016 to 2020

Specification	2016	2017	2018	2019	2020
Sales revenues [thous. CZK]	252 573	345 142	422 279	481 309	441 835
Labor costs [thous. CZK]	51 158	54 877	56 648	60 238	63 778
Wage costs [thous. CZK]	36 901	39 381	41 261	43 830	46 186
Social and health insurance costs [thous. CZK]	12 320	13 183	13 793	14 655	15 366
Other costs [thous. CZK]	1 937	2 313	1 594	1 753	2 226

Source: own work according to MJ CZ (2023).

The data obtained shows that the share of labor costs in the company's sales revenues is 15.30% on average in the given years. The share of social security and health insurance and other costs in wages was also analyzed, i.e., how much the employer has to pay the employee in addition to his gross wages. The average figure for the period was determined to be 38.16%. See Table 3 for details.

TABLE 3. Observed shares for the years 2016 to 2020

Specification	2016	2017	2018	2019	2020	AVG	<i>Me</i>
Share of labor costs on sales revenues [%]	20.25	15.90	13.41	12.52	14.43	15.30	14.43
Share of insurance and other costs on wage costs [%]	38.64	39.35	37.29	37.44	38.09	38.16	38.09

Source: own work.

Labor costs are not just wage costs but consist of several items. A very important part represents the compulsory health and social insurance paid by the employer on behalf of the employee, as well as all training, travel and meal allowances, various compensations, etc. All such other costs are shown in Table 3. It contains all the employee-related costs of the company for the year 2019. The labor costs in Table 4 were determined based on a discussion with the construction company's economist where these costs were identified in the accounting records, analyzed and a summary value was determined. The value of labor costs identified in Table 4 is not broken down into costs related to workers and technical and economic employees. The workers likely have lower wages than the salaries of the technical and economic employees. It is important to show that the personnel costs do not consist solely of wage costs, health and social insurance costs, and other costs (Table 2), but also of costs that enter the profit and loss statement under other cost items and that can only be identified personally.

The individual labor costs per employee for 2019 were quantified in Table 5 based on the information. Table 5 shows that the ratio of the sum of social and health insurance costs and other costs to the total wage costs is 53.66%.

The ratio Σ of social and health insurance costs to wage costs = $23,262,298.70 / 43,352,832.00 = 53.66\%$.

The above-stated data shows that this construction company must add to its wage costs 53.66% of these costs to get the total labor costs. These costs, quantified as a percentage share, are reflected within the overhead costs in the cost of the construction contract.

TABLE 4. Labor costs for 2019

Type of cost	Value [CZK]
Wage costs	43 352 832.00
Travel – construction contracts	834 989.40
Fares – TES	678.02
Travel – meals	1 485 571.00
Training, occupation safety and health	604 259.30
Services – workers’ compensation	3 104 413.00
Compensation – doctor	398 059.00
Statutory social insurance	10 763 332.00
Statutory health insurance	3 892 259.00
Supplementary pension scheme – employer’s contribution	208 400.00
Other social costs	65 672.54
Liability insurance – company	443 756.52
Statutory social costs	1 460 908.92
Total labor costs per year	66 615 130.70

1 EUR = 24.50 CZK.

Source: own work according to Bellayova (2020).

TABLE 5. Summary of labor costs per employee for 2019

Type of cost	Costs [CZK]
Labor costs	66 615 130.70
Wage costs	43 352 832.00
Social and health insurance	14 655 591.00
Other costs	8 606 707.70

1 EUR = 24.50 CZK.

Source: own work.

In the next section, the study focused on quantifying the labor costs on a specific construction contract involving the renovation of a single-family house. The renovation took place at the turn of 2019/2020. This contract involved both the company's own employees and subcontractors. The subcontracts involved roof repairs, the supply and installation of UPVC windows and plumbing. Other work was carried out by the company's employees. The total cost of the contract was 950,000 CZK. All the invoices related to the work of the subcontractors, as well as the statements of work of its own employees who had participated in the contract, were obtained from the company's accounts.

Table 6 quantifies the direct wage costs of the contract. The wage costs were determined from accounting data as the product of the actual hours worked by the employee and his hourly rate of pay, i.e. the time wage. Various employees with different wage rates and different working hours worked on the contract during construction. The amount of costs for direct wages was found to be 116,285 CZK from the accounting statements. However, if we require to quantify the total labor cost of the company's own employees, it is necessary to add all other costs, the percentage of which has been determined and declared in Table 5.

The total cost of subcontracting was determined from the invoices received and from the purchase orders provided by the company. It was possible to allocate the amount on material and labor costs of the individual subcontracted companies from a detailed description of the individual invoices and consultation with the economist of the selected construction company. When invoices do not include material costs, a tradesman was hired only for work. The company uses piecework pay for subcontractors or tradesmen hired. Most of the time, it is up to the contractor to decide how to charge for the work. For example, for earth or demolition work, the unit is m³ and the corresponding unit price. Detailed description can be found in Table 7.

TABLE 6. Total company's labor costs on own employees on the contract

Document type	Number of hours	Wage rate	Amount [CZK]
Work timesheet – employees	4.00	160.00	640.00
Work timesheet – employees	26.00	160.00	4 160.00
Work timesheet – employees	58.25	160.00	9 320.00
Work timesheet – employees	54.00	160.00	8 640.00
Work timesheet – employees	35.00	159.00	5 565.00
Work timesheet – employees	19.00	155.00	2 945.00
Work timesheet – employees	46.00	159.00	7 314.00

TABLE 6 (cont.)

Work timesheet – employees	51.00	160.00	8 160.00
Work timesheet – employees	28.00	164.00	4 592.00
Work timesheet – employees	16.00	164.00	2 624.00
Work timesheet – employees	12.00	164.00	1 968.00
Work timesheet – employees	30.50	200.00	6 100.00
Work timesheet – employees	33.00	160.00	5 280.00
Work timesheet – employees	3.00	159.00	477.00
Work timesheet – employees	42.50	160.00	6 800.00
Work timesheet – employees	54.00	164.00	8 856.00
Work timesheet – employees	10.00	160.00	1 600.00
Work timesheet – employees	16.00	157.00	2 512.00
Work timesheet – employees	35.00	160.00	5 600.00
Work timesheet – employees	70.00	160.00	11 200.00
Work timesheet – employees	35.00	160.00	5 600.00
Work timesheet – employees	36.45	160.00	5 832.00
Total direct labor costs on the contract			116 285.00
Other labor costs (53.66% of direct wages)			62 398.53
Total labor costs per employee on the contract			178 683.53

1 EUR = 24.50 CZK.

Source: own work according to Bellayova (2020).

TABLE 7. Subcontractors' labor costs on the contract

Document type	Subcontract type	Total amount [CZK]	Material costs [CZK]	Labor costs [CZK]
Invoice received	Construction work	14 700	0	14 700
Invoice received	Roof repair	32 425	18 725	13 700
Invoice received	Delivery and installation of plastic elements	101 818	78 820	22 998
Invoice received	Supply and installation of piping	32 717	15 425	17 292
Invoice received	Demolition and earthworks	31 500	0	31 500
Invoice received	Earthworks and demolition work	19 200	0	19 200
Invoice received	Earthworks	1 950	0	1 950
Invoice received	Construction work	2 250	0	2 250
Total		236 560	112 970	123 590

1 EUR = 24.50 CZK.

Source: own work according to Bellayova (2020).

The total labor cost on the contract can be determined by summing up all company's own employees' labor costs and subcontractors' labor costs (Table 8).

It was calculated from the information obtained from the profit and loss statement for the years 2016 to 2020 of the selected construction company that the share of labor costs of the company in the sales revenue was 15.30% on average and that the share of social and health insurance and other costs in labor costs is on average 38.16%. However, it was subsequently found from the internal data of the company that the actual share of compulsory insurance (social and health insurance) and other wage costs forms 53.66% of the wage costs of the company which is a significantly higher amount.

TABLE 8. Labor costs on the contract

Type of costs	Amount
Own employees' labor costs [CZK]	178 683.53
Subcontractors' labor costs [CZK]	123 590.00
Total labor costs [CZK]	302 273.53
Total cost of the contract [CZK]	950 000.00
Share of labor costs on the contract price [%]	31.82

1 EUR = 24.50 CZK.

Source: own work.

It was possible to quantify the total labor cost of the contract thanks to the labor information obtained from the subcontractors' invoices, which was found to be 31.82% of the contract price. This figure is more than double the assumed proportion of labor costs from the company's profit and loss statement.

Conclusions

The paper aimed to quantify all the labor costs in the company and to show the labor costs on a construction contract, both in terms of own employees' labor costs and subcontractors' labor costs. This is important information for any company in times of rising wages and other costs due to huge inflation.

The data was obtained from publicly available sources – from accounting statements mandatorily published on the website of the Ministry of Trade and Industry, and from internal information in a medium-sized construction company. All employee-related costs were collected and analyzed. Furthermore, the specific construction

contract was analyzed so that the work of subcontractors and tradesmen hired for specific works was quantified.

This allowed us to accurately quantify the total labor costs in the company, which is more than double the figure from the accounting statements. The profit and loss statement of the selected construction company, on which the case study was based, shows that the average percentage representation of labor costs, which include wage costs and social and health insurance costs, is 15.30%. However, when all costs associated with employees as a labor force are identified in detail, it is evident that the total labor costs represent 31.82% of the sales remuneration. It results in doubled the value.

Acknowledgements

This paper has been developed under the project of the specific research at the Brno University of Technology Cost analysis of construction objects within the life cycle (FAST-J-22-7963 Socio-economic impacts of green space development in the context of land development projects).

References

- Act No. 563/1991 Coll. on accounting.
- Act No. 2/1991 Coll. on collective bargaining.
- Act No. 589/1992 Coll. on social security contributions and contributions to the State Employment Policy.
- Act No. 592/1992 Coll. on general health insurance contributions.
- Act No. 586/1992 Coll. on income tax, as amended.
- Act No. 1/1992 Coll. on wages.
- Act No. 435/2004 Coll. on employment.
- Act No. 262/2006 Coll. Labour Code.
- Act. No. 110/2019 Coll. on the processing of personal data.
- Bellayova, M. (2020). *Náklady na pracovní sílu ve stavebním podniku [Analysis of cost on the workforce in construction company]* (bachelor's thesis). Brno University of Technology, Brno. Retrieved from: https://www.vut.cz/studenti/zav-prace?zp_id=128654 [accessed: 06.06.2023].
- Chen, V. W., Wu, H. X. & Van Ark, B. (2009). More costly or more productive? Measuring changes in competitiveness in manufacturing across regions in China. *Review of Income and Wealth*, 55, 514–537. <https://doi.org/10.1111/j.1475-4991.2009.00329.x>
- Cruz, M. D. (2023). Labor productivity, real wages, and employment in OECD economies. *Structural Change and Economic Dynamics*, 66, 367–382. <https://doi.org/10.1016/j.strueco.2023.05.007>

- Czech Statistical Office [CSO], (2023). *Wages – time series*. Retrieved from: https://www.czso.cz/csu/czso/pmz_cr [accessed: 06.06.2023].
- Darrat, A. F. (1994). Wage growth and the inflationary process: a reexamination. *Southern Economic Journal*, 61 (1), 181–190. <https://doi.org/10.2307/1060139>
- Domash, A. & Summers, L. H. (2022). *How tight are U.S. labor markets?* Cambridge, MA, USA: National Bureau of Economic Research. <https://doi.org/10.3386/w29739>
- Government Regulation No. 567/2006 Coll. on the minimum wage.
- Government Regulation No. 531/2021 Coll. on salary rates in Public Services and Administration.
- Hamza, M., Shahid, S., Bin Hainin, M. R. & Nashwan, M. S. (2022). Construction labour productivity: review of factors identified. *International Journal of Construction Management*, 22 (3), 413–425. <https://doi.org/10.1080/15623599.2019.1627503>
- Jang, H., Kim, K., Kim, J. & Kim, J. (2011). Labour productivity model for reinforced concrete construction projects. *Construction Innovation*, 11 (1), 92–113. https://doi.org/10.1108/14714171111104655_
- Jordà, Ò. & Nechio, F. (2023). Inflation and wage growth since the pandemic. *European Economic Review*, 156, 104474. <https://doi.org/10.1016/j.euroecorev.2023.104474>
- Ministry of Industry and Trade [MIT CZ], (2020). *Stavebnictví České Republiky [Construction industry, Czech Republic]*. Retrieved from: https://www.mpo.cz/assets/cz/stavebnictvi-a-suroviny/informace-z-odvetvi/2019/11/Stavebnictvi-2019.pdf?fbclid=IwAR-19HwPK2dJoHuwaVF_g5N1JlcV3rI9LjKTAIBIXLF97nOuU6V9NN5Zpa8o [accessed: 06.06.2023].
- Ministry of Industry and Trade [MIT CZ], (2023). Retrieved from: www.mpo.cz [accessed: 06.06.2023].
- Ministry of Justice [MJ CZ], (2023). Retrieved from: <https://www.justice.cz> [accessed: 06.06.2023].
- Naoum, S. G. (2016). Factors influencing labor productivity on construction sites: A state-of-the-art literature review and a survey. *International Journal of Productivity and Performance Management*, 65 (3), 401–421. <https://doi.org/10.1108/IJPPM-03-2015-0045>
- Rabušic, L. (2001). *Kde ty všechny děti jsou? [Where have all the children gone?]*. Praha: Sociologické nakladatelství (SLON). Retrieved from: <https://is.muni.cz/publication/382976/cs/Kde-ty-vsechny-deti-jsou/Rabusic> [accessed: 06.06.2023].
- Šimková, M. (2016). *Sociální a ekonomické aspekty stárnutí populace ČR [Social and economic aspects of population ageing of the Czech Republic]* (PhD thesis). Vysoká škola ekonomická v Praze, Praha.
- Smart Stavebnictví (2012). *Deloitte Česká republika, SPS v ČR, ÚRS Praha, 2012*. Retrieved from: https://www2.deloitte.com/content/dam/Deloitte/cz/Documents/about-deloitte/smart/SmartConstruction_1212_CZ.pdf [accessed: 17.02.2021].

Summary

Labor costs in a construction company in the Czech Republic – a case study. This article focused on quantifying the company's total labor costs in percent. Moreover, it aimed

to show the labor costs on a construction contract both from the terms of the company's labor costs of its own employees and the subcontractors' labor costs. Have been accurately quantified the total labor costs in the company from the profit and loss statement of the selected construction company, on which the case study was based, shows that the average percentage representation of labor costs, which include wage costs and social and health insurance costs, is 15.30%. However, when all the costs associated with employees as a labor force are identified in detail, it is evident that the total labor costs represent 31.82% of the sales remuneration. It results in the doubled value.

Irwan LAKAWA ✉  <https://orcid.org/0000-0002-9983-6531>

SYAMSUDDIN  <https://orcid.org/0009-0005-4458-4225>

HUJIYANTO  <https://orcid.org/0009-0005-4648-3110>

Vickky A. ILHAM  <https://orcid.org/0000-0001-5665-5637>

Universitas Sulawesi Tenggara, Faculty of Engineering, Civil Engineering Department, Kendari, Indonesia

Noise mapping due to motor vehicle activities in the by-pass ring road area of the city of Kendari

Keywords: traffic, noise exposure, mapping, ring road

Introduction

The issue of traffic noise constitutes a critical concern and a pervasive transportation challenge in urban areas, primarily driven by the rapid growth of motorized vehicles. This is also stated by Shvetsov (2021) that the noise level in modern cities continues to increase every year, primarily attributed to motor vehicles on highways. At certain intensities, this auditory intrusion can detrimentally affect the well-being and comfort of people in settlements, as well as road users themselves. Recent data indicates an annualized growth rate of 3% in motorized vehicles over the past three years in Indonesia (Kepolisian Republik Indonesia, 2021). Paradoxically, this surge in vehicles is not proportionately matched by the development of the road infrastructure, with the road growth rate languishing at a mere 0.6% per annum (Kementerian Pekerjaan Umum dan Perumahan Rakyat, 2021).

This lopsided growth dynamic creates problems that permeate the transportation system's comfort, notably manifesting as traffic congestion. Simultaneously, the escalating prevalence of motorized vehicles contributes to the degradation of environmental quality, with noise pollution emerging as a prominent byproduct. In the urban milieu, evading traffic noise has become a challenging feat (Kim et al., 2012). Despite the numerical preponderance of two-wheeled vehicles, it is the light vehicles that emerge as the principal contributors to noise pollution in urban areas, even when their numerical representation is dwarfed by that of two-wheeled vehicles in Indian urban settings (Agarwal & Swami, 2011).

As the capital of Southeast Sulawesi Province and a major city in Indonesia, the city of Kendari is poised to grapple with noise phenomena similar to developed countries and other major urban centers. Prior research in control locations has discerned noise levels reaching 75 dB (Lakawa, Sufrianto & Jusrin, 2021). This aligns with preliminary observations at various points in the by-pass ring road area of the city of Kendari, identifying noise levels peaking at 73 dB, surpassing the noise threshold stipulated in Indonesia (KEP-48/MENLH/11/1996).

Thus far, information on traffic noise distribution on highways has predominantly relied on numerical data, portraying trend descriptions that might not be readily comprehensible to the wider public. Moreover, the delineation of noise distribution across various land uses, particularly in the city of Kendari, remains an unexplored territory. This study seeks to address these gaps by presenting traffic noise variables as vector data, translating points of noise elevation into digitized representations. This approach aims to visually articulate information on traffic noise exposure.

The by-pass ring road in the city of Kendari connects the city center with the developing hinterland areas on the outskirts. Sections of this ring road include Edi Sabara Street, M. Joenoes, MT. Haryono, AH. Nasution, Malaka, ZA Sugianto, and Tapak Kuda. These road segments experience heavy motor vehicle traffic, leading to occasional congestion at specific hours. This situation has the potential to escalate traffic noise levels on the highways. The key question is the extent of traffic noise intensity and its distribution in the by-pass ring road area. In light of these considerations, a study was conducted in the by-pass ring road area of the city of Kendari. The research aims to determine roadside noise levels, predict noise exposure in land use, and map the distribution of noise.

Material and methods

Transportation challenges in urban areas encompass a spectrum of issues, including traffic congestion, parking, public transportation, pollution, and traffic order. While considerable attention is often directed toward mitigating traffic congestion, an equally

crucial concern stems from the noise generated by motorized vehicles on highways, known as traffic noise. Existing prediction models for traffic noise on collector roads incorporate independent variables such as vehicle volume, motorcycle speed, light vehicle speed, heavy vehicle speed, and noise measurement distance (Wedagama, 2012).

Numerous international studies highlight that highways constitute the primary source of noise in urban areas. This prevalence arises from the extensive use of motorized vehicles, including two-wheelers, four-wheelers, and those with more than four wheels. Notably, heavy vehicles (trucks, buses) and passenger cars emerge as the primary contributors to road noise, with motorcycles dominating at 60% (Mondal, 2013).

Predicting traffic noise extends beyond vehicle-related variables, encompassing traffic parameters, road characteristics, environmental conditions, weather variables, and residential parameters. Noise prediction involves not only vehicle volume and the percentage of heavy vehicles, but also factors like average vehicle speed and road conditions such as height, width, and gradient (Tripathi, Mittal & Ruwali, 2012). The level of traffic noise is further influenced by the distance between the noise source and the receiver, with an average reduction of 1.3 dB as the distance increases (Handayani, Rahadi & Hadiani, 2016). According to Lakawa, Hujiyanto and Haryono (2023), the parameters triggering urban traffic noise include traffic factors such as vehicle volume, speed, density, and vehicle composition. Physical road factors encompass superelevation, gradient, road width, road type, and road surface conditions. Environmental road factors include building density, tree density, leaf volume, ground surface type, and air temperature. However, from a different perspective, Kuehnel, Moeckel and Ziemke (2021) argue that responses to noise exposure differ between high and low-income households.

Despite the prevalence of road noise, comprehensive studies addressing its multifaceted nature have been limited. The intricacies lie in the diverse sources contributing to road noise, with heavy vehicles, constituting 4%, playing a crucial role on arterial roads but demonstrating lesser significance on collector roads, where their composition is 3%. In these settings, noise is more prominently influenced by motorcycles and light vehicles (Lakawa, Samang, Selintung & Hustim, 2015). The dispersion of noise exposure on highways occurs in all directions, involving absorption, transmission, and reflection.

International studies have leveraged advanced technologies to predict and address traffic noise. In Korea, a study utilized SoundPLAN software to predict noise distribution and facilitate noise reduction initiatives during and after road construction projects. The results revealed that increased traffic volume due to industrial area development had a more substantial impact on the surrounding area than on the industrial zone itself (Jeong, Din, Otsuru & Kim, 2010). Sotiropoulou, Karagi-

annis, Vougioukas, Ballis and Bouki (2020) conducted measurements and predictions of traffic noise in front of high-rise buildings in Athens using the calculation of road-traffic noise (CRTN) method. They found a high consistency between the predicted and measured noise levels. This model is suitable for predicting traffic noise in front of tall buildings during the planning and design phases.

Similarly in Surat, India, traffic noise mapping was conducted using the RLS-90 computer simulation model, integrating noise data, road inventory, geometric features, vehicle volume, speed, and meteorological data. The approach allowed for the incorporation of horn correction values to assess heterogeneous traffic conditions (Sonaviya & Tandel, 2020).

Novel methods, such as utilizing Google API for traffic flow data, have been employed to predict noise levels in Rome and Pisa. The BPR model estimated traffic volume, and the resulting noise mapping generated conventionally and from big data, offered valuable insights (Licitra, Moro, Teti & Del Pizzo, 2021). In the Delhi region, India, digital maps generated through optimization techniques illustrated horizontal and vertical noise level profiles with variations in measurement distances (Akhtar, Ahmad & Gangopadhyay, 2012).

A road traffic noise model developed using a graph theory approach, incorporating variables like vehicle speed, traffic volume, road width, the number of heavy vehicles, and horn sound, has demonstrated satisfactory performance. Despite slightly elevated results, this method proves effective in predicting future noise levels (Gilani & Mir, 2021).

Based on the research objectives of obtaining roadside noise levels, predicting noise exposure in land use, and mapping the distribution of noise in the area, the data collection activities are systematically conducted following survey procedures. Stage 1 involves the identification and analysis of traffic data. The survey is carried out at 11 points in the by-pass ring road area of the city of Kendari (Fig. 1), with observation times of $10 \text{ min} \cdot \text{h}^{-1}$. The observation time is set at 10 min based on the noise survey procedures (KEP-48/MENLH/11/1996). Location selection is varied to represent various land use types along the road, such as settlements, commercial, services, and school areas.

The identification and analysis of noise levels aims to obtain existing traffic noise values at the roadside. The noise survey is carried out simultaneously with the traffic survey, utilizing a sound level meter (SLM) for noise measurement (Fig. 2). Additionally, field coordinates are digitized during this stage. The existing noise data are then analyzed using mathematical equations. The final stage involves mapping the noise distribution using an overlay approach in ArcGIS. In the mapping process, noise values are treated as elevation points, and colors are assigned based on noise interval levels. This method provides a visual representation of noise levels across the area.

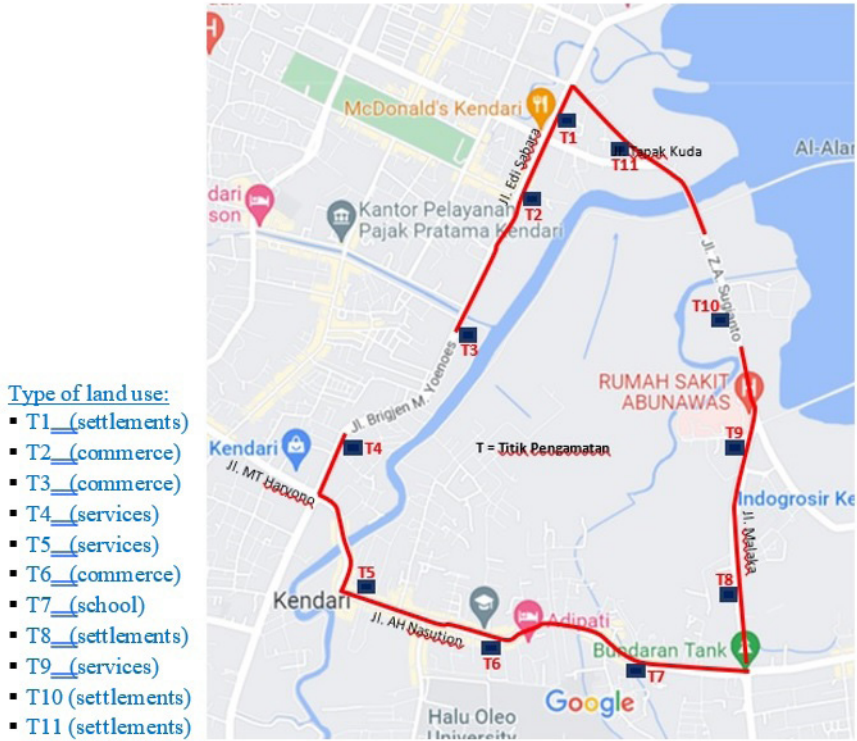


FIGURE 1. Observation point locations

Source: own work.

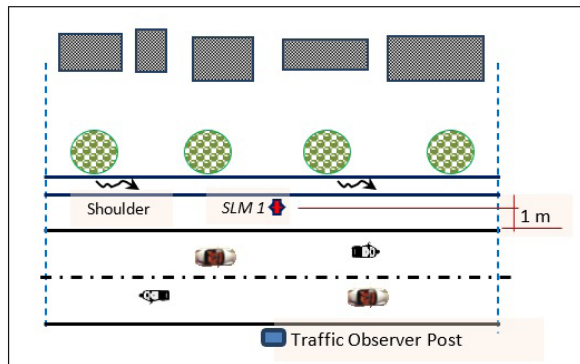


FIGURE 2. Noise measurement scheme

Source: own work.

Integral to this investigation is the establishment of a threshold value for noise levels. This value represents the maximum allowable noise limit to be emitted into the environment without causing health disturbances for humans and environmental discomfort. The calculation of the equivalent noise level (L_{eq}) was conducted using the following equation:

$$L_{eq} = L_{50} + 0.43(L_1 - L_{50}), \tag{1}$$

where: L_{eq} is the equivalent noise level [dB], L_{50} is the 50% noise percentile [dB], and L_1 is the 1% noise percentile [dB].

The values of L_{50} and L_1 are obtained from the readings of the SLM during the survey, according to the following equation:

$$L_{eq2} = L_{eq1} - 10\log(r_2/r_1), \tag{2}$$

where: L_{eq2} is the noise level at r_2 distance from the center of the road noise source [dB], L_{eq1} is the noise level at r_1 distance from the center of the road noise source [dB], r_1 is the distance from the noise source to the SLM measuring position [m], and r_2 is the distance from the noise source to the building wall [m].

The threshold value for noise levels represents the maximum permissible limit of noise released into the environment, aiming to prevent health risks and ensure environmental comfort. Table 1 outlines the noise standards in Indonesia, referring to the Minister of State for the Environment of the Republic of Indonesia’s decree KEP-48/MENLH/11/1996.

TABLE 1. Noise level quality standard

Type of land use	Noise level standards [dB]
1. Appropriation of region	
a) housing and settlements	55
b) trade and services	70
c) office and commerce	65
d) green open space	50
e) industry	70
f) government and public facilities	60
g) recreation	70

TABLE 1 (cont.)

h) specifically	
– airport*	
– railway station*	
– harbor	70
– cultural heritage	60
2. Surrounding activity	
a) hospital or the like	55
b) school or the like	55
c) worship place or the like	55

*In accordance with the regulations of the Minister of Transportation PM 62/2021 and PM 175/2015.

Source: Minister of State for the Environment of the Republic of Indonesia's decree KEP-48/MENLH/11/1996.

Results and discussion

The study focuses on traffic volume, particularly the number of motorized vehicles traversing the by-pass ring road area, serving as a vital connection to developing suburban regions (Fig. 3). Calculations are based on observed vehicle counts at various locations during the study period, converted into passenger car units per hour [pcu·h⁻¹].

Notably, the highest vehicle volume is recorded on ZA Sugianto Street at 2,734 pcu·h⁻¹, followed by MT. Haryono Street (1,937 pcu·h⁻¹), M. Joenoes Street (1,868 pcu·h⁻¹), Edi Sabara Street (1,630 pcu·h⁻¹), Malaka Street (1,375 pcu·h⁻¹), Tapak Kuda Street (1,300 pcu·h⁻¹), and the lowest on AH Nasution Street (1,229 pcu·h⁻¹). Motorcycles dominate the composition at 68%, followed by light vehicles at 27%, and heavy vehicles at 5%. Peak traffic hours vary; MT Haryono and AH Nasution streets peak in the morning, Edi Sabara and Brigjen M. Joenoes streets peak during the day, while Malaka, ZA Sugianto, and Tapak Kuda streets peak in the evening. Notably, motorcycle compositions in medium and large cities typically range from 60–70%. Survey results include the coordinates of each location (refer to Table 2), while L_{eq} noise values are obtained using Equation (1).

Figure 4 illustrates that traffic noise levels along the by-pass ring road surpass the environmental noise threshold outlined in the Minister of State for the Environment of the Republic of Indonesia's decree (KEP-48/MENLH/11/1996) for settlements/school, office, and commerce/service areas. The average noise level on the highways is 76 dB, with the level reaching the receiver at 67 dB, indicating an average noise

reduction of 9 dB. The average distance from the receiver to the noisy road source is 14 m, resulting in a noise reduction of $2 \text{ dB} \cdot \text{m}^{-1}$. Noise levels are influenced by land use, with the commerce area exhibiting the highest noise levels, followed by service and school areas, and the lowest in front of settlement areas. These variations are intricately linked to the activities associated with each land use (Table 3).

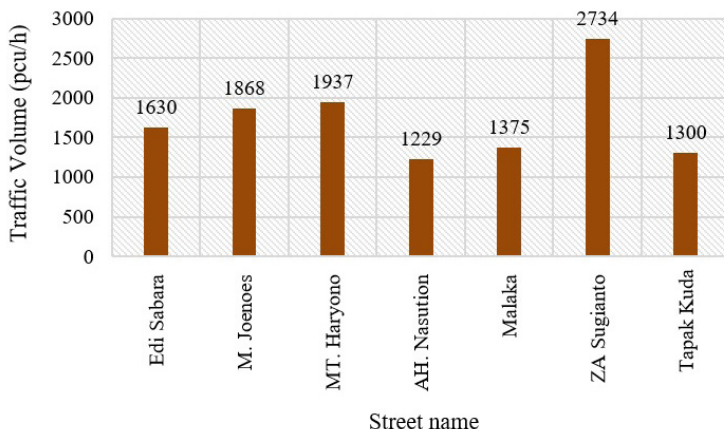


FIGURE 3. Volume traffic on seven regional roads traversing the by-pass

Source: own work.

TABLE 2. Point coordinates and noise values

Street name	Location code	Point 1 (1 m from the roadside)			Noise level [dB]		
		coordinate	east longitude	south latitude	L_1	L_{50}	L_{eq}
Jl. Edi Sabara	T.1	1183	122° 31' 30.54" E	3° 58' 29.60" S	81.9	71.7	75.7
Jl. M. Joenoes	T.2	1185	122° 31' 21.90" E	3° 58' 47.43" S	84.4	73.1	78.0
Jl. M. Joenoes	T.3	1187	122° 31' 11.91" E	3° 59' 8.55" S	88.4	72.6	79.4
Jl. M. Joenoes	T.4	1189	122° 30' 53.22" E	3° 59' 25.00" S	85.2	72.2	77.8
Jl. MT. Haryono	T.5	1191	122° 30' 55.52" E	3° 59' 53.91" S	83.6	71.6	76.8
Jl. AH. Nasution	T.6	1197	122° 31' 14.57" E	3° 59' 59.69" S	83.8	69.3	75.5
Jl. AH. Nasution	T.7	1199	122° 31' 46.97" E	4° 0' 5.17" S	87.6	68.2	76.5
Jl. Malaka	T.8	1203	122° 32' 2.49" E	3° 59' 28.33" S	83.6	69.7	75.7
Jl. Malaka	T.9	1201	122° 32' 1.27" E	3° 59' 56.09" S	81.7	70.2	75.1
Jl. ZA Sugianto	T.10	1205	122° 32' 1.26" E	3° 59' 10.50" S	85.6	71.9	77.8
Jl. Tapak Kuda	T.11	1207	122° 31' 42.54" E	3° 58' 36.36" S	81.8	70.7	75.5

Source: own work.

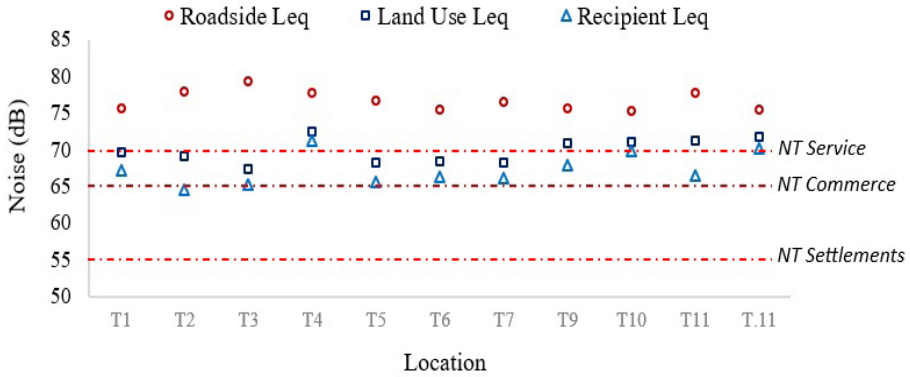


FIGURE 4. Traffic noise level on the highway, NT Settlements 55 dB, NT Commerce 65 dB, and NT Service 70 dB

Source: own work.

TABLE 3. Types of land use and exposure distance

Street name	Location code	Type of land use	Exposure distance [m]	
			source-SLM (r_1)	source-land use (r_2)
Jl. Edi Sabara	T1	settlements	9	18
Jl. M. Joenoes	T2	commerce	9	36
Jl. M. Joenoes	T3	commerce	9	26
Jl. M. Joenoes	T4	services	9	16
Jl. MT Haryono	T5	services	7	19
Jl. AH Nasution	T6	commerce	8	19
Jl. AH Nasution	T7	school	8	21
Jl. Malaka	T8	settlements	9	20
Jl. Malaka	T9	services	9	18
Jl. ZA Sugianto	T10	settlements	7	32
Jl. Tapak Kuda	T11	settlements	5	13

Source: own work.

Based on the roadside noise level (L_{eq}) values in Table 2 and the r_1 and r_2 exposure distances, the predicted results of noise distribution in land use are obtained using Equation (2), as seen in Figure 5.

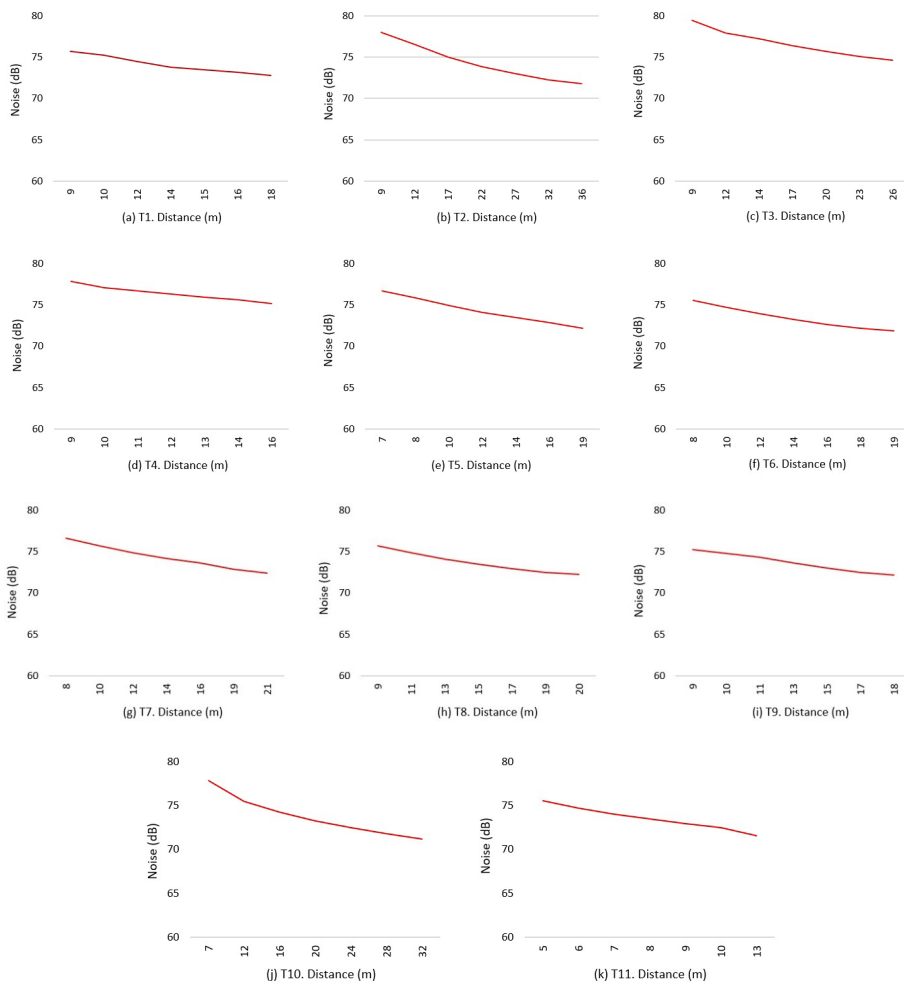


FIGURE 5. Prediction of noise exposure in land use based on the distance from the roadside
Source: own work.

Figure 5 illustrates the varying noise exposure across different land uses in the research area. The service area at Point T4 exhibits the highest noise level at 75.2 dB, succeeded by the commerce area at Point T3 with a measurement of 74.6 dB. Other notable levels include the settlements area at Point T1 (72.8 dB), school area at Point T7 (72.4 dB), service area at Point T5 (72.2 dB), settlements area at Point T8 (72.2 dB), service area at Point T9 (72.2 dB), commerce area at Point T6 (71.8 dB), settlements area at Point T11 (71.5 dB), and the lowest in the settlements area at Point T10 (71.2 dB).

The analysis emphasizes that noise intensity diminishes with increased distance from the noise source to the receiver. According to Lakawa, Hujiyanto, Sulaiman and Haryono (2022), a reduction in noise levels within an area may occur due to increased distance, resulting in an average decrease of 1.3 dB. Consequently, the determination of noise exposure hinges on the intensity within a specific area and the duration of exposure. Disparities in noise reduction among the eleven areas stem from both the augmented distance and the magnitude of the roadside noise level. Additionally, variations are influenced by the type of land surface transitioning from the roadside to land use, along with the extent and density of greenery or tree planting along the roadside.

The mapping results indicate that the noise intensity in the by-pass ring road area is best understood by observing the color intervals of contour lines. Yellow and red colors signify a moderate level of noise (Fig. 6). Furthermore, the noise exposure reaching land use planning exceeds the noise threshold set in Indonesia. This potential overstep poses a threat to the health and comfort of both road users and residents living along the road. For instance, hearing impairment can be temporary or permanent, depending on the duration and frequency of exposure to noise.

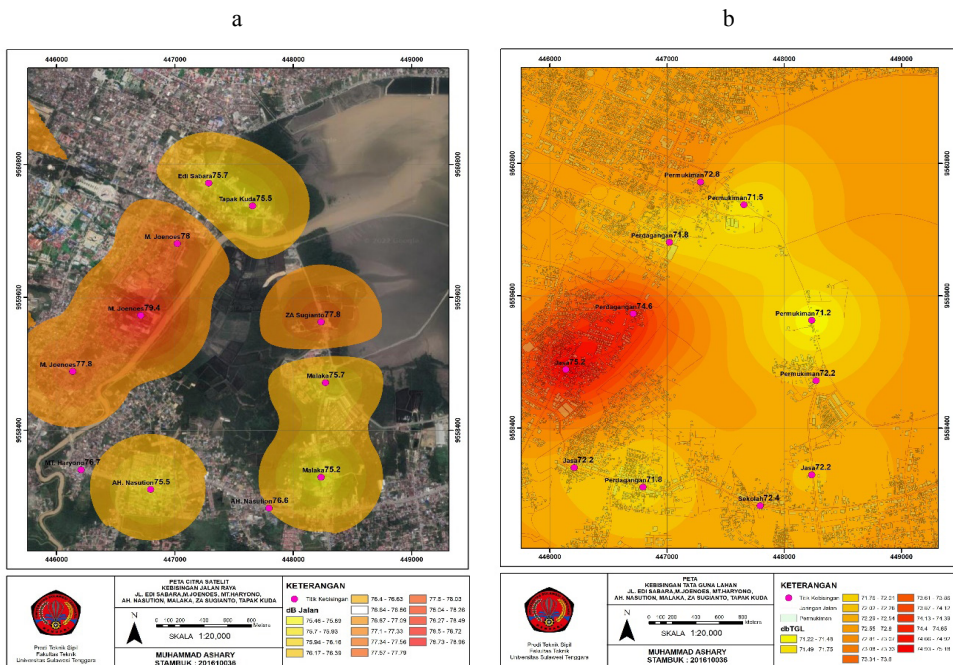


FIGURE 6. Noise distribution map: a – noise distribution at the roadside; b – noise exposure that reaches land use
Source: own work.

In a comparative context, noise level mapping was conducted in Rome during the COVID-19 pandemic, focusing on strategies to control the virus. The mapping generated a noise emission map, exploring scenarios of restricting private vehicle travel and scenarios of easing private vehicle use (Aletta et al., 2020). Notably, this mapping exercise did not explicitly depict noise level limits. Similarly, noise mapping was undertaken to evaluate noise disturbances stemming from the operations of Athens International Airport. The analysis revealed that the community experienced noise levels surpassing 70 dB. The mapping exercise involved a comparative analysis of strategic noise maps between 2017 and 2019, considering daytime and nighttime noise indices. Furthermore, this study formulated an action plan for Athens International Airport, commencing in 2007 (Vogiatzis, Dimitriou & Gerolymatou, 2019). Similarly, noise measurements were conducted in Tehran using the FHWA TNM software. This model considers barrier parameters, trees, sidewalks, and slopes. The research produced a traffic noise map based on a combination of modeling and field measurement results. The study's findings highlighted that a significant number of trucks in Tehran are outdated, contributing to elevated noise levels (Mohamady, Noorpoor & Bayatian, 2021).

Distinctively, the present research has successfully generated a traffic noise map for the highway, delineating its distribution across various land uses and receivers. This distribution encompasses commerce areas, services, schools, and settlements areas. The mapping results provide a visual indication of areas where noise levels surpass the regulatory limits set forth in Indonesia.

Conclusions

The vehicle composition along the by-pass ring road is dominated by motorcycles at 68%, followed by light vehicles at 27%, and heavy vehicles at 5%. The average noise level on the highway is 76 dB, with land use patterns significantly influencing noise fluctuations on the road. The highest noise levels occur in the commerce area, followed by service and school areas, while the lowest levels are observed in front of residential areas. This correlation is closely related to the movement patterns associated with each land use. Notably, the trend is consistent: the farther the distance from the noise source to the receiver, the lower the intensity of the noise. This highlights the crucial role of spatial distance in determining noise exposure levels.

To mitigate traffic noise in the by-pass ring road area of the city of Kendari, it is recommended to implement green landscaping, specifically by planting trees along the road. This strategic tree planting approach can effectively reduce traffic noise. Additionally, combining tree planting with creeping plants can further enhance the noise reduction efforts.

Acknowledgements

The authors express their gratitude to all those who played vital roles in facilitating the execution of this research, particularly the dedicated survey team and research members. This study was made possible through the grant provided by Universitas Sulawesi Tenggara in 2023, as per the decision letter from the Rector of Universitas Sulawesi Tenggara (Number: 435.a/R/09/N/IX/2023). Thus, the authors extend their thanks to the Rector of Unsultra for the invaluable support and motivation. It is hoped that the findings of this research will prove beneficial in advancing scientific knowledge, especially in the field of environmental transport.

References

- Agarwal, S. & Swami, B. L. (2011). Comprehensive approach for the development of traffic noise prediction model for Jaipur City. *Environment Monitoring and Assessment*, 172, 113–120. <https://doi.org/10.1007/s10661-010-1320-z>
- Akhtar, N., Ahmad, K. & Gangopadhyay, S. (2012). Road traffic noise mapping and a case study for Delhi Region. *International Journal of Applied Engineering and Technology*, 2 (4), 39–45.
- Aletta, F., Brinchi, S., Carrese, S., Gemma, A., Guattari, C., Mannini, L. & Patella, S. M. (2020). Analysing urban traffic volumes and mapping noise emissions in Rome (Italy) in the context of containment measures for the COVID-19 disease. *Noise Mapp*, 7, 114–122. <https://doi.org/10.1515/noise-2020-0010>
- Gilani, T. A. & Mir, M. S. (2021). Modelling road traffic Noise under heterogeneous traffic conditions using the graph-theoretic approach. *Environmental Science and Pollution Research*, 28 (27), 36651–36668. <https://doi.org/10.1007/s11356-021-13328-4>
- Handayani, D., Rahadi, R.S. & Hadiani, R.R. (2016). Prediksi kebisingan pada jalan kolektor (Studi kasus: Jalan Monginsidi Surakarta) [Prediction of noise on collector roads. Case study: Jalan Monginsidi Surakarta]. *e-Jurnal Matriks Teknik Sipil*, 4 (3), 649–657. <https://doi.org/10.20961/mateksi.v4i3.37069>
- Jeong, J. H., Din, N. C., Otsuru, T. & Kim, H. C. (2010). An application of a noise maps for construction and road traffic noise in Korea. *International Journal of the Physical Sciences*, 5 (7), 1063–1073.
- Kementerian Pekerjaan Umum dan Perumahan Rakyat [Ministry of Public Works and Housing (Indonesia)] (2021). *Panjang Jalan Menurut Jenis Permukaan 2019–2021 [Road length by surface type 2019–2021]*. Jakarta: Kementerian Pekerjaan Umum dan Perumahan Rakyat.
- Kepolisian Republik Indonesia [The Indonesian National Police]. (2021). *Perkembangan jumlah kendaraan bermotor menurut jenis 2019–2021 [Number of motor vehicle by type (unit) 2019–2021]*. Jakarta: Kepolisian Republik Indonesia.

- KEP-48/MENLH/11/1996, tentang baku tingkat kebisingan [KEP-48/MENLH/11/1996 Minister of State for the Environment of the Republic of Indonesia's decree No. 48, the year 1996, concerning noise limits].
- Kim, M., Chang, S. I., Seong, J. C., Holt, J. B., Park, T. H., Ko, J. H. & Croft, J. B. (2012). Road traffic noise: annoyance, sleep disturbance, and public health implications. *American Journal of Preventive Medicine*, 43 (4), 353–360. <https://doi.org/10.1016/j.amepre.2012.06.014>
- Kuehnel, N., Moeckel, R. & Ziemke, D. (2021). Traffic noise feedback in agent-based integrated land-use/transport models. *The Journal of Transport and Land Use*, 14 (1), 325–344. <https://doi.org/10.5198/jtlu.2021.1852>
- Lakawa, I., Hujiyanto, H. & Haryono, H. (2023). A study of heterogeneous traffic noise trigger parameters for urban areas. *Technium*, 13, 79–87. <https://doi.org/10.47577/technium.v13i.9572>
- Lakawa, I., Hujiyanto, H., Sulaiman & Haryono, H. (2022). The determination of noise area criteria based on prediction distance. *International Journal of Development Research*, 12 (11), 60589–60593. <https://doi.org/10.37118/ijdr.25779.11.2022>
- Lakawa, I., Sufrianto, S. & Jusrin, J. (2021). Application of overlay method in interpreting of traffic noise distribution in land use. *IOP Conference Series: Earth and Environmental Science*, 847 (1), 012023. <https://doi.org/10.1088/1755-1315/847/1/012023>
- Lakawa, I., Samang, L., Selintung, M. & Hustim, M. (2015). Relationship models of traffic volume vs noise level. *International Journal of Development Research*, 5 (9), 5463–5466.
- Licitra, G., Moro, A., Teti, L. & Del Pizzo, L. G. (2021). The influence of link characteristics on road traffic noise mapping by using Big Data. *INTER-NOISE and NOISE-CON Congress and Conference Proceedings*, 263 (1), 5225–5232. <https://doi.org/10.3397/IN-2021-3010>
- Mohamady, Z., Noorpoor, A. & Bayatian, M. (2021). Investigating of environmental traffic noise modelling by using FHWA TNM in Tehran township. *EQA – International Journal of Environmental Quality*, 45, 42–48. <https://doi.org/10.6092/issn.2281-4485/12482>
- Mondal, N. K. (2013). Vehicle noise interference and its impact on the community. *International Journal of Current Science*, 5 (20), 161–169.
- Shvetsov, A. (2021). Aspects of traffic noise reduction. *Akustika*, 39 (39), 27–29.
- Sonaviya, D. R. & Tandel, B. N. (2020). Integrated road traffic noise mapping in urban Indian context. *Noise Mapping*, 7 (1), 99–113. <https://doi.org/10.1515/noise-2020-0009>
- Sotiropoulou, A., Karagiannis, I., Vougioukas, E., Ballis, A. & Bouki, A. (2020). Measurements and prediction of road traffic noise along high-rise building façades in Athens. *Noise Mapping*, 7 (1), 1–13.
- Tripathi, V., Mittal, A. & Ruwali, P. (2012). Efficient road traffic noise model for generating noise levels in Indian scenario. *International Journal of Computer Applications*, 38 (4), 1–5.
- Vogiatzis, K., Dimitriou, D., Gerolymatou, G. & Konstantinidis, A. (2019). Strategic noise mapping in Athens International Airport: a tool for balanced approach & health effects evaluation. *Noise Mapping*, 7 (1), 87–98. <https://doi.org/10.1515/noise-2020-0008>
- Wedagama, D. M. P. (2012). The influence of local traffic on noise level (case study: bypass Ngurah Rai and Sunset Road, Bali). *Jurnal Bumi Lestari*, 12 (1), 24–31.

Summary

Noise mapping due to motor vehicle activities in the by-pass ring road area of the city of Kendari. The by-pass ring road in Kendari serves as a crucial artery, facilitating accessibility and mobility between the city center and the expanding outskirts. However, heightened traffic has led to a notable upswing in noise along the highway. This study aims to systematically map the distribution of this noise across various land uses in the vicinity. To accomplish this, measurements were taken at eleven specific points along the road, utilizing a sound level meter (SLM). The collected data, encompassing noise levels on the highway and its impact on different land uses, underwent a thorough analysis through mathematical equations. Subsequently, mapping was executed using the overlay method based on coordinate points. The findings reveal a vehicular composition predominantly comprised of motorcycles (68%), followed by light vehicles (27%), and heavy vehicles (5%). Notably, although heavy vehicles constitute a mere 5%, they significantly influence the elevation of noise levels. The highest noise intensity impacting land use is observed in service areas, succeeded by commercial and school zones, with the lowest levels recorded in settlement areas. The mapped results depict a noise exposure of 67 dB reaching receptors, coupled with an average noise reduction of 9 dB. Remarkably, as the average distance from the noise source on the highway to the receptors increases (averaging 14 m), there is a discernible reduction in noise intensity. This visually apparent trend is corroborated by the noise mapping results.

Instruction for Authors

The journal publishes in English languages, peer-reviewed original research, critical reviews and short communications, which have not been and will not be published elsewhere in substantially the same form. Author of an article is required to transfer the copyright to the journal publisher, however authors retain significant rights to use and share their own published papers. The published papers are available under the terms of the principles of Open Access Creative Commons CC BY-NC license. The submitting author must agree to pay the publication charge (see Charges).

The author of submitted materials (e.g. text, figures, tables etc.) is obligated to restricts the publishing rights. All contributors who do not meet the criteria for authorship should be listed in an Acknowledgements section of the manuscript. Authors should, therefore, add a statement on the type of assistance, if any, received from the sponsor or the sponsor's representative and include the names of any person who provided technical help, writing assistance, editorial support or any type of participation in writing the manuscript.

Uniform requirements for manuscripts

The manuscript should be submitted by the Open Journal System (OJS) at <https://srees.sggw.edu.pl/about/submissions>. All figures and tables should be placed near their reference in the main text and additionally sent in a form of data files (e.g. Excel, Visio, Adobe Illustrator, Adobe Photoshop, CorelDRAW). Figures are printed in black and white on paper version of the journal (color printing is combined with an additional fee calculated on a case-by-case basis), while on the website are published in color.

The size of the manuscript should be limited up to 10 pages including overview, summary, references and figures (the manuscript more than 13 pages is unacceptable); Please set the text format in single column with paragraphs (A4 paper format), all margins to 25 mm, use the font Times New Roman, typeface 12 points and line spacing one and half.

The submitted manuscript should include the following parts:

- name and SURNAME of the author(s) – up to 5 authors
- affiliation of the author(s), ORCID Id (optional)
- title of the work
- key words
- abstract (about 500 characters)
- text of the paper divided into: Introduction, Material and Methods, Results and Discussion, Conclusions, References and Summary
- references in APA style are listed fully in alphabetical order according to the last name of the first author and not numbered; please find the details below
- post and mailing address of the corresponding author:

Author's address:

Name, SURNAME

Affiliation

Street, number, postal code, City

Country

e-mail: address@domain

- Plagiarism statement (<https://srees.sggw.edu.pl/copyright>)

Reference formatting

In the Scientific Review Engineering and Environmental Sciences the APA 6th edition style is used.

Detailed information

More information can be found: <https://srees.sggw.edu.pl>

